THE IMPACT OF ATMOSPHERIC MODELS ON THE DYNAMICS OF SPACE TETHER SYSTEMS

Vishal Siewnarine

A THESIS SUBMITTED TO THE FACULTY OF GRADUATE STUDIES IN PARTIAL FULFILMENT OF THE REQUIREMENTS FOR THE DEGREE OF MASTER OF SCIENCE

Graduate Program in Physics and Astronomy
York University
Toronto, Ontario

September 2015

Abstract

Space debris has become an increasingly larger concern for aerospace travel and exploration. One idea to control the space debris population is to de-orbit defunct satellites using a space tether system.

A space tether system is often made up of three parts: the main satellite, the tether and the sub-satellite. The tether connects the main satellite and the sub-satellite. Space tether systems make use of the Lorentz force as an electrodynamic drag for de-orbit.

We use an established model of a space tether system to observe how satellites de-orbit. This model was constructed in MATLAB (Simulink) and uses the 1976 U.S. Standard Atmosphere. However, we wish to investigate how the model behaves using newer and more accurate atmospheric models, namely, the Jacchia-Bowman 2008 model and the Drag Temperature Model 2013. We also investigate the effect of controlling the tether's libration energy under the three aforementioned atmospheric models.

Acknowledgements

First of all, I would like to thank God for bringing me to this point. Without her, nothing is possible. Next, I would like to thank Professor Zheng Hong Zhu for his enduring patience and effort in being my supervisor and mentor whose sincerity, encouragement, late nights and tireless efforts helped shape my focus and inspire me as I hurdle all the obstacles and barriers in the completion of this work. Professor Zhu has provided a wealth of experience and knowledge in the field of science and engineering.

I also wish to acknowledge the comprehensive assistance from Mr. Gangqiang Li for helping me implement libration energy control strategy and conduct simulations. I would also like to pay special thanks to the members of the Space Engineering Design Laboratory for their friendship and help during the undertaking of the current study.

Finally, I want to extend thanks to my friends and family for believing in me and supporting me through the study.

List of Notations

All units are given in SI derived units, time in seconds (s), distance in metres (m), velocity in metres per second (m/s), except where otherwise noted.

A	Cross-sectional area of object (satellite)
A_{1i}	Constant
$\vec{B}$	Local geo-magnetic field
$\overline{c}_i$	Mean velocity of the i^{th} component of the gas
C_D	Drag coefficient
$d\vec{l}$	Differential element of length
D	Diameter of the tether
$\hat{e}_r$	Unit vector in radial direction
$f(z)$	Relation between the amplitude of the variation and the height, z
$F_{10.7}$ / $\overline{F}_{10.7}$	Tabulated solar indices
F_D	Drag force
$\vec{F}_{Gr}$	Gravitational force between two objects
$\vec{F}_{Lo}$	Lorentz force
F_{gas}	Weight of gas

$g(t)$	Average density variation (amplitude normalised to 1)
$g, g(z)$	Acceleration due to gravity
g_{120}	Acceleration due to gravity at 120 km
H	Hour angle of Sun
i	Inclination angle
$I(l)$	Current flowing through tether
k	Boltzmann constant
K_p	Three-hour planetary index for geomagnetic activity
L	Length of tether
m_{gas}	Mass of the gas in the column
m_i	Molecular mass of the i^{th} constituent
m_{Sat}	Mass of satellite
M_E	Mass of Earth
M_{mol}	Molecular mass of the gas
n	Mean orbital motion
$n(H)_{500}$	Number density of Hydrogen at 500 km
n_i	Number density of the i^{th} atmospheric constituent
$n_{i,7}$	Set of number density values corresponding to each atmospheric constituent
n_{mol}	Number of moles of gas
P	Pressure of gas

r	Distance between Earth and satellite
R_E	Radius of Earth (in kilometres)
R_{gas}	Molar gas constant
s	Constant that depends on specific atmospheric constituent (N_2, O_2 etc.)
T	Temperature
T_{120}	Temperature at 120 km altitude
T_7	Temperature at 86 km
T_C	Global exospheric temperature
T_l	Exospheric temperature
T_∞	Exospheric temperature
$\vec{v}$	Relative velocity vector of tether with respect to geo-magnetic field
v_{obj}	Speed of object (satellite) with respect to flow of atmosphere
V_c	Non-dimensional libration energy
V_{gas}	Volume of the container
z	Altitude in kilometres
α_i	Thermal diffusion factor for the i^{th} constituent
δ	Sun's declination
ϕ	Given latitude
ϕ_{roll}	Roll angle
Φ	Induced voltage
γ_{dist}	Distance between centre of mass of space tether system and sub-satellite

μ	Gravitational constant of the Earth
ω_E	Rotational velocity
θ_{pitch}	Pitch angle
ρ	Density of atmosphere
ρ_{gas}	Density of gas

List of Abbreviations

ATMOP	Advanced Thermosphere Modelling for Orbit Prediction
CHAMP	CHAllenging Minisatellite Payload
CIRA	COSPAR International Reference Atmosphere
CNES	Centre National d'étudesspatiales
COSPAR	COmmittee on SPAce Research
EDT	Electrodynamic Tether
EUV	Extra Ultra-Violet
FUV	Far Ultra-Violet
GOCE	Gravity field and steady-state Ocean Circulation Explorer
LEO	Low Earth Orbit
NASA	North American Space Agency

CONTENTS

List of Tables

List of Figures

List of Appendices

Chapter 1 INTRODUCTION

1.1 The Problem

1.1.1 Space Tethers and Their Applications

Space tether systems comprise a tether that connects one or more satellites: the base or mother satellite and her sub-satellites [1]. Space tethers are long cables, made of long strands of high strength fibres or conducting wires and they provide a mechanical connection that enables the transfer of energy and momentum from one object to the other(s) [2]. Tethers are typically very long, ranging from a few hundred metres to several kilometres with a relatively small diameter [3]. Space tether systems have many potential applications. The most promising use of space tether systems is that they are able to change (raise and lower) their orbit around Earth without expensive propellants [4] [5]. There are also other uses for space tether systems, such as the collection (and removal) of space debris [6] [7] and the exploration of other planets (such as Mars and Jupiter) and their atmospheres [8] [9]. Another, perhaps more novel, use of the tether is in space elevators, where payloads travel along the tether from the ground to space [10]. A final application for the space tether is de-orbiting satellites from the upper atmosphere [11] which is the one considered in this dissertation.

Space tether systems orbit the Earth in the upper atmosphere and, as a result, their

dynamics is influenced by its location. The upper atmosphere is an unpredictable environment and this provides a challenge to both the stability and the dynamics of space tether systems. In this dissertation, we will study the impact of the different models of the upper atmosphere on the dynamic stability of the space tether systems. With a proper atmospheric model, we can better understand the behaviour of space tether systems as they work. In our case, we will concentrate specifically on using the tether to de-orbit a space system. We will examine the different atmospheric models and see how they influence the dynamics of our space tether system during de-orbit.

1.2 Justification of the Research

1.2.1 Satellite De-orbit by a Space Electrodynamic Tether

Over the years, the Earth orbits, specifically the geosynchronous orbits that are ideal for communication satellites and the Sun synchronous orbits that are favoured for Earth observing satellites, are becoming increasingly crowded because more and more man-made objects are launched into the space, see Fig. 1.1. Pardini et al. [12] stated that there are over 9000 satellites and other trackable objects in the Earth's orbit in 2007. The debris population has grown by approximately 200 every year since the beginning of the space age [13]. Since that time, two major events (the Chinese Anti-Satellite test in 2007 and the collision of the Cosmos-Iridium satellites in 2009) have added approximately 40% to the amount of debris in LEO [14] indicative of Kessler syndrome. Since then, Levin et. al. has estimated the number of lethal impactors to be 500,000 [15]. De-orbiting 5 main bodies (such as satellites) yearly from densely populated orbital regions will keep the space environment stable [16]. As such, there is a need to control the amount of

debris that result from man-made spacecraft in Earth's orbit.

Over the years, many technologies have been proposed for the space debris removal, for instance, the chemical propulsion, electrical propulsion, drag sail, solar radiation augmentation sail, tethered momentum exchange, electrodynamic tethers (EDT), laser propulsion, ion-beam shepherd satellite and hybrid EDT ion-beam shepherd systems. Among them, the chemical and electrical propulsion has the highest Technology Readiness Level (TRL) of 9, followed by the EDT with a TRL 6-7 and the rest with TRLs below 5. Compared with the chemical and electrical propulsion, the EDT technology appeals most due to its advantages of low mass, compact size, fuel-less and ease of operation. Particularly, it is able to function independently and does not rely on having a working satellite it resides to re-enter.

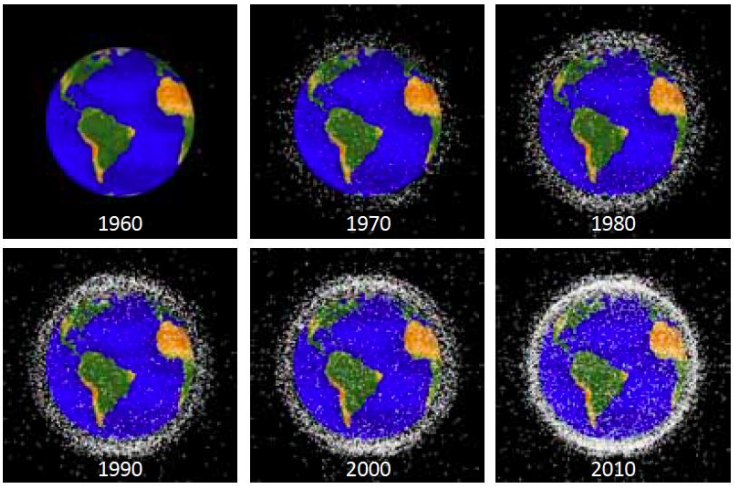

Figure 1.1 Satellites and space debris in Earth orbit from 1960 to 2010. (Courtesy NASA)

Khan and Sanmartin [17] investigated the survivability of the tether by conducting simulations using a taped tether to reduce the impact of the collisions on the tether from existing space debris. Their results depended on the model used for space debris but declared them to be optimistic.

The first introduction of using a tether to de-orbit a satellite in academic literature was made by Hoyt et. al. [18]. Hoyt is also a founder of the company Tethers Unlimited, Inc. which is a private American aerospace company. Their initial paper asserts that the electrodynamic drag created from the tether causes a typical communication satellite to de-orbit orders of magnitude faster than with just aerodynamic drag. Tethers Unlimited, Inc. have coined terms like 'Terminator Tether' and 'Remora Remover' [19] to commercially describe the function of the space tether i.e. to de-orbit satellites.

A more detailed explanation of how the EDT de-orbits the satellite is given by Pardini et al. [20]. The tether, when deployed from the satellite, will induce an electrodynamic drag due to the Lorentz force created by the interaction between the current flowing in the conductive tether and the Earth's magnetic field. This Lorentz force, $\vec{F}_{Lo}$, depends on the orbit, the state of the local ionosphere and the design parameters of the system.

$$\vec{F}_{Lo} = \int_0^L I(l)d\vec{l} \times \vec{B} \tag{1.1}$$

The current can be sustained by the induced voltage, ∅, generated by the relative motion of the tether across the Earth's magnetic field, such that,

$$\Phi = \int_0^L (\vec{v} \times \vec{B})d\vec{l} \tag{1.2}$$

This is the main principle behind the EDT used to de-orbit a satellite.

1.2.2 Importance of the Atmospheric Model

The atmospheric model is important in the analysis of tethered spacecraft system for one main reason. The atmospheric model is used to provide us with the information about the density of the surrounding atmosphere. Though the tethered spacecraft system dwells in

the upper atmosphere (commonly called ‘space’) for most of its lifetime, there is still an atmospheric density present. For a spacecraft without electrodynamic tethers, the drag force is the second most influential force below 700 km (after gravity) [21].

This density is significant because it directly influences the drag force the tethered spacecraft system experiences during de-orbit process [22]. It also directly contributes to the total of perturbative forces acting on the tether [22]. Atmospheric drag is especially important in the prediction of satellite trajectories (such as re-entries and manoeuvres) because of its energy dissipating nature [23]. Additionally, the influence of the atmospheric drag on the de-orbit of towed space debris (using a tether) has been considered by Aslanov and Ledkov [24].

Moreover, the process of the satellite de-orbit by the EDTs is slow. Besides, the design guideline for the end-of-mission satellite de-orbit, which is suggested by the Inter-Agency Space Debris Coordination Committee (IADC) Organization for Standardization and the UN International Telecommunication Union, allows a maximum 25 years for the end-of-mission satellite to lower its altitude to 250 km. Thus, the mission analysis of the satellite de-orbit is sensitive to errors caused by the atmospheric density model.

The atmospheric density in the upper atmosphere varies based on a number of factors such as altitude, latitude [25], time of year, heat from solar radiation and different kinds of ultra-violet radiation and the presence of geo-magnetic activity among other factors. Further, the increase in the concentration of greenhouse gases has affected the atmosphere. While the lower atmosphere is warmed by this increase, the upper atmosphere is cooled instead [26].

Many efforts have been devoted to the development of proper atmospheric density

model based on the satellite observation data and some semi-analytical models. For instance, Clausen et al. [27] analysed the detailed perturbations to the atmospheric density due to the magnetic sub-storms from 2001-2005. The thermosphere makes up the bulk, if not all, of the upper atmosphere that we are interested. The study founds the influence of the magnetic activity is especially noteworthy since it is rather unpredictable. Bruinsma [28] detailed the effect of solar rotation on the atmospheric density and suggested to use the F10.7 solar proxy in the measure of the influence of ultraviolet (UV) radiation on the density. However, in other work by Bruinsma [29], he made another solar proxy, MgII, to account for the influence of extra ultra-violet (EUV) radiation on the atmospheric density. All of these proxies account for the influence of all kinds of solar radiation on the atmospheric density. In a more recent work (2014), radio proxies are being used in the upper atmosphere modelling [30]. These highlights the atmospheric models in the literature are continuously being improved to give us more accurate density values.

The continuous improvement of the atmospheric models, although is very necessary, is imposing challenges to engineers who conduct space mission analysis: (i) what is the impact on the accuracy of residual orbital life prediction of the de-orbit satellite by different atmospheric models and (ii) how often should the atmospheric model be updated in the dynamic model of space tether system in engineering analysis.

Therefore, it is necessary to have an atmospheric model that can account for the multiple factors that affect the atmospheric density. A better estimate of density gives us a better estimate for the drag force on the satellite and the tether as well as the residual orbital life of the space tether system.

1.2.3 Limitations of Existing Treatments of Previous Approaches

The current work is a continuous effort to improve the dynamic modelling codes of EDT system developed by Zhong and Zhu [22, 31-34], who described the dynamics of de-orbiting a nanosatellite with an EDT and developed control law to stabilize the EDT in the satellite de-orbit process. The majority the assumptions in their works are adopted in the current work, such as,

(i) The tether is successfully deployed and remains undamaged throughout the entire de-orbit;

(ii) The tether is not extensible, conductive and bare. The induced current in the tether obeys orbit motion limited (OML) theory;

(iii) The space environmental perturbations include the electrodynamic force, atmospheric drag, Earth's oblateness, lunisolar attraction and solar radiation pressure as outlined by Zhong and Zhu [22]; and

(iv) The optimal current control strategy developed by Zhong and Zhu [32] is used for the stability control of the EDT.

One of the notable aspects of their work is in the atmospheric model used to calculate the drag force on the satellite and tether. All their works made use of the US 1976 Standard Atmosphere [35], which assumes the upper atmospheric density is a function of altitude only. It is noted that the latest models considered other factors that affect the density, such as, solar radiation, geo-magnetic activity, latitude etc. and are more noticeably more accurate than the US 1976 Standard Atmosphere model. However, the US 1976 Standard Atmosphere model is still used in some mission analyses in space engineering due to its simplicity and easy implementation. Thus, the main work of this

thesis is to estimate the induced error in the residual orbital life prediction in the satellite de-orbit process by the grossly simplified atmospheric model in comparison with the latest models.

Another area of the current work is to improve the libration control strategy of the EDT in the satellite de-orbit process. The current method of control (angle control), used in the works of Zhong and Zhu [32], may prove to be inferior to other methods of control (such as energy control). When subject to the Lorentz force, the EDT deviates from the local vertical, an equilibrium position if the current in the EDT is zero. When it deviates too far from the local vertical by exceeding a critical libration angle, the current passing through the tether should be turned off so that no Lorentz force can be generated. This allows the tether to gradually return to its natural equilibrium position, the local vertical, by the gravity. Once below this angle threshold, the current is turned on to once again generate the Lorentz force to lower the altitude of the tether. This is a brief description of the angle control used by Zhong and Zhu [32].

Additionally, we wish to consider the de-orbit of a microsatellite by the EDT whereas the previous works by Zhong and Zhu only considered the de-orbit of a nanosatellite. Furthermore, the IGRF and IRI models used on the previous works of Zhong and Zhu are also updated in the current work.

1.3 Objectives of the Current Research

The objectives of this work are to:

(i) Investigate the state-of-the-art atmospheric models;

(ii) Compare the atmospheric models in use;

(iii) Implement the new atmospheric models into the Simulink model for the space

EDT system;

(iv) Conduct parametric study on microsatellite de-orbit by the EDT with the Simulink model; and

(v) Implement and test the libration energy control in the Simulink model for microsatellite de-orbit by the EDT.

1.4 Method of Approach

The methodology chosen to achieve the above objectives is given as follows. The first step is to conduct a literature review of the relevant topics found in this dissertation. Broadly, these are space tethers, space EDT systems, methods of libration control used in space EDT systems, the upper atmospheric structures and models of the upper atmosphere. The literature review provides us with information about the most recent works that have been done in the modelling of the EDT systems and the upper atmosphere models. From there, we can take steps to further our research.

Following the literature review, we identify appropriate atmospheric models and compare the impact of these models on the orbital life prediction of the EDT systems and their libration control to the previously used atmospheric model - the US 1976 Standard Atmosphere. We then implement these latest upper atmospheric models into our Simulink model of an EDT system with the necessary parameters for a microsatellite proposed by COM DEV [36]. Once implemented, we conduct parametric study on the microsatellite de-orbit by the EDT with different tether length, mass of main satellite and sub-satellite, and different atmospheric models.

The next step in our research is to improve the method of libration control implemented in our simulation codes. Particularly, we study the impact of the libration

energy control on the satellite de-orbit by the EDT system using the cases similar to those mentioned in the previous step.

Finally, we conclude the researches done in this thesis and outline some future study subjects on how to improve the current work.

1.5 Layout of Thesis

This thesis will be laid out using chapters. We first have the introduction in the first chapter that gives us the context for the research that was done. It tells us the motivation for conducting this work and the justification for doing so. In Chapter 2, we have the literature review. In the literature review, we not only go through the information collected during the course of the research but also develop the ideas that will take us to the results and its analysis. Chapter 3 contains comparisons between three atmospheric models in use. Chapter 4 contains a description of the space tether model that we used. It gives a list of the relevant parameters used in our simulations. Chapters 5, 6 and 7 contain the results from the different regimes we considered. Chapter 5 contains results based on our work of doubling of the sub-satellite mass to investigate its effect on the stability of the EDT system in satellite de-orbit. Chapter 6 contains results using a libration angle control strategy and the latest atmospheric models in simulations. Chapter 7 contains results using the libration energy control strategy with the latest atmospheric models. At the end of each of these chapters, we draw the conclusions from the simulation results. The final chapter (8) contains the conclusions drawn from the work done as well as areas of improvement for the current work. It also gives guidelines for future related work.

Chapter 2 LITERATURE REVIEW

2.1 State-of-The-Art of Dynamics of Space Tether Systems

2.1.1 Dynamics of Electrodynamic Tether Systems

The basic idea of the dynamics of space tether systems has been summarized by Dafu et. al. [37]. More specifically, an EDT system uses a conductive tether orbiting in a planet's magnetic field. As the conductive tether across the Earth's magnetic field, it generates a current in the tether. The current-carrying tether passing through the Earth's magnetic field experiences an electrodynamic force (the Lorentz force) that acts perpendicular to the tether to provide propellantless propulsion for spacecraft. This transverse electrodynamic force would change the orbit of the system. Hoyt further modelled the dynamics of an EDT system and its applications in satellite de-orbit [38]. The transverse electrodynamic force will cause the tether bow and swing away from the local vertical. However, as the tether swing away from the local vertical, the gravity gradient forces acting on the tethered satellites will bring the tether back to the local vertical. This results in a pendulum-like motion as shown in Figure 2.1. As EDT system orbiting the Earth, the local magnetic field strength naturally varies as well as the magnitude and direction of the induced electrodynamic force. As such, the EDT system is intrinsically instable due the periodic excitation of electrodynamic force pumping energy into the system.

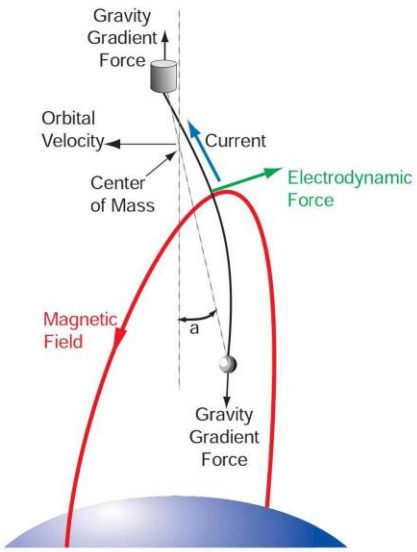

Figure 1. Electrodynamic tether, in drag mode.

Figure 2.1 Schematic of the dynamics of an EDT system in space. [38]

Williams summarised the dynamic motion of space tether systems in the following way: the rigid body in-plane and out-of-plane librational modes, the longitudinal elastic modes and the high-order transverse displacements [1]. Each of these factors has been studied in depth and results have been published in numerous papers on these factors.

Generally, the dynamics of such a system can be separated into two parts: orbital and libration dynamics [22]. The orbital dynamics consider the movement of the centre of mass of the system. Also included in the orbital dynamics are the space environmental perturbations to this system. The perturbations to the system's orbital dynamics include the electrodynamic force, atmospheric drag force, Earth's oblateness, lunisolar attraction and solar radiation pressure. An important note on the tether systems is the tether must be kept taut while in orbit [22]. If the tether is slack in orbit, then the entire system fails.

The dynamic characteristics of a space tether system are affected by several factors [22]:

- the specific application of the space tether system; and
- the mass ratio of the base satellite to the sub-satellite(s).

Depending on the application of the space tether system, some aspects of the dynamics may be more important than others.

2.1.2 Phases of Space Tether Systems

There are three phases in the operation of space tether systems and each of them has their own kind of dynamics. The three phases are:

- the deployment phase
- the station keeping phase
- the retrieval phase

Generally, the tether must be initially stowed inside the base satellite [1]. In the deployment phase, the tether is released from the base satellite into the surrounding atmosphere in a short period of time. Dynamics specific to this phase includes the ejection of the tether at the pre-defined velocity so that it can be deployed safely in a quick and stable manner. Generally, the atmospheric drag and other space environmental perturbation forces are not considered in the dynamics of tether deployment except the primary external load (the Earth's gravity) [39] because of the short duration. Thus, it is outside the scope of the current thesis and the relative research works in the literature are not included here.

The station keeping phase starts once the tether is successfully deployed to the desired length and orbiting the Earth (or whatever object, Jupiter, say). In this phase, the type of model we use for the tether dynamics becomes more important. Williams in 2011 lists five tether models that are used in the literature for the dynamic modelling of space

tether systems. They are:

1. Continuous model that includes tether flexibility and extensibility;
2. Continuous, inextensible but flexible tether model;
3. Discrete lumped mass model that includes tether flexibility and extensibility;
4. Discrete lumped mass model that are flexible but inextensible; and
5. Single link extensible (or inextensible) massless or (massive) models.

In addition, there are other models that are used to describe the dynamics of space tether systems as given by Kristiansen et. al. [40], where a hierarchy of the most common models for space tether systems was provided.

At the top of this hierarchy is the massive tether model. In this model, tether flexibility is accounted for and a partial differential equation is used to model the dynamic motion of the tether. The satellites are considered point masses. Next on the hierarchy is the slack-spring model. This model replaces the tether with a spring that connects the two satellites. This is followed by the dumbbell model where the tethered system is assumed as rigid bar. Despite the deliberate omission of the tether folds and bends in this model, it is still quite popular in current research.

The dumbbell model is widely used in the preliminary design of controllers to control the libration of tether due to its simplicity. The other four models are more used to perform more detailed dynamic analysis of the space tether system [1]. A typical analysis of the system's dynamics in station keeping phase is given by Dafu et. al. [37] where the tether was considered to be continuous and flexible but not extensible. The relevant forces in this model in addition to the primary force the Earth gravity, such as, atmospheric drag and electrodynamic force were included in the system dynamics

because the long-term effects of these space environmental perturbations are not negligible. Different atmospheric models were used in existing works. However, there is no detailed and parametric study in the literature to compare the impact on the dynamic responses of space tether systems using different models and versions of atmospheric density, especially the long-term process of satellite de-orbit using the electrodynamic tether system.

The retrieval phase is far more complicated than the deployment phase because retrieval is inherently unstable. The governing equation of the dynamics of tether retrieval is the same as the dynamics of tether deployment. Therefore, the deployment and retrieval of space tether systems generally studied together. The same as the case of tether deployment, the atmospheric drag is usually not included in the study. Thus, it is outside the scope of the current thesis and the relative research works in the literature are not included here.

2.2 Space Environmental Perturbations to Space Tether Systems

The motion of a spacecraft orbiting the Earth obeys the Newton's law of motion and universal gravitation [41], such that,

$$m_{Sat}\ddot{\mathbf{r}} = \vec{\mathbf{F}}_{\mathbf{Gr}} = -\frac{GM_E m_{Sat}}{r^3}\vec{\mathbf{r}} \tag{2.1}$$

where $\vec{\boldsymbol{F}}_{\boldsymbol{Gr}}$ is the gravitational force acting on the spacecraft, G is the gravitational constant, M_E and m_{Sat} are the masses of the Earth and spacecraft respectively, and r is the distance between the centre of Earth and satellite.

This equation is valid only if the Earth is a perfect sphere and the spacecraft is not

influenced by any other force. In the region of low Earth orbit (LEO), there are other environmental forces that influence the motion of the spacecraft, although they are generally much smaller than the gravitational force. In other words, the other forces are perturbation forces, i.e., they are orders of magnitude smaller than the gravitational force. Nevertheless, they do influence the motion of a spacecraft, especially in long-term, and need to be studied.

A space tether system is effectively a satellite with a tether attached to it. Therefore, most of the perturbation forces that influence a satellite's motion will also influence a space tether system's motion. The main perturbation forces that are relevant to the EDT systems can be listed as follows [22] [41]:

- The atmospheric drag;
- The electrodynamic force;
- The oblateness of the Earth; and
- The gravitational attraction of the Sun and the Moon (lunisolar attraction)

In the current work, we focus on the influence of atmospheric models on the de-orbit dynamics of the EDT system. Thus, the models for the other space environmental perturbations used in the work of Zhong and Zhu [22] are adopted except the atmospheric drag.

2.2.1 Atmospheric Drag

The atmospheric drag F_D exerted on a spacecraft is generally given as [41] [42]

$$F_D = \frac{1}{2} \rho v_{obj}^2 C_D A \tag{2.2}$$

where ρ is the atmospheric density, v_{obj} is the orbiting velocity of the tether system with respect to the atmosphere, A is the cross-sectional area of the tether normal to the velocity, and C_D is the drag coefficient. The drag coefficient is shape dependent. For instance, $C_D = 2.2$ is used for a tether with circular cross-section and $C_D = 1.6$ for a cubic shaped satellite.

The critical component in the atmospheric drag is the density of atmosphere. This is because the atmospheric drag is directly dependent on the density [43]. Most models of the atmosphere are either empirical or semi-empirical. These models have been adjusted or calibrated using voluminous amounts of satellite observation data or from observations of satellites undergoing orbital decay. In addition, Mehta [44] described the recent development about the physics-based models of the atmosphere thanks to the rapid increase in computing power. These models solve the equations that govern the thermal, electromagnetic, chemical and flow dynamics of different regions of the atmosphere [21].

There are a plethora of semi-empirical models for the atmosphere. Vallado and Finkleman [45] provided a comprehensive list of the models as well as the subsequent evolutions (and predecessors) of these models, see Fig. 2.2. From this comprehensive list of atmosphere models, one can find the models that are most popular today, such as those from the work of Doornbos [46]. The four main groups for the atmosphere models are as follows:

- The Jacchia models
- The Drag Temperature Models (DTM) [47]
- The Horizontal Wind Models (HWM)
- The Mass Spectrometer and Incoherent Scatter (MSIS) Models [47]

We will review each group in turn and identify their main characteristics, particularly, the most recent evolution from each of these groups.

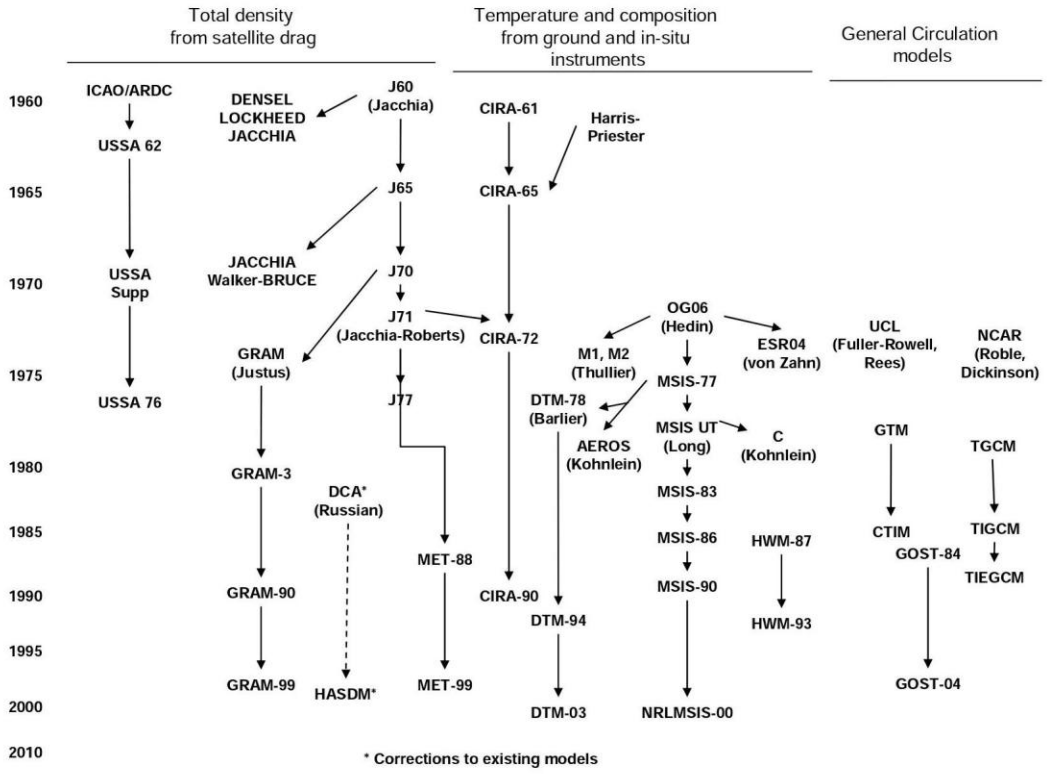

Figure 2.2 The development of various atmospheric models in the literature [45].

2.3 Jacchia Atmospheric Model

Jacchia atmospheric model is an atmospheric model that defines values for density and other properties at altitudes from 90 to 2500 km. It is semi-empirical and is mainly based on satellite drag database. Some of the equations used in this model are derived from data collected by observations of satellite drag and rocket measurements.The Jacchia model includes effects of latitudinal, seasonal, geomagnetic, and solar effects. The model is primarily used in the dynamic modelling of spacecraft.

2.3.1 Jacchia Model, 1965

The first model of Jacchia is called Jacchia 65 or J65 [48] [49]. Generally, J65 is a static diffusion model, i.e., Jacchia assumed that the atmosphere was in diffusive equilibrium at all times. Montenbruck and Gill [41] pointed out that this model is based only on the primary parameters of geodetic height and temperature. The J65 employs two steps to calculate the density of the upper atmosphere (from 120 km to the exosphere):

- Find a temperature profile for the atmospheric constituent under scrutiny; and
- Integrate the diffusion equation for the given atmospheric constituent with this profile.

The first step is to find a temperature profile for the desired atmospheric constituent. Early work in finding a temperature profile for the atmosphere was done by Jacchia [50] in the 1950s. As time passed, he refined his initial work and created a temperature profile suitable for use in his first major model of the atmosphere. In this static diffusion model, Jacchia [49] considered the main atmospheric constituents to be nitrogen, oxygen, atomic oxygen and helium.

Each of these constituents has their own temperature profile throughout the entire atmosphere and need to be calculated separately. This is because the constituents are not thoroughly mixed in the heterosphere. According to CIRA-2012 [51], the heterosphere is defined as the portion of the atmosphere that begins at approximately 125 km where diffusive separation of species dominates and atmospheric composition depends on height as shown in Fig. 2.3 [41].

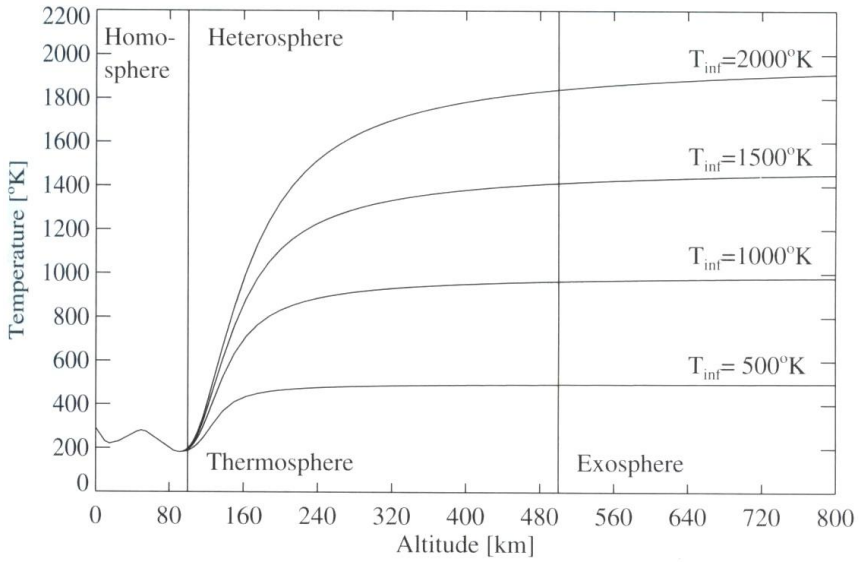

Figure 2.3 Temperature stratification in the atmosphere with respect to altitude [41].

Jacchia [49] noted that the temperature profiles can be represented by the following empirical equation derived from the work of Harris, Priester and Nicolet [52], such that,

$$T(z) = T_\infty - (T_\infty - T_{120})e^{-s(z-120)} \tag{2.3}$$

with

$$s = 0.0291 \cdot e^{x^2/2} \quad \text{and} \quad x = \frac{T_\infty - 800}{750 + 1.722 \times 10^{-4}(T_\infty - 800)^2} \tag{2.4}$$

where T_∞ is the exospheric temperature, T_{120} is the temperature at 120 km, z is the altitude in kilometres, and s is a constant that depends on the specific atmospheric constituent.

Once the temperature profile is determined, it is used to numerically solve the diffusion equation with the appropriate boundary conditions, such that,

$$\frac{1}{n_i}\frac{dn_i}{dz} = -\frac{1}{H_i} - \frac{1}{T}\frac{dT}{dz}(1+\alpha_i) \tag{2.5}$$

where T is the temperature, n_i is the density of the i^{th} constituent, α_i is the thermal diffusion factor for the i^{th} constituent, $H_i = kT/m_i g$ is the scale height that is defined as the distance over which the concentration of the particular atmospheric constituent decreases by a factor of e, k is the Boltzmann constant, m_i is the molecular mass of the constituent, and g is the acceleration due to gravity.

The boundary conditions for the diffusion equation at z = 120 km are given as,

$$\left.\begin{array}{ll} T & = 335K \\ n(N_2) & = 4.0 \times 10^{11} \\ n(O_2) & = 7.5 \times 10^{10} \\ n(O) & = 7.6 \times 10^{10} \\ n(He) & = 3.4 \times 10^{7} \end{array}\right\} \quad (2.7)$$

Furthermore, there is an additional boundary condition for hydrogen to account for a change in its distribution above 500 km, such that,

$$\log_{10} n(H)_{500} = 73.13 - 39.40 \log_{10} T_\infty + 5.5(\log_{10} T_\infty)^2 \quad (2.6)$$

where $n(H)_{500}$ is the density of hydrogen at the altitude of 500 km.

The calculation of T_∞ was not discussed in the Jacchia's original work [49]. However, it includes a number of corrections to the exospheric temperature. The corrections considered were the influence of the solar cycle, of one solar rotation, of the diurnal variation and of the variation due to geomagnetic activity. The associated equations for these variations can be found in Jacchia's paper [49]. These equations make use of solar and geomagnetic indices that have been calculated from satellite data. For example, the $F_{10.7}$ solar proxy or solar flux is used in some of the corrections to the

exospheric temperature. This index is a measure of the solar radio flux at a wavelength of 10.7 cm.

The subsequent models in the Jacchia family are all based on this first model. These descendants make use of new solar indices, new geomagnetic indices, and different equations to model the corrections to exospheric and account for recently discovered phenomenon among other changes.

2.3.2 Jacchia Model, 1971

The Jacchia model was released in 1971 and is called J71 in the literature. It is a modification of the J65 model [44] [53], in which the lower boundary was lowered to 90 km from 120 km in the J65 model. J71 assumes that the atmosphere is properly mixed up to 105 km; beyond this altitude is the heterosphere. In addition, this model makes use of the analysis conducted on satellite accelerations due to drag [41].

Among all the changes to the variations that influence the exospheric temperature, two were most notable. A new seasonal-latitudinal variation was added for all constituents in the lower thermosphere (90 - 170 km) and an additional variation for the winter helium bulge was added in the J71 model.

Jacchia's paper [53] provided readers with an example of how to use the model he had developed and corresponding algorithm was presented in Doornbos' book [46].

2.3.3 Altered Versions of Jacchia Model

It was around 1971 that slightly altered versions of Jacchia's model started to appear. Often, these slightly altered versions were created in an effort to reduce the computational time needed to run the Jacchia's model. The bulk of the computational

time in the Jacchia's model was in the numerical integration of the diffusion equation.

An example of such an altered version of Jacchia's model is the Jacchia-Lineberry model [54] that was used by the North American Space Agency (NASA). The Jacchia-Lineberry model closely follows the J71 model with one major change. Lineberry assumed that the logarithm of the density may be expressed as a truncated Laurent series in temperature and altitude, in order to reduce the computational time of the J71 model.

There are a few other models that are slightly altered versions of the J71 model. However, none of them produced results that were significantly more accurate than the original J71 model [41]. The reduction in computational time did not compensate enough for the less accurate results from the slightly altered models and, so, the J71 model was the best of its time.

Analytic versions of Jacchia's model were also created following the release of his model in 1971 [55].

2.3.4 Jacchia-Bowman 2006 Model

The Jacchia-Bowman 2006 model for the upper atmosphere was developed in 2006 (JB2006). It was constructed using J71 as its foundation. Bowman et. al. [56] compared this model with other similar models and found the JB2006model is significantly more accurate than its contemporaries.

Among the changes made was the use of more solar indices in the equation that calculates T_C. These new solar indices account for the heating of the atmosphere that occurs through EUV radiation and far ultra-violet radiation (FUV), which provides us a more complete picture of the heating in the atmosphere. These indices are based on the observed phenomenon and validated from data collected by satellites. They were first

tested and validated in the JB2006 model [57].

Also, the equation modelling the semi-annual variation has been improved by the introduction of Fourier series. Another significant change is the introduction of density correction factors that improve the accuracy between 100 km and 400 km. Bowman et. al.'s paper [56] is quoted as having standard deviations of 10% at 400 km for JB2006. This is lower than the 16% obtained from the J70 model at the same height (the J70 and J71 model are very similar).

2.3.5 Jacchia-Bowman 2008 Model

Jacchia-Bowman 2008 model (JB2008) is the most recent that have descended from Jacchia's work in the 1960s. It is simply a revised edition of its immediate predecessor, JB2006 model. The major change in this model is the use of a new geomagnetic index that improves the accuracy especially during geomagnetic storms [51]. This model is the one we have used in the thesis. The model is coded in FORTRAN and the source codes are available online from http://sol.spacenvironment.net/~jb2008/code.html.

According to CIRA-2012 [51], JB2008model describes the neutral temperature and density in the Earth's thermosphere and exosphere. The valid range for this model is between 120~2,500km. This model uses four solar indices and two geomagnetic activity indices that have been derived from the data of weather satellites.

In the work by Bowman et. al. [58], the density data used in the JB2008 model was collected from four different sources. They are

- US Air Force daily density values from 1997 to 2007;
- US Air Force High Accuracy Satellite Drag Model (HASDM) density values

from 2001 to 2005;

- Challenging Mini-satellite Payload (CHAMP) accelerometer density values from 2001 to 2005; and
- Gravity Recovery and Climate Experiment (GRACE) accelerometer density values from 2002 to 2005.

In addition, there are two new features that make JB2008 model different to its predecessors. First, it accounts for the semi-annual variation of atmospheric density, which was discovered in 1961. Second, it adopts new formulations for the solar indices that are derived from more realistic relationships between the dependence of heat and energy inputs from solar radiation to specific altitude regions and the heating processes within the upper atmosphere.

From Bowman's work [58], there are a few conclusions that are noteworthy. First, there is a great reduction in the density errors compared to previous models, especially during major geomagnetic storms. Second, the use of the new global exospheric equations greatly improves the density modelling, especially at solar minimums.

The algorithm of the JB2008 model is available for free download at http://sol.spacenvironment.net/~jb2008/code.html.

Finally, the CIRA-2012 [51] also provides a quantifiable measure of the accuracy of the JB2008 model. For mean conditions, the estimated standard uncertainty of the total density within the atmosphere is of the order of 10%. This number also depends on altitude. However, in extreme conditions i.e. high solar or geomagnetic activity, this uncertainty increases dramatically to approximately 100%.

2.4 Mass Spectrometer and Incoherent Scatter Model

The mass spectrometer and incoherent scatter (MSIS) model is an empirical model of neutral temperature and composition of the upper atmosphere (above 90km). This class of models was published in several papers by Hedin [59]. It is based on the in-situ mass spectrometer data from various satellites and sounding rockets (in space) and ground-based incoherent scatter radar data [41].

The first MSIS model (MSIS-77) was published in 1977 [59] [60]. The increase in availability of data brought several upgrades to this model in 1983 [61] (MSIS-83) and in 1986 (MSIS-86). MSIS-86 model was adopted by COSPAR to be the CIRA 1986 reference model. MSIS-86 model is relatively complex because it requires more computational time than its contemporaries. It makes use of over 850 coefficients to evaluate atmospheric density and other constituents. Hedin also created MSISE-90 model [62] in 1990, which is an extension of MSIS-86 into the middle and lower atmosphere [62].

The last model in this series is the Naval Research Laboratory Mass Spectrometer Incoherent Scatter Radar Extended Model released in 2000, which we will discuss below.

2.4.1 Naval Research Laboratory Mass Spectrometer Incoherent Scatter Radar Extended Model

The Naval Research Laboratory Mass Spectrometer Incoherent Scatter Radar Extended Model (NRLMSISE-00) is the most recent addition to the MSIS class of models [63]. It calculates the neutral temperature, composition and total mass density of the upper atmosphere and is valid from the ground to the exosphere.

The CIRA-2012 further goes on to state that the NRLMSISE-00 model has been extensively tested within the international scientific community and is currently accepted as a sufficiently robust model in engineering applications and the standard for international space research [64]. In addition, the NRLMSISE-00 model has a flexible mathematical background. The NRLMSISE-00 can be found and used in MATLAB's Aerospace Toolbox.

2.5 Drag Temperature Models

The purpose of this section is to briefly describe the first DTM model so that we could compare with the early Jacchia models. In particular, we show here that the DTM uses spherical harmonics for the exospheric temperature and for each main atmospheric constituent whereas Jacchia does not. Additionally, this model incorporates data from mass spectrometer measurements, optical measurements and incoherent scatter sounders.

2.5.1 DTM-78

The first Drag Temperature Model (DTM) came from Barlier et al. [65] [41] [46] in 1978. This model, DTM-78, was based on total density data that came from observations of satellite drag. It used a more general model than its contemporaries. The total density was obtained by integrating the diffusion equation with an empirical temperature profile. However, this model was considerably less accurate to its Jacchia contemporary at the time. Like all atmospheric models, the DTM-78 begins with some fundamental assumptions. First, Barlier et al. [65] recognized that diffusive separation occurs above 100km altitude with molecular nitrogen (N_2), atomic oxygen (O), and helium (He) being more plentiful as altitude increased. It made use of a popular expression for temperature

in terms of altitude (which was also used in Jacchia's work) that was suggested by Walker [55], such that,

$$T(z) = T_\infty - (T_\infty - T_{120})e^{(-\sigma\varphi)} \tag{2.7}$$

$$\varphi = \frac{(z-120)(R_E+120)}{R_E+z} \tag{2.8}$$

$$\sigma = s + (R_E+120)^{-1} \tag{2.9}$$

where T_∞ is the thermopause (region between thermosphere and exosphere) temperature, T_{120} is the temperature at 120km altitude (the lower boundary), φ is the geo-potential altitude, R is the radius of the Earth (in km), σ is a quantity related to the temperature gradient parameter s.

Furthermore, the DTM-78 assumes constant values for s and T_{120}, which are 0.02 and 380 K, respectively. In addition, DTM-78 uses the model given by Thuillier et al. [66] for T_∞ and makes a special accommodation for the amount of molecular oxygen (O_2) and atomic hydrogen (H).

The significant difference between the DTM and the Jacchia's series of models is the density of each atmospheric constituent (N_2, O, He) in the DTM is expanded in terms of spherical harmonics, such that,

$$n_i(z) = A_{1i}e^{[G_i(L)-1]}f_i(z) \tag{2.10}$$

The function $f_i(z)$ results from the integration of a diffusive equilibrium distribution with the temperature profile given by the Walker's equation above, such that,

$$f_i(z) = \left(\frac{1 - a}{1 - ae^{sf}} \right)^{1+a_i+g_i e^{[-sg_i f]}} \tag{2.11}$$

where $a = (T_\infty - T_{120})/T_\infty$, $\frac{m_i g_{120}}{\sigma k T_\infty}$, α_i is the thermal diffusion factor (equal to -0.38 for He and 0 for N_2 and O), m_i is the molecular mass of each constituent, *k* is the Boltzmann constant, g_{120} is the acceleration due to gravity at 120 km, A_{1i} is a constant, $G_i(L)$ are functions in the developments in spherical harmonics that depend on the local time, *t*, the co-latitude and the day count in the year, *d*, the daily 10.7 cm solar flux measured at day, *d*-1 is the average flux over three solar rotations centred on the day, *d* and the three hour planetary index taken three hours before time, *t*. The aforementioned spherical harmonics is a modification of those previously formulated by Hedin et. al. [67]

Barlier et al. [65] further elaborated the functions that use spherical harmonics and also discussed some geophysical characteristics of the model. These include the solar activity effect, geomagnetic activity, daily variations and annual variations.

The significant update to DTM-78 was done in 1994 by Berger et. al. [68] who used an extended dataset gathered from various satellites. Further work was done on this model in 2000 [66] when a new solar proxy, Mg II [29], was introduced along with more data from the CHAMP accelerometer.

The next update was done in 2009. The DTM-2009 model [69] describes the neutral temperature and most of the species densities in the atmosphere between 120 km and 1500 km. CIRA-2012 states that this model is based on essentially the same data that the NRLMSISE-00 was based on. The source code for this model can be found online at atmop.eu. The model itself was developed and is maintained by Centre national

d'étudesspatiales (CNES), a French space agency.

Though CIRA-2012 states that the DTM-2009 model is the most recent, ATMOP disagrees. They have released a more recent version in 2012. This DTM-2012 makes uses of more accurate solar indices to improve the accuracy of their model. Further, DTM-2012 is the first step in a two-step plan by CNES to produce a superior model. CNES has released a newer model in the fall of 2013, which has new geomagnetic indices and assimilates new data that will further improve the model's accuracy.

The DTM-2013 model makes the use of a new solar proxy, F-30, that replaces the usual F-10.7 and makes the use of 2.5 years of measurements at 270km from the Gravity Field and Steady-State Ocean Circulation Explorer (GOCE) satellite. In a preliminary report by Bruinsma [70] [71], it was concluded that, of the most recent models discussed above (JB2008, NRLMSISE-00, DTM-2009 and DTM-2012), the DTM-2013 is the most accurate model in the altitude ranging from 270km to 1000km. Accordingly, we will use the codes for DTM-2013 in our analysis.

ATMOP's website provides the source code for DTM-2009, DTM-2012 and DTM-2013 to registered users (registration is free). The website also allows users to run the models online if given a set of input.

2.6 Horizontal Wind Models

The Horizontal Wind Model (HWM) is based on gradient winds from CIRA- 86 plus rocket soundings, incoherent scatter radar, MF radar and meteor radar data. It accepts the same input as the MSIS series of density models and return zonal and meridional wind speeds. Further development of the HWM model is now also continued at the Naval

Research Lab. The latest edition is HWM07 [51].

2.7 The US 1976 Standard Atmosphere

The US 1976 Standard Atmosphere is the atmospheric model that was used in the simulations of the space tether system that we discuss later. It is an idealised, steady-state representation of the Earth's atmosphere from the surface to 1000 km [35] as stated in the handbook associated with this model. The key point of this model is that it is entirely height dependent. The density given by this model only takes into account the height above the Earth's surface. The sole height-dependence of this model was the area of concern that motivated this research. We sought to find atmospheric models that accounted for other variables in the atmosphere (which would ultimately be a more accurate atmospheric model) to improve the prediction of orbital life of a space tether system by our dynamic simulation codes of space tether system. Throughout this thesis, we refer to this model either by its name (US 1976 Standard Atmosphere) or as the 'old (atmospheric) model'.

2.8 Outstanding Issues and Limitations of Atmosphere Models

The atmosphere models listed above are subject to some common limitations. The behaviour of the upper atmosphere is complex by nature [51] and is influenced by many variables. While some of these variables are deterministic, others remain more unpredictable. For example, it is not currently possible to make predictions in the lower atmosphere (below the thermosphere) past 3 - 5 days. These conditions do affect the composition of the atmosphere and make modelling it accurately more difficult. Chapter 5 of CIRA-2012 [51] gives some insight into the outstanding issues concerning the

atmosphere models.

In the subsequent Chapters, we will investigate the impact of different atmospheric models, namely the DTM-2013 model and the JB2008 model, on the dynamic prediction of space tether systems. In our current model of a space tether system, we use the US 1976 Standard Atmosphere model that describes the atmospheric drag changes only in altitude. The JB2008 and DTM-2013 both account for other factors (such as diurnal variations) and claim to be more accurate models than the one currently used. We will determine if the newer models will significantly change the output from our model of a space tether system in comparison with the US 1976 Standard Atmosphere model.

In this thesis, we will not consider the latest models from the MSIS and HWM groups. This is because these two do not accommodate for as many variations in the density of the thermosphere as the two (JB2008 and DTM-2013) we wish to consider. Also, we are seeking to find the most advanced model for the density and this hampers the choice of the candidates from the MSIS and HWM groups. In addition, we are not concerned with the influence of winds in the thermosphere and, so, the HWM group models become even less important.

2.9 Methods of Libration Control of Space Tether System

The first method that we discuss is the angle control. An example of this kind of control is given by Williams [72]. He describes the state of the electrodynamic tether system using the in-plane (pitch) and out-of-plane (roll) angles of the tether together with their rates of change. The state makes up part of a cost function that is to be minimised using time-delayed predictive control. The time-delayed predictive control estimates the state of the system at some future time and forces the system to achieve that future state from

its initial state. Another example of the angle control is given by Zhao et. al. [73]. In their paper, they used a linear-quadratic regulator to damp the libration angle when it becomes too large. This stabilises the libration attitude of the space tether system.

Another method is to control the libration energy. In this method, the libration energy is expressed in a Hamiltonian function and subjected to some upper bound (threshold) for the energy. If this upper bound is exceeded, the space tether system is prone to tumbling. The simplest method of control for the electrodynamic tether is to remove the current from the tether once the threshold has been exceeded since the electrodynamic force is the source of instability. Once the libration energy drops below the threshold, the current is turned on to flow through the tether once more to allow the de-orbit to continue. This method of control is described by Tortora et. al. [74] and by Corsi and Iess [75]. This is also the method of control that we added to our Simulink model as an alternative to our previous method of control, which is the angle control.

2.10 Comparison of the Atmospheric Density Models

2.10.1 Comparison of Mean Density

The current work seeks to use the new atmospheric models in applications of space tether systems. In particular, we wish to determine whether the new atmospheric models significantly alter the results obtained from simulations of the space tether system that use an older atmosphere model. However, before we investigate the results from the simulations of the space tether system, we will make some remarks about the atmosphere models in concern: the JB2008 model, the DTM 2013 model and the US 1976 Standard Atmosphere model that was used in our simulation codes of the space tether system.

We used these models to get atmospheric density values between 200 km and 1000 km, where the majority of space debris resides. Also, we are only interested in the space tether system's de-orbit until 250 km. To properly compare the densities, we fixed the day, time and location before generating the density profile from each model. The fixed day, time and location is midnight on January 1st, 2011 at 90^{0} N latitude and 0^{0} longitude, i.e., January 1st at 12:00 am. Below are graphs that illustrate the density profile as given by the JB2008 model, the DTM-2013 model and the US 1976 Standard Atmosphere. Note that the US 1976 Standard Atmosphere is solely height dependent, i.e. it does not account for latitude, longitude etc.

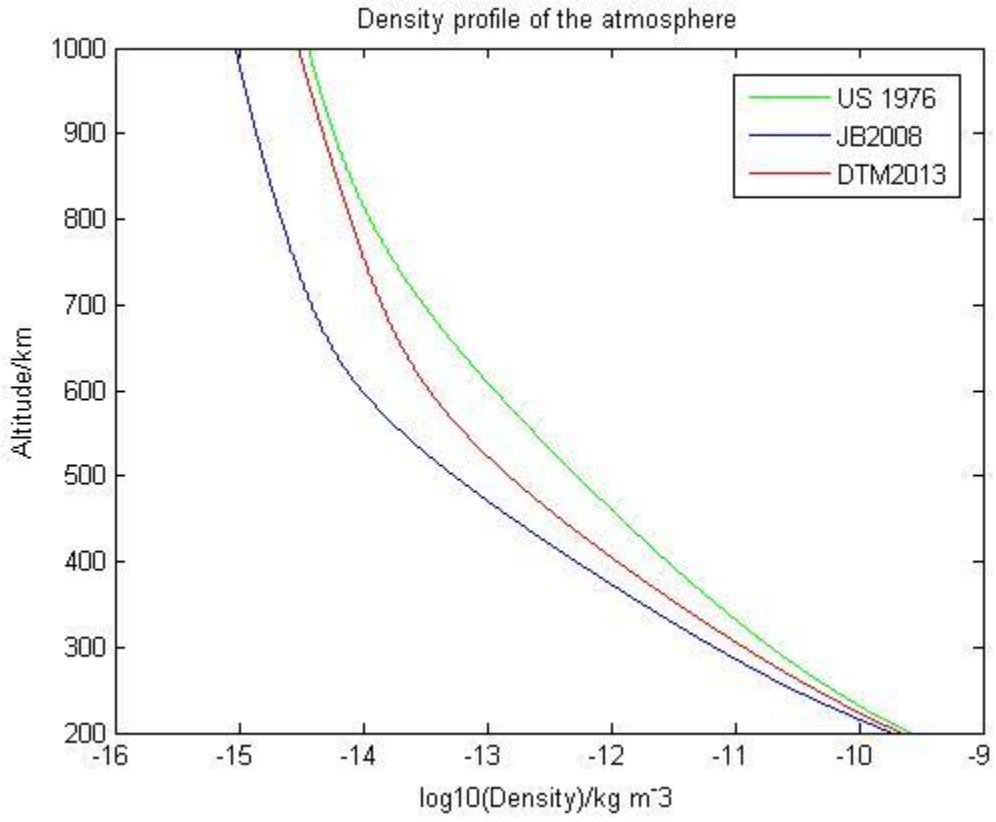

Figure 2.4 The comparison of the mean density of the atmospheric models.

The density values of DTM-2013, JB2008 and US 1976 Standard Atmosphere models

shown in Fig. 2.4 were calculated by taking an average of the densities at each height increment (the height intervals were 10m each) on the aforementioned day. This also proves useful for our space tether simulation since, for some simulations, the time extends past the capacity of both new atmospheric models. As such, we chose to adopt an average of the atmospheric densities for those cases.

We compare the mean density values of the three atmospheric models in an attempt to highlight the differences between the models. Again, we only use the densities between 200 km and 1000 km because this is our region of interest.

The mean densities of the US 1976 Standard Atmosphere, JB2008 and DTM-2013 (within the given range) are 1.1649×10^{-11} kg m^{-3}, 7.2950×10^{-12} kg m^{-3} and 7.3825×10^{-12} kg m^{-3}, respectively. It is obvious from the numbers that the newer atmospheric models predict densities that are lower than that given by the US 1976 Standard Atmosphere. It is also evident that the newer atmospheric models are in close agreement with each other.

2.10.2 Comparison with Actual Data

Unfortunately, there appears to be no official statement of how accurate these models are when compared to the actual densities found in the atmosphere. Instead, there is an evaluation report [34] that makes numerous comparisons between the JB2008 model, the DTM-2013 model and data from various satellites. However, the papers that document these models do say that the models have been developed using the densities that have been observed by satellites. In addition, they also mention that they have improved the accuracy of their models with each subsequent model update.

Chapter 3 DYNAMIC SIMULATION OF SPACE TETHER DE-ORBIT

3.1 Description of the Simulation Codes of Space Tether System

The model that we use for the simulation of the space tether system was written in MATLAB. More specifically, it is a series of Simulink models within MATLAB that was constructed originally by Dr. Rui Zhong [22]. The Simulink models essentially describe the complete de-orbit process of the space tether system from the given starting altitude until the system reaches the 250 km altitude. The Simulink models output various important quantities associated with the space tether system such as altitude, semi-major axis (and other orbital elements), magnitude of the Lorentz force, pitch and roll angles and other useful quantities. The models have been used to generate results that have been published by several journals so far. In this work, we added the latest atmospheric models into the codes. Furthermore, we improved and updated its implementation of the Earth's magnetic field by making use of the most recent International Geomagnetic Reference Field (IGRF). Its implementation of the Earth's ionosphere was also revised using the most recent International Reference Ionosphere (IRI) model.

Another notable modification to the original Simulink model is the addition of libration energy control strategy. The libration control strategy implemented in the original codes is the maximum libration control. In this case, the maximum of libration

angles is limited to 15 degrees (0.26 rad). Should the upper bound be breached, the current in the tether was turned off allowing the libration angles to return below the upper bound under the combination of gravity field and dissipative perturbation forces such as the atmospheric force. Once the libration angles are less than the upper bound, the current is turned on to de-orbit the tether again. The libration energy control strategy does not control the angle directly. Instead, it controls the libration energy of the system. The comparisons between two control strategies are conducted and the results are presented in the thesis.

The chosen model outputs various .mat files during each simulation. These .mat files record different kinds of information about the tether system as it de-orbits, i.e. for every time step. These include its altitude, its pitch and roll angle, its semi-major axis, the eccentricity of the orbit, the magnitude of the Lorentz force, the current in the tether and the torque due to the Lorentz force among other useful quantities. Should we include the libration energy control strategy in the Simulink model, we output similar useful quantities with the addition information viz. the libration energy.

3.1.1 Orbital dynamics equations

The orbital dynamic equations can be expressed in two ways. We first establish the co-ordinate system used in either of these two descriptions. We assume a geocentric inertial frame of Earth with the origin at the Earth's centre, the x-axis points to vernal equinox, the z-axis is in the direction of Earth's rotation axis and the y-axis is perpendicular to both aforementioned axes [33].

If we consider a space tether system as made up of two masses, m_1 and m_2 (representing the main satellite mass and the sub-satellite mass), then the two body

problem of a de-orbiting space tether system subject to perturbations can be written as

$$\ddot{\vec{\mathbf{r}}} = -\frac{\mu}{\left|\vec{\mathbf{r}}\right|^3}\vec{\mathbf{r}} + \vec{\mathbf{F}} \tag{3.1}$$

where $\vec{\mathbf{r}} = \vec{\mathbf{r}}(x, y, z)$ is the position vector, μ is the gravitational parameter of the Earth and $\vec{\mathbf{F}}$ is the perturbation force vector acting on the space tether system. Equation 3.1 is non-linear and, as such, presents challenges to solve using numerical methods.

The second description of the orbital dynamics employs the Gaussian perturbation equations [81]. The Gaussian perturbation equations use the orbital elements to describe the orbital dynamics of the space tether systems. The six orbital elements are sufficient to uniquely identify the specific orbit of any object in space and are eccentricity, e, semi-major axis, a, inclination, i, longitude of the ascending node, Ω, argument of periapsis, ω and mean anomaly, M. The Gaussian perturbation equations take the form shown below.

$$\frac{d\upsilon_j}{dt} = f(\upsilon_1, \upsilon_2, \upsilon_3, \upsilon_4, \upsilon_5, \upsilon_6, T, S, W) \tag{3.2}$$

In Eq. (3.2), $\upsilon_j, (j = 1..6)$ are the orbital elements, T, S, W are the three orthogonal perturbation force components in the orbital frame previously described [33]. T is in the radial direction, S is in the direction of satellite motion and W is perpendicular to them both. We use this description of orbital dynamics in our simulations because 5 out of 6 orbital elements are constant in the two-body problem and because using the orbital elements provides less numerical issues than with the Cartesian co-ordinate system.

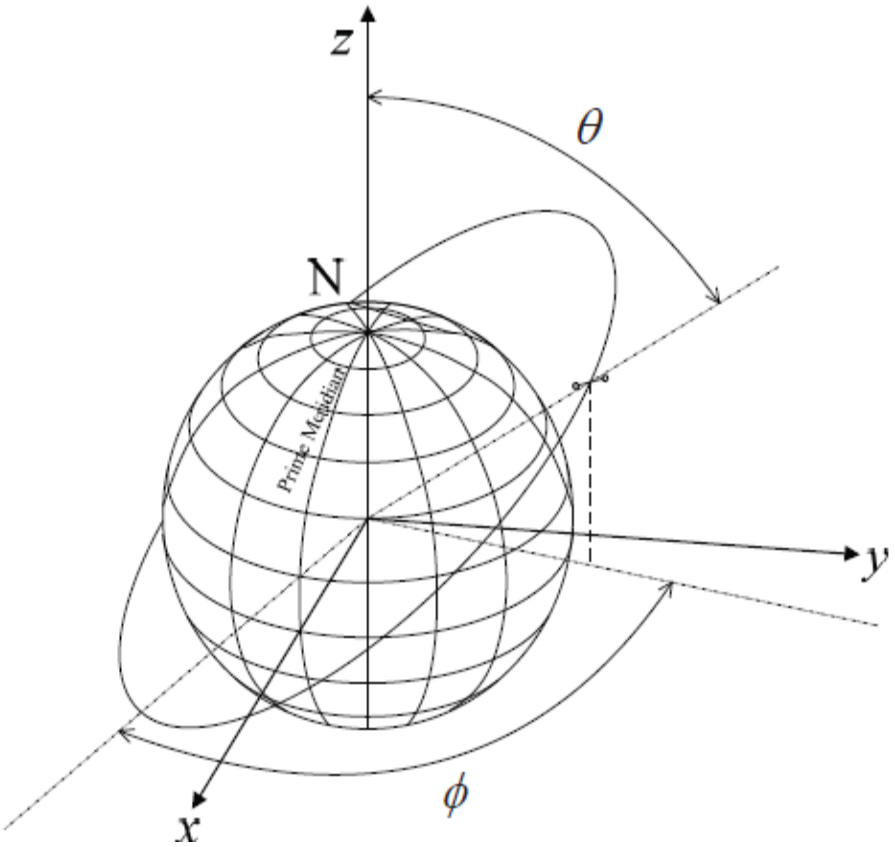

Figure 3.1 The co-ordinate system used in the description of the space tether system

We now give a more detailed description of the Gaussian perturbations equations shown in Eq. (3.3) ~ (3.8) below [34].

$$\frac{da}{dt} = \frac{2}{n\sqrt{1-e^2}}\left(Te\sin f + S\frac{p}{r}\right) \tag{3.3}$$

$$\frac{d\Omega}{dt} = \frac{Wr\sin u}{na^2\sqrt{1-e^2}\,\sin i} \tag{3.4}$$

$$\frac{di}{dt} = \frac{Wr\cos u}{na^2\sqrt{1-e^2}} \tag{3.5}$$

$$\frac{de_x}{dt} = \frac{\sqrt{1-e^2}}{na}\left\{T\sin u + S\left[\left(1+\frac{r}{p}\right)\cos u + \frac{r}{p}e_x\right]\right\} + \frac{d\Omega}{dt}e_y\cos i \tag{3.6}$$

$$\frac{de_y}{dt} = \frac{\sqrt{1-e^2}}{na}\left\{-T\cos u + S\left[\left(1+\frac{r}{p}\right)\sin u + \frac{r}{p}e_y\right]\right\} - \frac{d\Omega}{dt}e_x\cos i \tag{3.7}$$

$$\frac{d\eta}{dt} = n - \frac{1}{na}\left[\begin{array}{l} T\left(\frac{2r}{a} + \frac{\sqrt{1-e^2}}{1+\sqrt{1-e^2}}e\cos f\right) \\ -S\left(1+\frac{r}{p}\right)\frac{\sqrt{1-e^2}}{1+\sqrt{1-e^2}}e\sin f \end{array}\right] - \frac{Wr\cos i\sin u}{na^2\sqrt{1-e^2}\sin i} \tag{3.8}$$

Equations (3.3) ~ (3.8) contain the mean orbital angular rate, n, the true anomaly of the orbit, f, the semilatus rectum of the orbit, p, the geocentric radius of the space tether system, r and $e_x = e\cos\omega, e_y = e\sin\omega, \eta = M + \omega$.

We replace the classical orbital elements with e_x, e_y, η respectively to avoid computational errors in near circular orbits i.e. when e is close to zero.

3.1.2 Perturbation Forces on the Orbital Dynamics

Various orbital perturbation effects induce the perturbation force components T, S, W previously mentioned. The perturbative forces considered in our simulations are (i) the electrodynamic force on the current-carrying tether, (ii) the aerodynamic drag, (iii) the oblateness of the Earth, (iv) forces from third bodies viz. the sun and the moon, (v) solar radiation pressure, and (vi) spacecraft thrust (if present) [33]. We will discuss the electrodynamic force, the aerodynamic force and the oblateness individually below. The remaining perturbation forces are not considered in the simulation because their effects are negligible for our purposes.

3.1.2.1 Electrodynamic Drag

In our consideration of electrodynamic drag, we assume that the tether has been fully

deployed, is kept taut pointing vertically downwards due to gravity and undergoes no libration. When the tether crosses the Earth's magnetic field with some velocity (due to the satellite's motion), an electromotive force, E_m, is generated along the length of tether given by [33]

$$E_m = \frac{dV_p}{ds} = \left(\vec{\mathbf{v}} \times \vec{\mathbf{B}}\right) \cdot \vec{\mathbf{l}} \tag{3.9}$$

Equation (3.9) contains the induced voltage, V_p, the local co-ordinate along the tether, s, the velocity vector of the tether with respect to the Earth's magnetic field, $\vec{\mathbf{v}}$, Earth's local magnetic field strength, $\vec{\mathbf{B}}$, and the unit vector along the tether, $\vec{\mathbf{l}}$.

We updated the Earth's magnetic field in Zhong's codes to the IGRF-10 model from the IGRF2000 model. We maintained the same Legendre polynomials that he used to describe the magnetic field components in the three directions [33].

The resultant electromotive force will cause one end of the tether to be slightly positively charged and the other end to be slightly negatively charged. The positively charged end will attract the electrons from the surrounding ambient plasma while the negatively charged end will attract the positively charged ions from the surrounding plasma. This results in a current across the tether provided there is an appropriate emitting device at each end of the tether to complete a current loop.

The potential in the tether is dependent on the current because of its dependence on ohmic loss. Consequently, we can write the relationship between potential and current as

$$\frac{d\Delta V}{ds} = \frac{I}{\sigma A} - E_m \tag{3.10}$$

Equation (3.10) contains the conductivity of the tether, σ and the cross-sectional area

of the tether, A.

Now, the induced current in the tether will interact with the Earth's magnetic field to generate a Lorentz force, $\vec{\mathbf{F}}_B$, on the tether as follows

$$d\vec{\mathbf{F}}_B = -\vec{\mathbf{B}} \times I(s)\vec{\mathbf{l}}ds \tag{3.11}$$

Thus, the power, P, dissipated by the tether is

$$P = \int_0^L \vec{\mathbf{v}} \cdot d\vec{\mathbf{F}}_{\mathbf{B}} = -\int_0^L \vec{\mathbf{v}} \cdot \left(\vec{\mathbf{B}} \times \vec{\mathbf{l}}\right) I(s)ds = -\int_0^L \left(\vec{\mathbf{v}} \times \vec{\mathbf{B}}\right) \cdot \vec{\mathbf{l}} I(s)ds \tag{3.12}$$

Substituting Eq. (3.9) and Eq. (3.10) into Eq. (3.12) yields

$$P = -\int_0^L E_m I(s)ds \le -\int_0^L \frac{\sigma A}{2}\left(\frac{I^2}{(\sigma A)^2} + E_m^2\right)ds \le 0 \tag{3.13}$$

Equation (3.13) tells us that the power dissipated by the tether's motion is negative which implies that the Lorentz force always opposes the motion of the tether even in polar orbits. In this way, the electrodynamic force is used as drag to de-orbit the space tether system.

3.1.2.2 Aerodynamic Drag

The aerodynamic drag or the atmospheric drag on the tether is given by the well-known equation,

$$d\vec{\mathbf{F}}_A = \frac{1}{2}\rho C_d A|\vec{\mathbf{v}}_r|\vec{\mathbf{v}}_r ds \tag{3.14}$$

$$\vec{\mathbf{v}}_r = \vec{\mathbf{v}} - \vec{\omega} \times \vec{\mathbf{r}} \tag{3.15}$$

where $\vec{\mathbf{v}}_r$ is the relative air velocity with respect to the tether, $\vec{\omega}$ is the Earth's self-rotational rate and $\vec{\mathbf{r}}$ is the position of the tether in the geocentric inertial frame.

The density term in Eq. (3.14) will be determined from each of the atmospheric models that we have chosen: the US Standard Atmosphere 1976, the JB2008 model and the DTM-2013 model. The drag coefficient is taken as a constant of 2.2 [33].

3.1.2.3 Oblateness of the Earth

The Earth is a geoid; it is not perfectly spherical. This irregular shape causes satellites to be attracted to both the Earth's centre and the equator. Thus, once the satellite crosses the equator at an angle, the orbital angular momentum vector regresses slightly [33]. We can account for this change using the daily increase in the ascending node as follows,

$$\Delta\Omega = -9.97\left(\frac{r_E}{a}\right)^{\frac{7}{2}}\cos i_0 \tag{3.16}$$

where i_0 is the orbital inclination angle.

3.1.3 Libration dynamics

We first define the co-ordinate system we work in when we consider the libration of the tether segment. The z-axis points from the centre of the Earth to the centre of mass of the space tether system, the x-axis is in the direction of the orbital plane and the y-axis is perpendicular to both to make up a right-hand co-ordinate system. The unit vectors of this co-ordinate system are denoted by $\vec{\mathbf{e}}_{0x}, \vec{\mathbf{e}}_{0y}, \vec{\mathbf{e}}_{0z}$. Additionally, we introduce a co-ordinate system fixed with respect to the tether segment with unit vectors $\left(\vec{\mathbf{o}}, \vec{\mathbf{n}}, \vec{\mathbf{l}}\right)$ to describe the attitude of the tether with respect to the previously established co-ordinate system inthis

section. The attitudes are described by the pitch or in-plane angle, α, and the roll or out-of-plane angle, β. We can now write the position vector, $\vec{\mathbf{r}}_s$, and velocity vector, $\vec{\mathbf{v}}_s$, of any point along the tether.

$$\vec{\mathbf{r}}_s = \vec{\mathbf{r}} + (s-\lambda)\vec{\mathbf{l}} \tag{3.17}$$

$$\vec{\mathbf{v}}_s = \vec{\mathbf{v}} + (s-\lambda)\vec{\omega}_t \times \vec{\mathbf{l}} \tag{3.18}$$

Equations (3.17) and (3.18) contain $\vec{\mathbf{r}}$, the orbital position of the tether's centre of mass, s, measured from the main satellite to the sub-satellite, $\lambda = \dfrac{(m_1 + 0.5m_t)L}{(m_1 + m_2 + m_t)}$, $\vec{\mathbf{v}}$ is the orbital velocity of the tether and $\vec{\omega}_t$ is the absolute angular velocity of the tether [22].

We can further decompose the absolute angular velocity into the sum of the pitch and roll angles as show below in Eq. (3.19).

$$\vec{\omega}_t = \dot{f}\vec{\mathbf{e}}_{0y} + \dot{\beta}\vec{\mathbf{o}} + \dot{\alpha}\cos\beta\vec{\mathbf{n}} \tag{3.19}$$

Equation (3.19) contains f, the true anomaly.

We can now formulate expressions for the kinetic energy, E_k, and potential energy, E_p, of the space tether system using the position and velocity vectors given in Eqs. (3.17) and (3.18). These expressions are shown in Eqs. (3.20) and (3.21) below.

$$\begin{aligned} E_k &= \frac{1}{2}m_1(\vec{\mathbf{v}}_s \cdot \vec{\mathbf{v}}_s)_{s=L} + \frac{1}{2}m_2(\vec{\mathbf{v}}_s \cdot \vec{\mathbf{v}}_s)_{s=0} + \frac{1}{2}\int_0^L (\vec{\mathbf{v}}_s \cdot \vec{\mathbf{v}}_s)\rho_t ds \\ &= \frac{1}{2}\left[\left(\dot{f} + \dot{\alpha}\right)^2 \cos^2\beta + \beta^2\right]\hat{m}L^2 + \frac{1}{2}m_{tot}v^2 \end{aligned} \tag{3.20}$$

$$E_p = -\frac{\mu m_1}{r_s}\Big|_{s=L} - \frac{\mu m_2}{r_s}\Big|_{s=0} - \int_0^L \frac{\mu \rho_t}{r_s} ds$$
$$= \frac{1}{2}\mu r^{-3}\left(1 - 3\cos^2\alpha\cos^2\beta\right)\hat{m}L^2 - \frac{\mu m_{tot}}{r} + \mathrm{O}\left(\left(\frac{L}{r}\right)^3\right) \tag{3.21}$$

$$\hat{m} = \frac{\left[m_1 m_2 + \frac{1}{3}(m_1 + m_2)m_t + \frac{1}{12}m_t^2\right]}{m_{tot}}, m_{tot} = m_1 + m_2 + m_t \tag{3.22}$$

Here we have ρ_t, the linear density of the tether and L, the tether length.

We can now derive the Lagrangian function, L, of the space tether system as follows

$$= E_k - E_p$$
$$\approx \frac{1}{2}\left[\left(\dot{f} + \dot{\alpha}\right)^2\cos^2\beta + \dot{\beta}^2 - \mu r^{-3}\left(1 - 3\cos^2\alpha\cos^2\beta\right)\right]\hat{m}L^2$$
$$+ \frac{1}{2}m_{tot}v^2 + \frac{\mu m_t}{r} \tag{3.23}$$

Ignoring terms higher order than third and applying Lagrange's equation, we can deduce the equation of libration of the space tether system.

$$\ddot{\alpha} + \ddot{f} - 2\left(\dot{\alpha} + \dot{f}\right)\dot{\beta}\tan\beta + 3\mu r^{-3}\sin\alpha\cos\alpha = \frac{Q_\alpha}{\hat{m}L^2\cos^2\beta} \tag{3.24}$$

$$\ddot{\beta} + \left(\dot{\alpha} + \dot{f}\right)^2\sin\beta\cos\beta + 3\mu r^{-3}\cos^2\alpha\sin\beta\cos\beta = \frac{Q_\beta}{\hat{m}L^2} \tag{3.25}$$

Equations (3.24) and (3.25) contain the generalised perturbative forces acting on the pitch, Q_α and the generalised perturbative forces acting on the roll, Q_β.

3.1.4 Perturbation forces on the libration dynamics

The perturbative forces on the libration dynamics are derived by considering virtual work

along the tether length. The derivation of the equations are done by Zhong and Zhu [22]. We only present the equations derived below. The equations describe the perturbative torques on both the pitch and roll due to the electrodynamic force, Q_{Ed}, the aerodynamic drag force, Q_{Air}, the oblateness of the Earth, Q_{Ob} and solar radiation pressure, Q_{Ra}. We present only the equations representing the perturbative torques due to atmospheric drag in a future chapter because these equations are the ones of most interest to this study.

3.1.5 Numerical procedure

A description of the numerical procedure followed to determine the current flowing in the tether by given by Zhong and Zhu [33]. First, we retrieve the expression that describes the flow of current in the closed loop that consists of the tether and the surrounding plasma.

$$\frac{dI}{ds} = en_{\infty} d \begin{Bmatrix} \left(\frac{2e\Delta V}{m_e} \right)^{\frac{1}{2}} \mapsto V_t > V_p \\ -\left(\frac{-2e\Delta V}{m_i} \right)^{\frac{1}{2}} \mapsto V_t < V_p \end{Bmatrix} \tag{3.26}$$

Equation (3.26) contains the tether voltage, V_t, the induced voltage, V_p, $\Delta V = V_t - V_p$, the charge of an electron, e, the unperturbed plasma density, n_{∞}, the mass of an electron, m_e and the mass of the ion, m_i.

We now introduce three dimensionless variables and their definitions with L_0 as the dimensionless length, I_0 as the dimensionless current and V_0 as the dimensionless voltage.

$$\varepsilon = \frac{s}{L_0}; i = \frac{I(s)}{I_0}; \lambda = \frac{\Delta V}{V_0} \tag{3.27}$$

$$L_0 = \left(\frac{9\pi m_e \sigma^2 E_m A}{128 e^2 n_\infty^2} \right)^{\frac{1}{3}}; I_0 = \sigma E_m A; V_0 = E_m L_0 \tag{3.28}$$

Substituting Eqs. (3.27) - (3.28) into Eqs. (3.10) and (3.26) gives a dimensionless set of equations relating current and voltage.

$$\frac{di}{d\varepsilon} = \frac{3}{4}\sqrt{\lambda} \tag{3.29}$$

$$\frac{d\lambda}{d\varepsilon} = i - 1 \tag{3.30}$$

The boundary conditions for Eqs. (3.29) and (3.30) above are given below.

$$\text{At } \varepsilon = 0, \qquad i = 0, \lambda = \lambda_A \tag{3.31}$$

$$\text{At } \varepsilon = \varepsilon_B, \qquad i = i_B = i_C, \lambda = 0 \tag{3.32}$$

Integrating Eqs. (3.29) – (3.30) using the given boundary conditions, we get

$$\lambda_A = \left(2 i_C - i_C^2\right)^{\frac{2}{3}} \tag{3.34}$$

$$\varepsilon_B = \int_0^{\lambda_A} \left(\lambda^{\frac{3}{2}} - \lambda_A^{\frac{3}{2}} + 1 \right) d\lambda \tag{3.35}$$

At this point, we can assume one of two things to calculate the necessary boundary conditions. The first option is to assume that the current at the negatively charged end of the tether, i_C is known. An immediate consequence of this is that the voltage at the positively charged end of the tether, λ_A, is known as well as the length of the positively

charged segment of the tether, ε_B. This completes the list of boundary conditions are the pair of differential equations can be solved accordingly.

The second option is to assume that the entire length of the tether is positively charged. We do this to estimate what is the maximum de-orbit potential of the tether. In this case, ε_B, is known and is constant. However, the integration of Eq. (3.35) requires i_C . At this point, we took a different approach to those described by Zhong and Zhu [33]. We chose to implement the golden section optimisation method using Gaussian interpolation coefficients to find a value for i_C which proved to be successful with no significant computational cost.

3.2 Simulation Parameters of COM DEV cases

The parameters of the space tether system used in the current study were taken from two parts. The parameters for the main satellite are taken from the microsatellite platform designed by COM DEV (a Canadian company) [36]. The parameters for the tether and the sub-satellite are chosen based on previous studies [22, 31-34]. To investigate the impact of the mass of the sub-satellite, we decided to experiment with doubling the mass of the sub-satellite to see what impact it would have on the whole system. The results will be presented in a separate section.

Once the parameters are defined, we conducted runs that compare the three atmospheric models and analyse their results to determine whether the new models are significantly different from the U.S. 1976 model previously used. All simulation runs are done for the polar orbits with 90 degrees inclination because it is the worst case to de-orbit the space tether system by the electrodynamic tether.

The simulation would terminate when one of following stop conditions occurs. These are:

- The tether system starts tumbling, such that, either the pitch or roll angle exceeds 90 degrees (1.57 rad),
- The deorbit time exceeds the time limit – the maximum of 25 years,
- The space tether system is successfully lowered to 250 km

We chose the 250 km as the final altitude because it is well known that the space tether system shall re-enter into the Earth's atmosphere to burn up quickly due to the dense atmosphere. Finally, a time step of 100 seconds was used for all simulations.

The parameters used in simulations are listed as follows.

- Main satellite dimensions: 0.6 m×0.85 m×0.6 m
- Masses of the main satellite: 75 kg, 100 kg, 150 kg
- Sub-satellite dimensions: (0.1 m×0.1 m×0.1 m) and (0.1 m×0.1 m×0.2 m).

  The first set of dimensions corresponds to the lighter sub-satellite while the second set of dimensions corresponds to the heavier sub-satellite (twice the mass of the lighter sub-satellite). The length was doubled in the z-direction i.e. pointing towards Earth
- Mass of the sub-satellite: mass of the tether (light sub-satellite) and twice the mass of the tether (heavier sub-satellite)
- Rigid tether with a mass of 0.5 kg for every kilometre
- Tether length: 1 km, 3km and 5 km
- Tether diameter: 0.5 mm

- U.S. Standard Atmosphere 1976
- Time step of 100s
- Initial altitude: 900 km and 500 km
- Orbital inclination: 90 degrees (polar orbit)
- Eccentricity: approximately 0

3.3 Results and Discussion

We conducted simulations on every combination of initial altitude (500 km, 900 km), tether length (1 km, 3 km, 5km), mass of the main satellite (75 kg, 100 kg, 150 kg) and mass of the sub-satellite (equal to the mass of tether and doubled). This gave us 36 cases in total. We divided the results into two parts: those that have an initial altitude of 900 km and those that have an initial altitude of 500 km.

3.3.1 Initial Altitude: 900 km

The simulation results are summarized in Table 3.1 and shown in Figs. 3.2 ~ 3.4.

It is noted that all the cases that had an initial altitude of 900 km and tether length of 1 km (see Fig. 3.2 (a), Fig. 3.3 (a), Fig. 3.4 (a)) do not de-orbit to the targeted altitude of 250 km within 25 years, although the libration of the EDT system is stable.

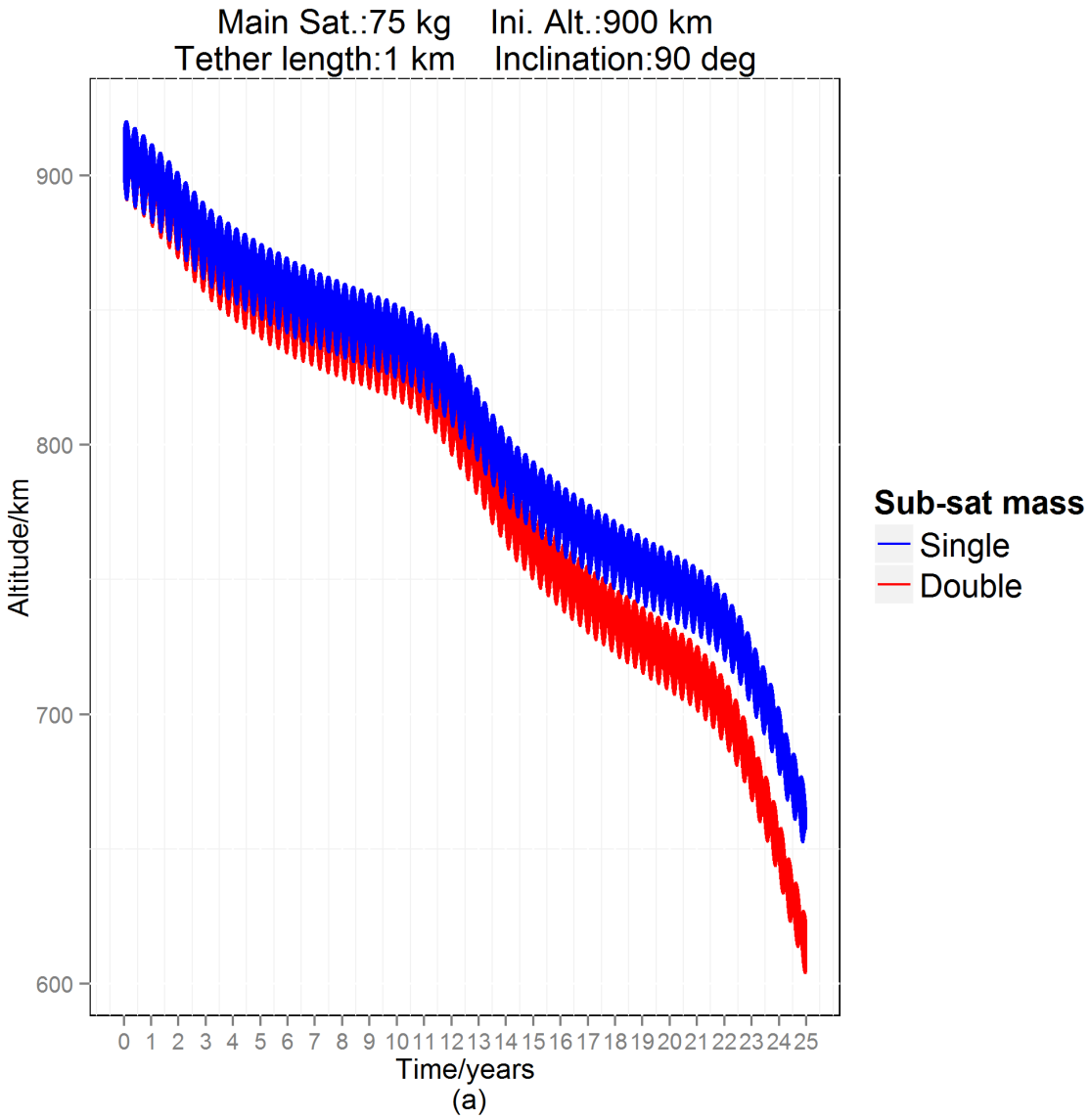
Main Sat.:75 kg Ini. Alt.:900 km
Tether length:1 km Inclination:90 deg
900
800
700
600
Altitude/km
0 1 2 3 4 5 6 7 8 9 10 11 12 13 14 15 16 17 18 19 20 21 22 23 24 25
Time/years
(a)
Sub-sat mass
Single
Double

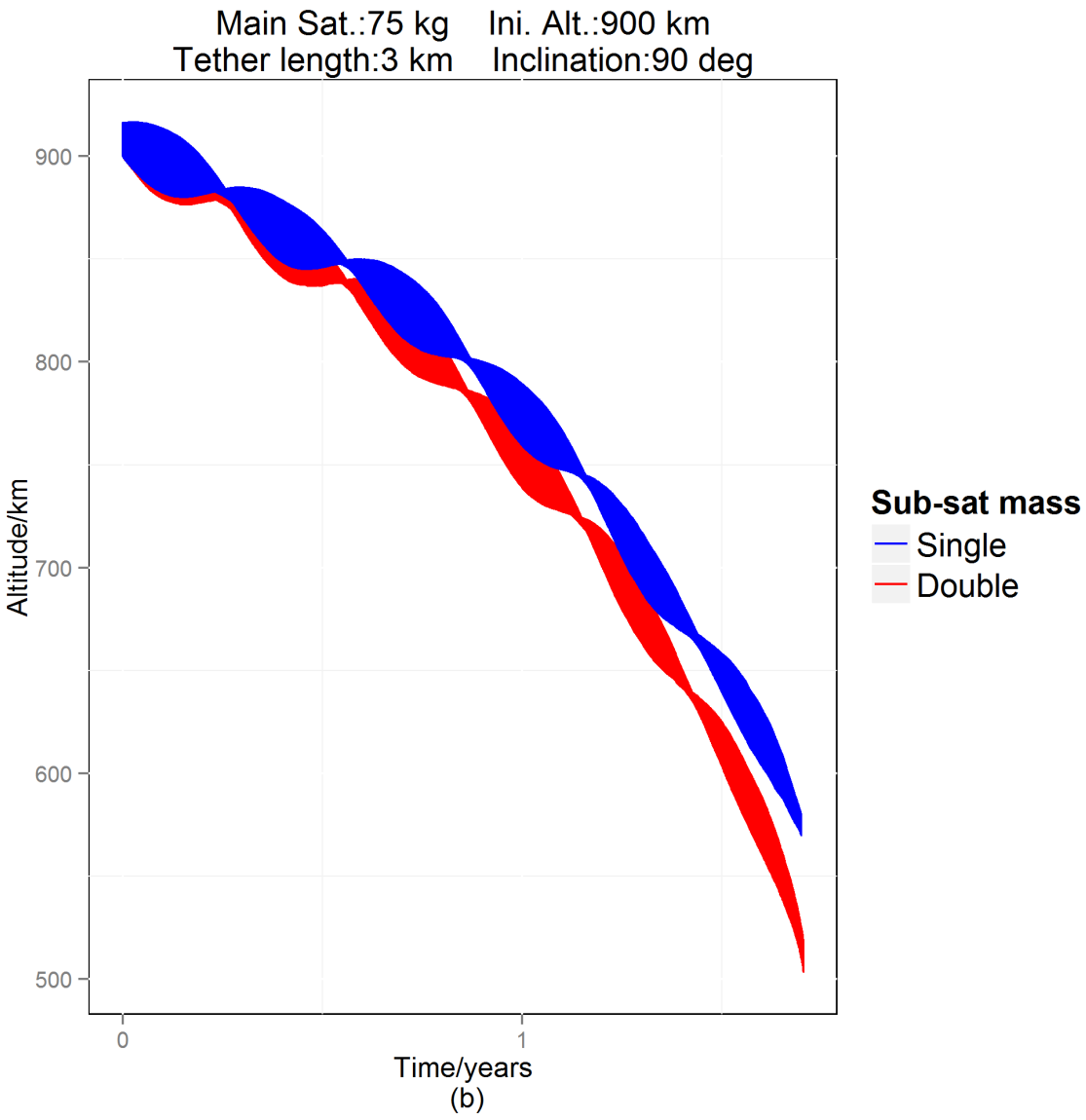
Main Sat.:75 kg Ini. Alt.:900 km
Tether length:3 km Inclination:90 deg
900
800
700
600
500
Altitude/km
0
1
Time/years
(b)
Sub-sat mass
Single
Double

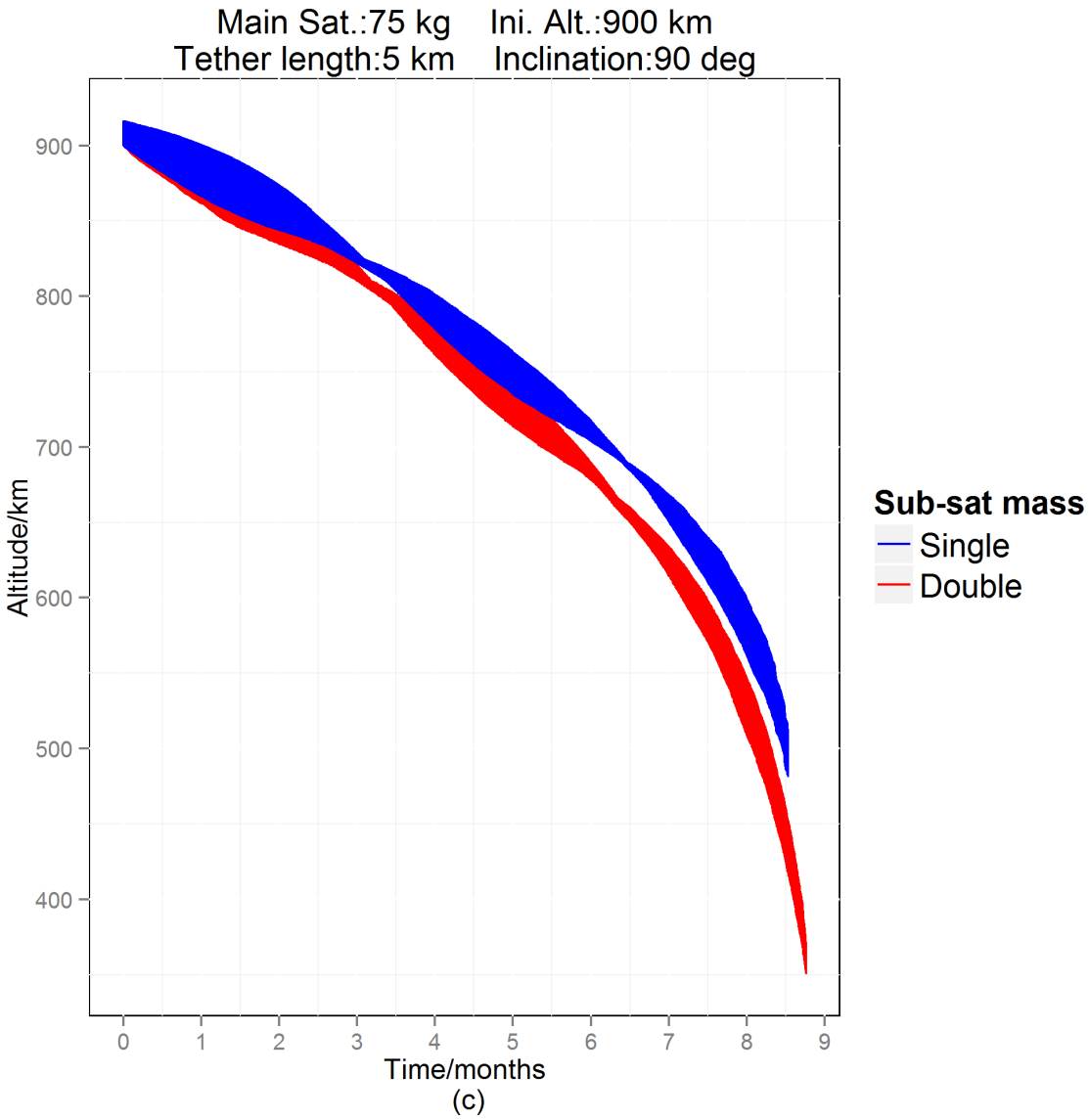

Figure 3.2 The results using the 75 kg main satellite, 900 km initial altitude and 1 km, 3 km and 5 km tether lengths (COMDEV)

For the cases with 3 and 5 km long tethers (see Fig. 3.2 (b) (c), Fig. 3.3 (b) (c), Fig. 3.4 (b) (c)), the EDT de-orbits the system to an altitude around 600 km very quickly with a few years. However, the EDT system becomes unstable and tumbling before it reaches the targeted altitude. We include this case merely for the sake of simulation. In real

missions, it is expected that the space tether system will de-orbit from this altitude by only air drag within 25 years if the altitude is less than 600 km. If one wants to de-orbit faster than 25 years, than a libration stability control is required. The controlled de-orbit is shown in the next Chapter.

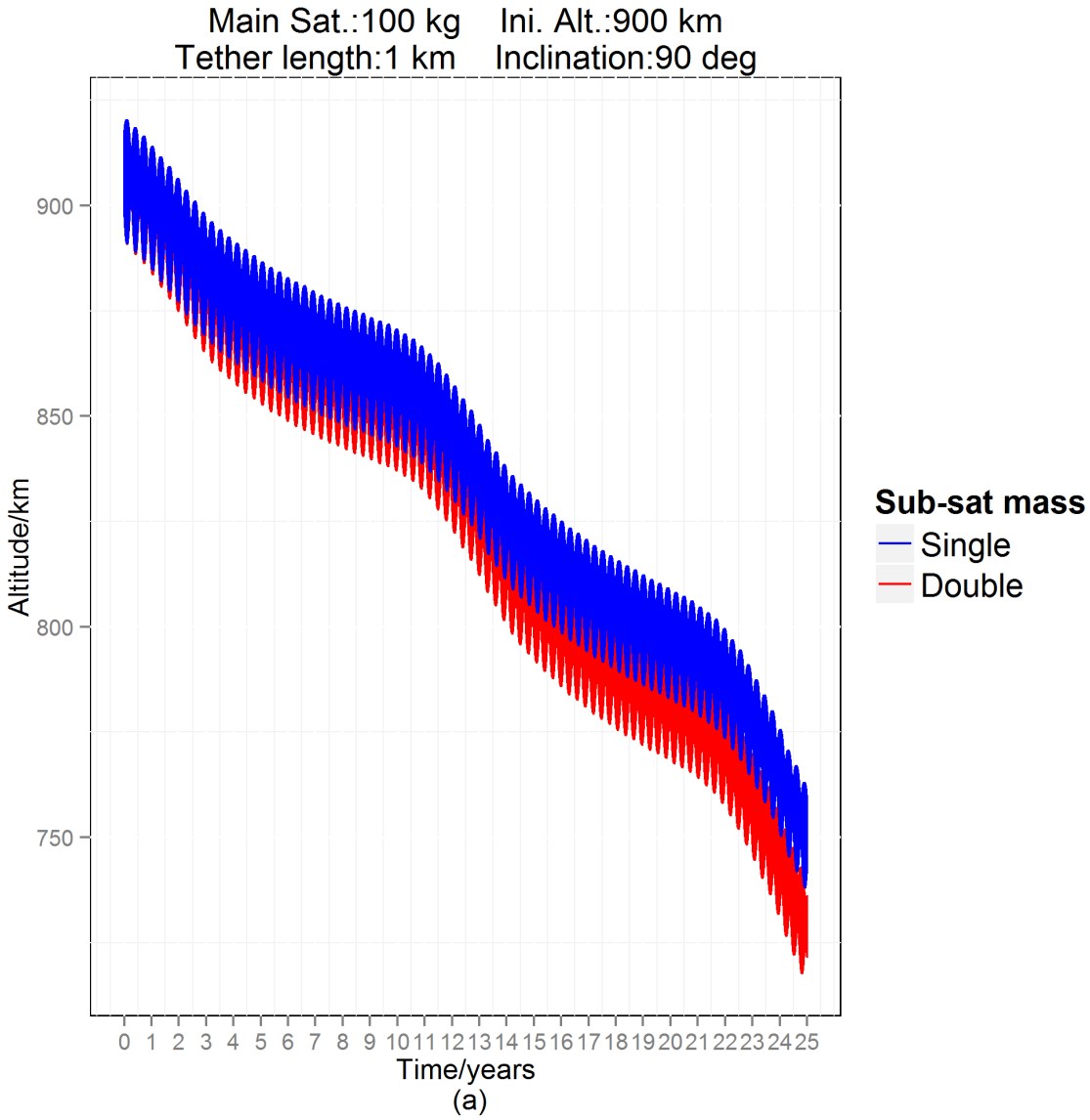

(a)

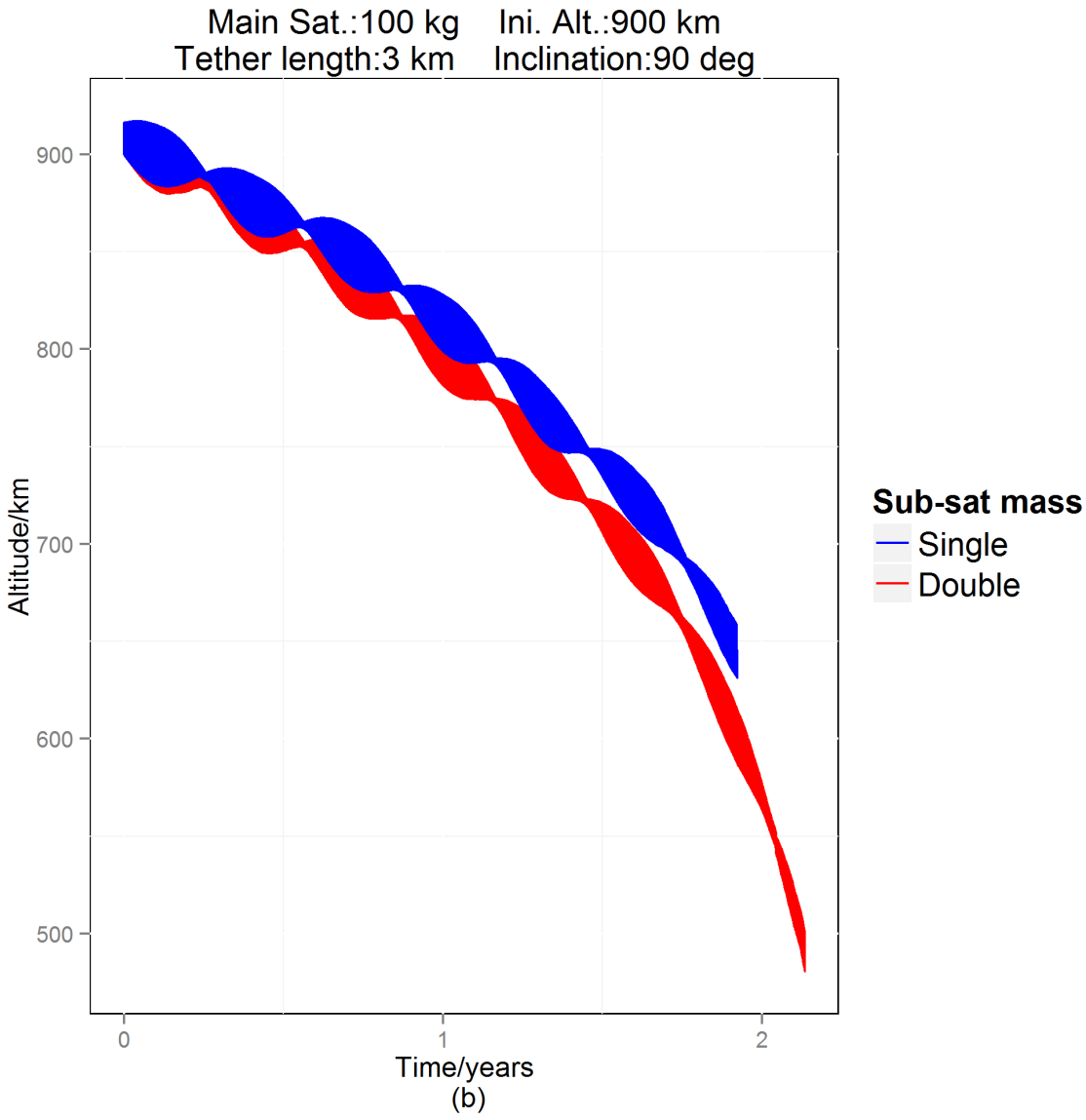
Main Sat.:100 kg Ini. Alt.:900 km
Tether length:3 km Inclination:90 deg
900
800
700
600
500
Altitude/km
0
1
2
Time/years
(b)
Sub-sat mass
Single
Double

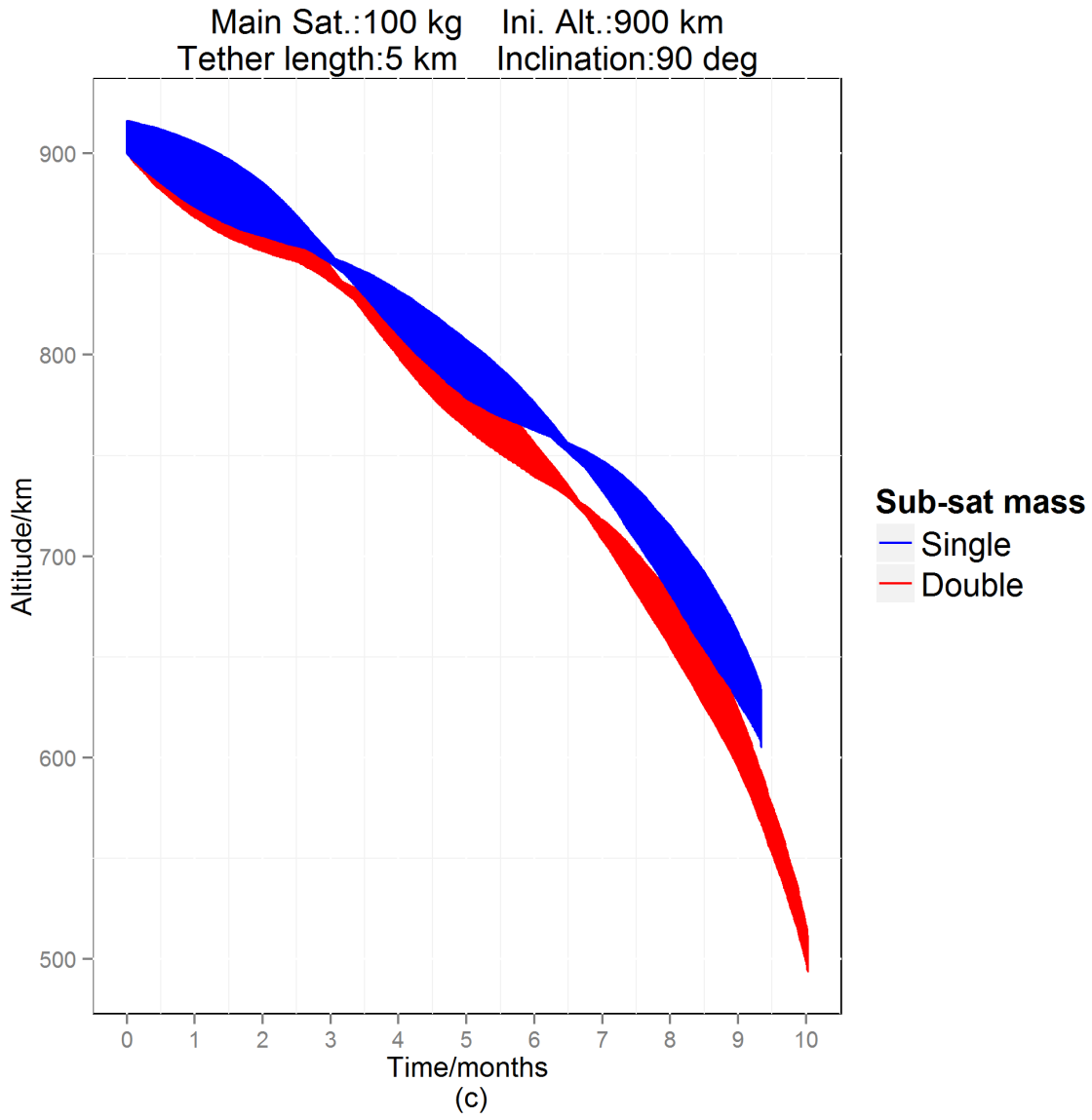

Figure 3.3 The results using the 100 kg main satellite 900 km, initial altitude and 1 km, 3 km and 5 km tether lengths (COMDEV).

Next, the tether system de-orbits to a lower altitude when the mass of the sub-satellite is doubled in all cases (keeping all other parameters the same) because a heavier sub-satellite increases the stability of the system. Similarly, the EDT system begins to tumble before 250 km in the cases with the 3 km tether and the 5 km tether (see Fig. 3.2 (b) (c), Fig. 3.3 (b) (c), Fig. 3.4 (b) (c)). For the case of the 1 km tether (see Fig. 3.2 (a), Fig. 3.3

(a), Fig. 3.4 (a)), the space tether system does not tumble within the given 25 years but also does not de-orbit to the target altitude of 250 km. Another point to note about the cases with the 1 km tether is the rate at which the space tether system de-orbits. There appears to be two different rates and this is attributed to angle control used in these simulations.

Table 3.1 De-orbit from 900km with a light sub-satellite.

Orbit Inclination	90°	Tether Length (km)	1	3	5
		Tether mass (kg)	0.5	1.5	2.5
		Sub-satellite mass (kg)	0.5	1.5	2.5
Masse of main satellite (kg)	75	De-orbit time (years)	25*	1.7	0.7
		Final altitude (km)	664	574†	504†
	100	De-orbit time (years)	25*	1.9	0.8
		Final altitude (km)	746	643†	610†
	150	De-orbit time (years)	25*	2.9	1.0
		Final altitude (km)	807	613†	676†

* -- Simulation stopped when the maximum allowed de-orbit time is reached.

† -- Simulation stopped when the EDT system starts tumbling.

Table 3.2 De-orbit from 900km with a heavy sub-satellite.

Orbit Inclination	90°	Tether Length (km)	1	3	5
		Tether mass (kg)	0.5	1.5	2.5
		Sub-satellite mass (kg)	1.0	3.0	5.0
Masse of main satellite (kg)	75	De-orbit time (years)	25*	1.7	0.7
		Final altitude (km)	621	508†	362†
	100	De-orbit time (years)	25*	2.1	0.8
		Final altitude (km)	729	487†	503†

	150	De-orbit time (years)	25*	3.1	1.2
		Final altitude (km)	802	476†	430†

* -- Simulation stopped when the maximum allowed de-orbit time is reached.

† -- Simulation stopped when the EDT system starts tumbling.

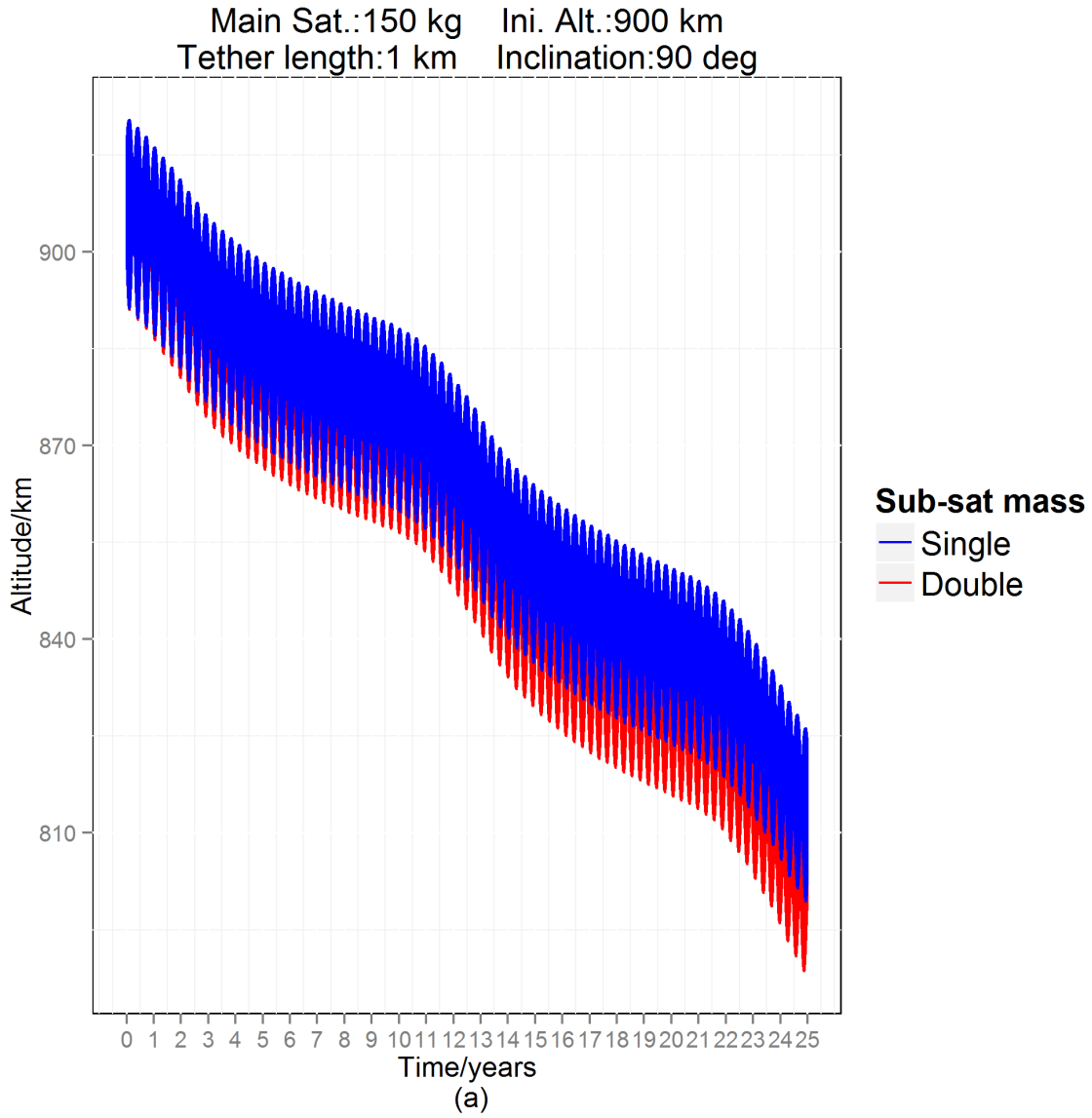

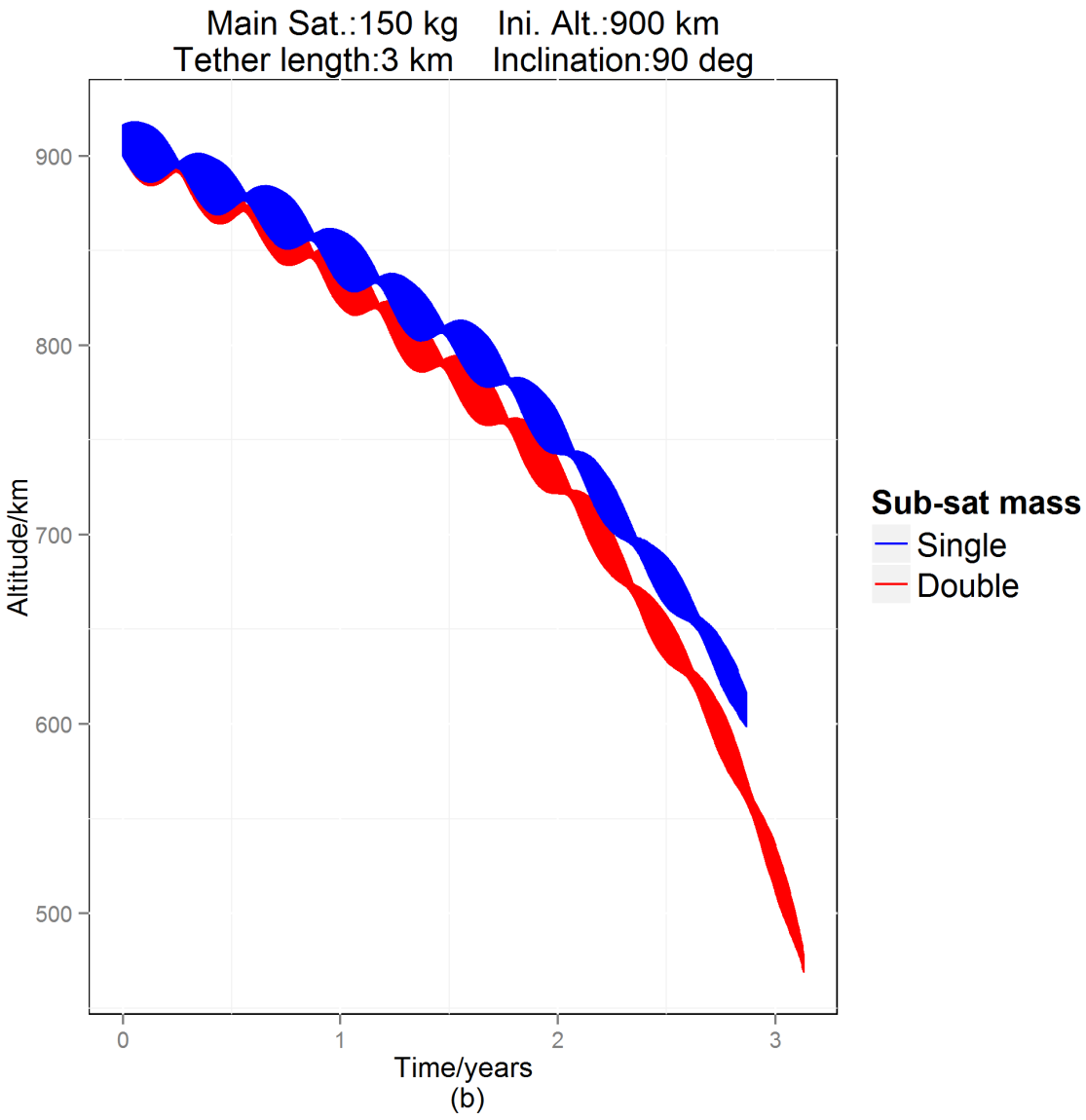
Main Sat.:150 kg Ini. Alt.:900 km
Tether length:3 km Inclination:90 deg
900
800
700
600
500
Altitude/km
0
1
2
3
Time/years
(b)
Sub-sat mass
Single
Double

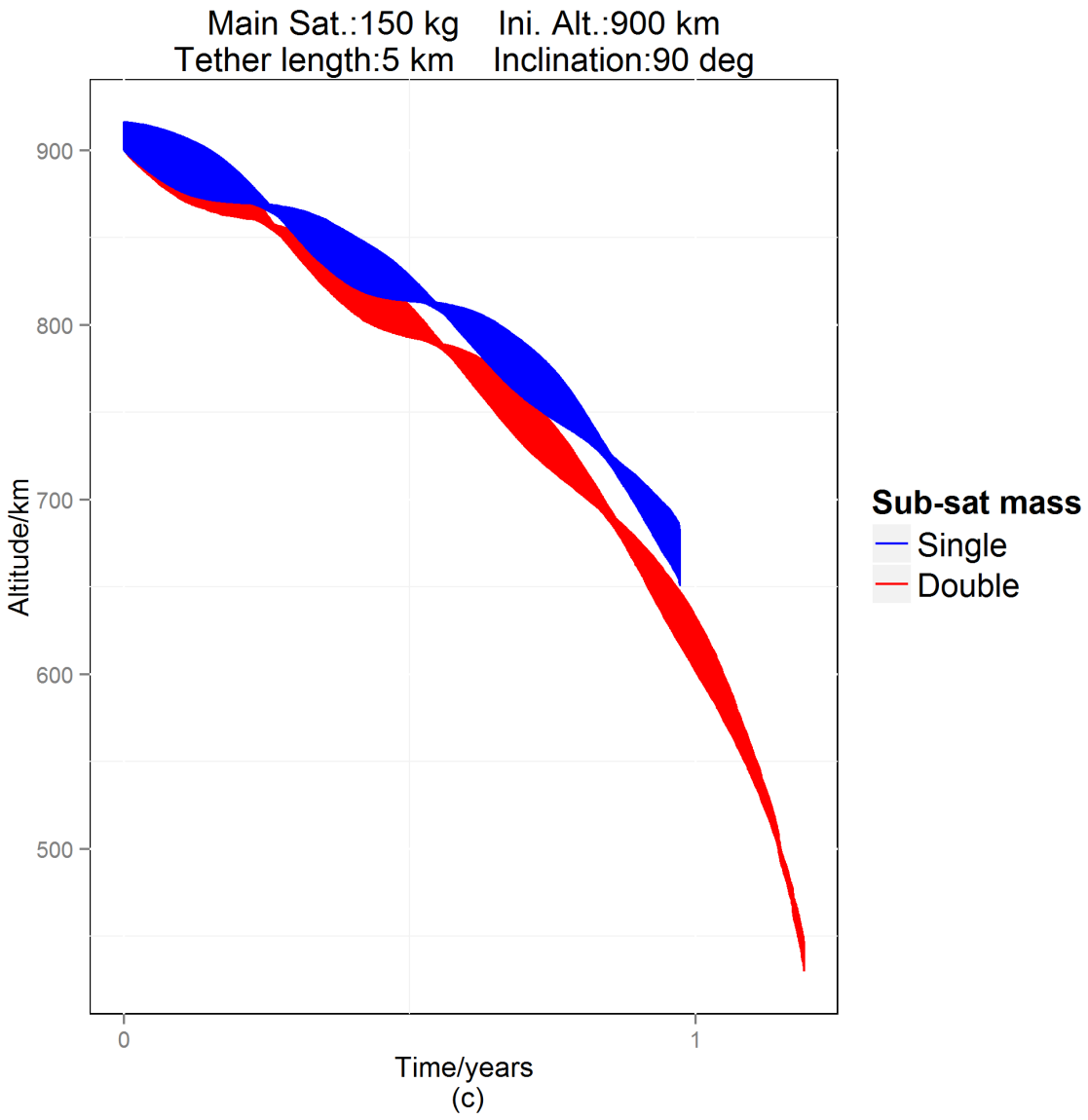

Figure 3.4 The results using the 150 kg main satellite, 900 km initial altitude and 1 km, 3 km and 5 km tether lengths (COMDEV)

3.3.2 Initial Altitude: 500 km

The simulation results are summarized in Tables 3.3-3.4 and shown in Figs. 3.5 ~ 3.8. First, the results show that the EDT system begins tumbling before reaching 250 km altitude very quickly in all but one case due to the strong electrodynamic force (see Fig.

3.5 (c)).

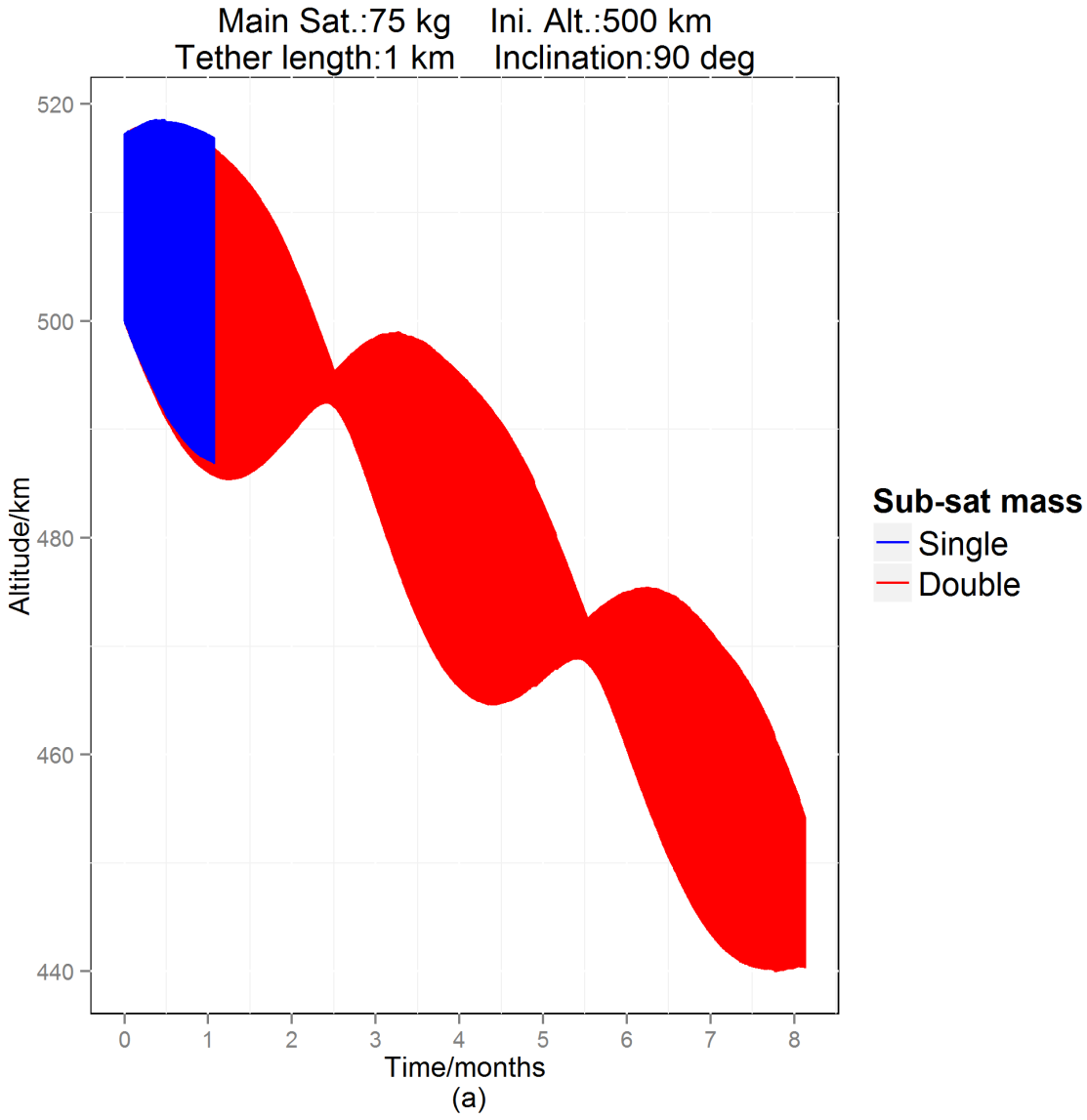
Main Sat.:75 kg Ini. Alt.:500 km
Tether length:1 km Inclination:90 deg
520
500
480
460
440
Altitude/km
0
1
2
3
4
5
6
7
8
Time/months
(a)
Sub-sat mass
Single
Double

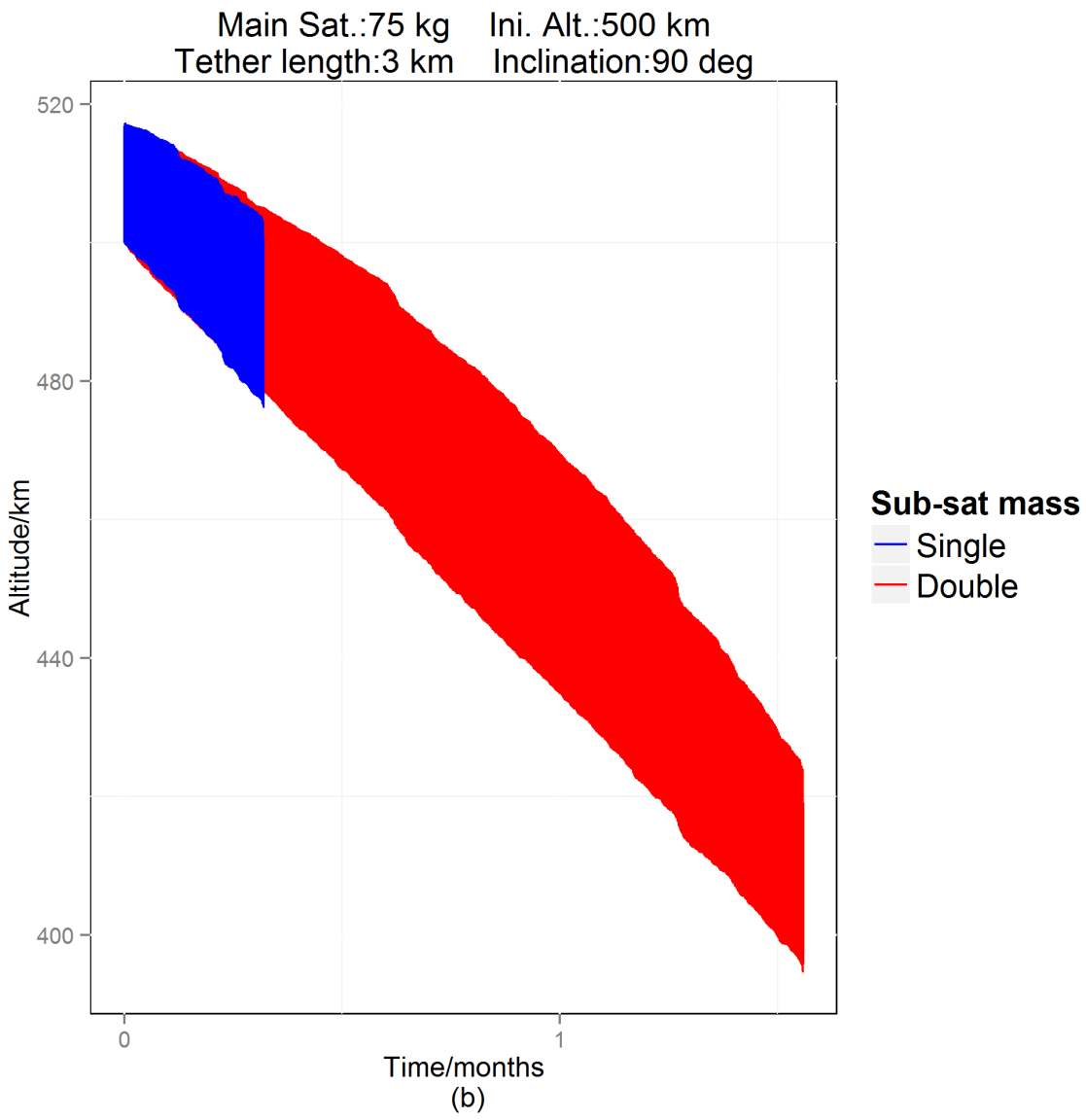
Main Sat.:75 kg Ini. Alt.:500 km
Tether length:3 km Inclination:90 deg
520
480
440
400
Altitude/km
0
1
Time/months
(b)
Sub-sat mass
Single
Double

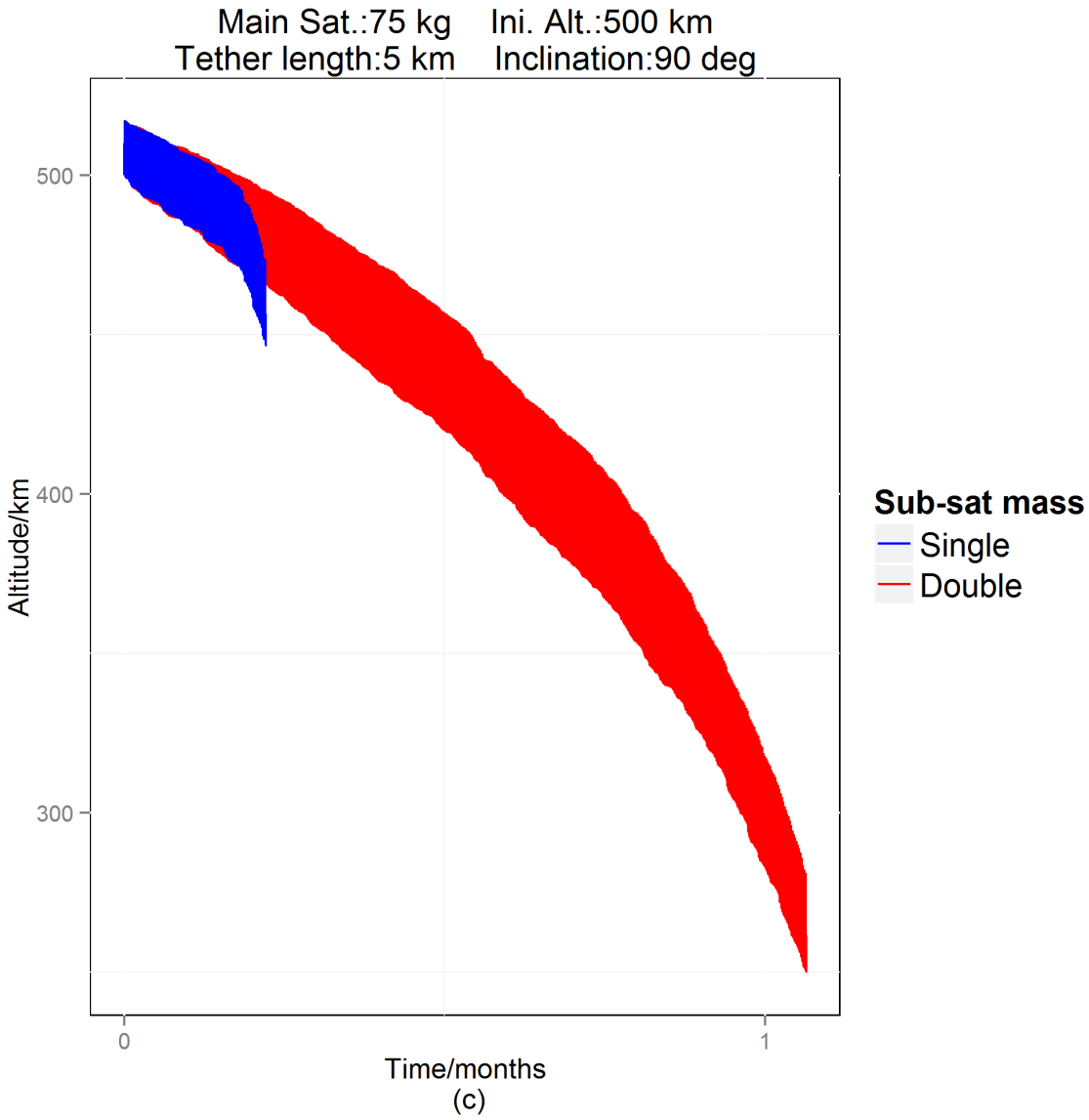

Figure 3.5 The results using the 75 kg main satellite, 500 km initial altitude and 1 km, 3 km and 5 km tether lengths (COMDEV)

Second, the systems with a heavier sub-satellite, which provides a larger gravity moment to stabilize the EDT system, can stably de-orbit for a longer time and to a lower altitude before tumbling than the systems with the lighter sub-satellite. The final altitude recorded in some of these simulations is larger than the initial altitude. This is because the orbit becomes more elliptical over time due to the inhomogeneity of the geo-magnetic

field and the system experiences larger electrodynamic force near the South Pole than the North Pole.

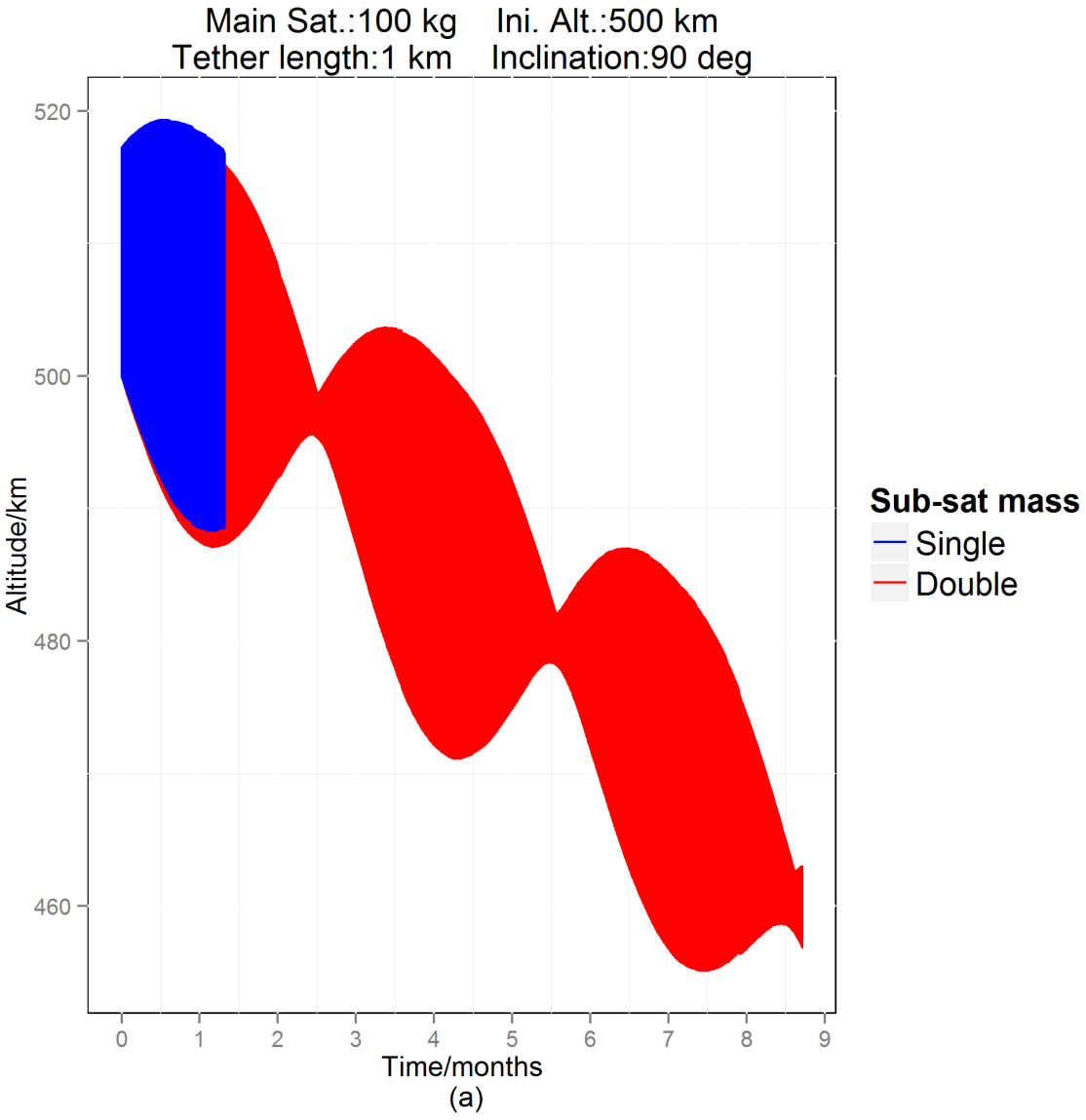

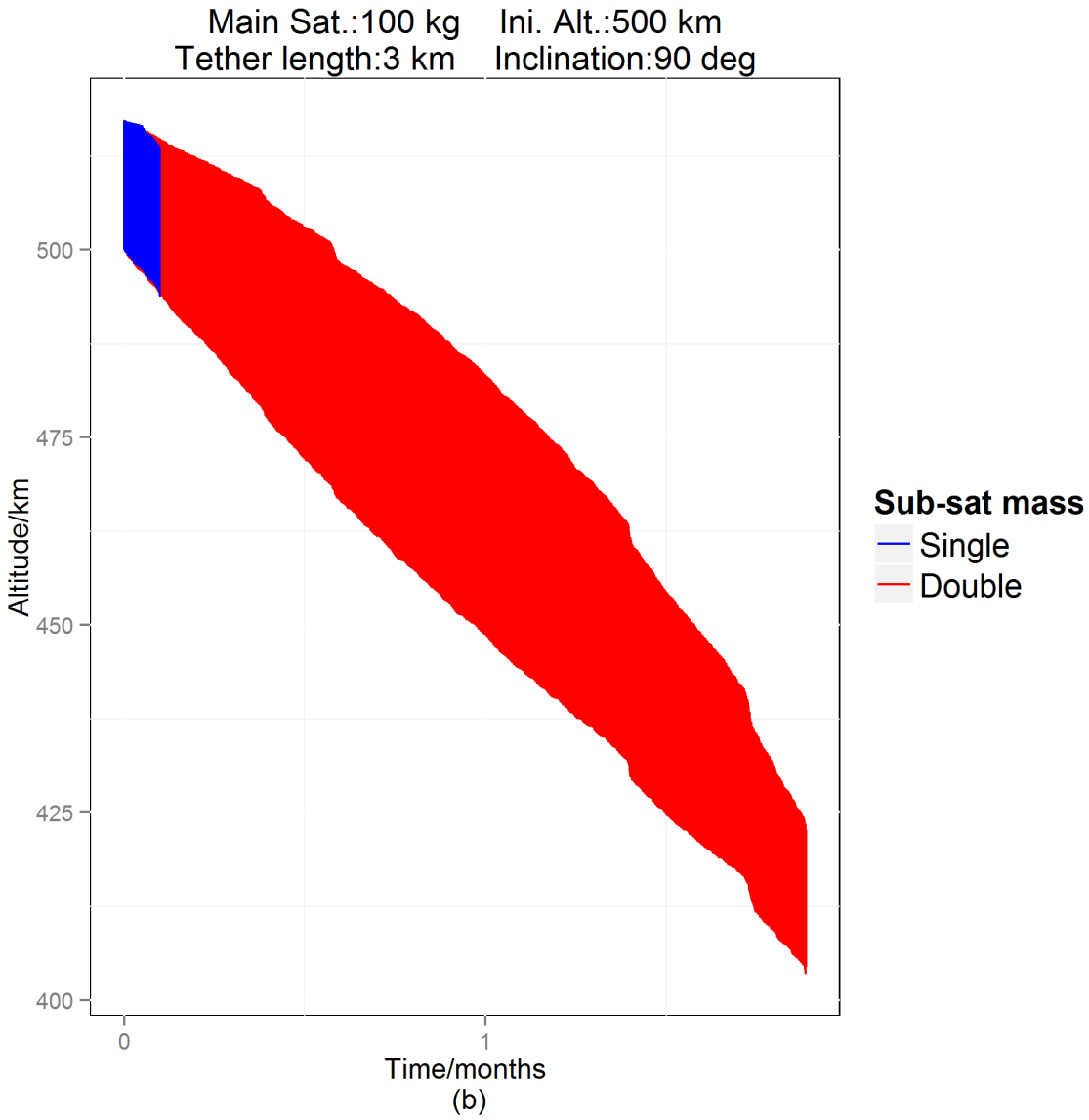
Main Sat.:100 kg Ini. Alt.:500 km
Tether length:3 km Inclination:90 deg
500
475
450
425
400
Altitude/km
0
1
Time/months
(b)
Sub-sat mass
Single
Double

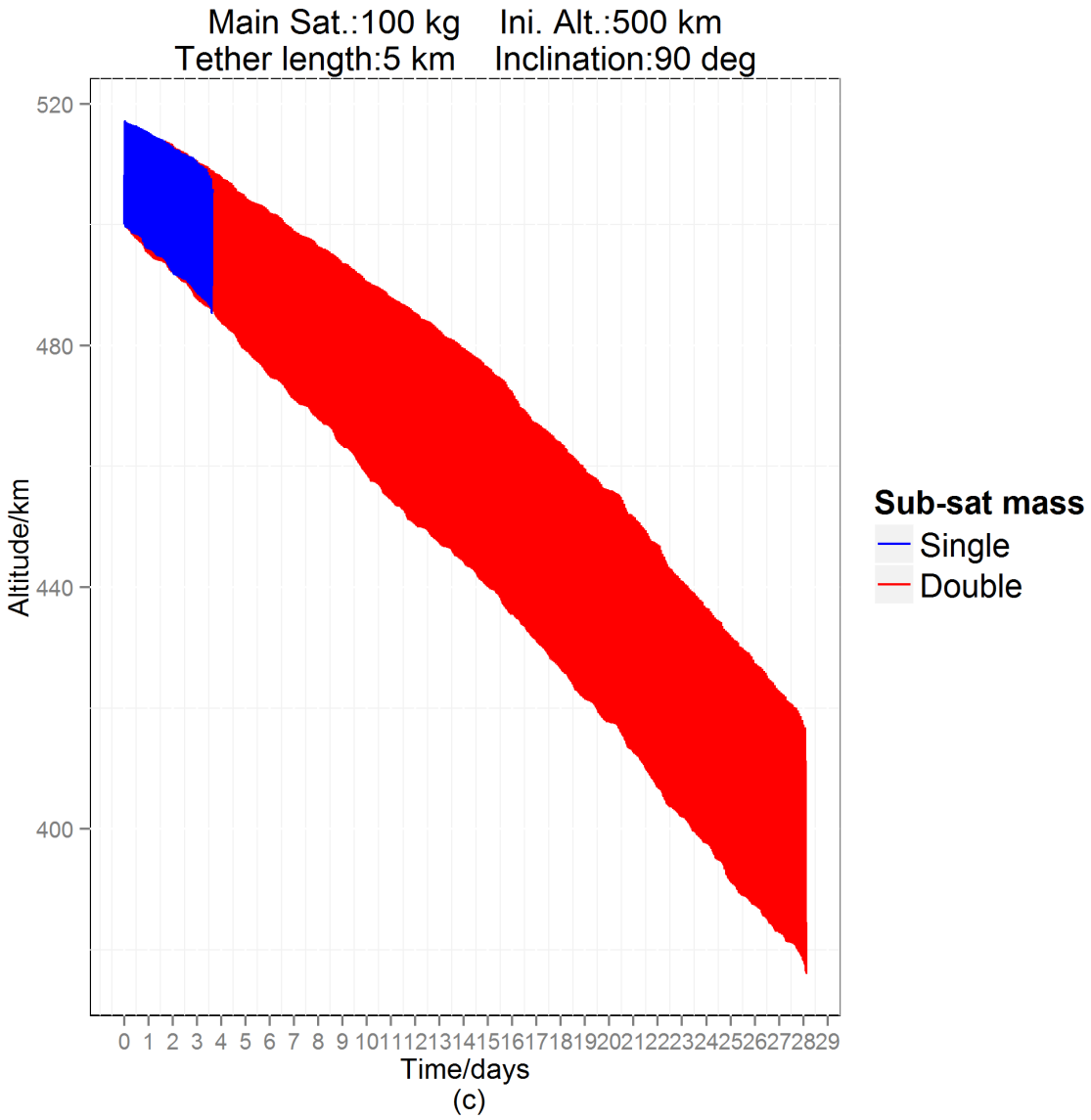

Figure 3.6 The results using the 100 kg main satellite, 500 km initial altitude and 1 km, 3 km and 5 km tether lengths (COMDEV)

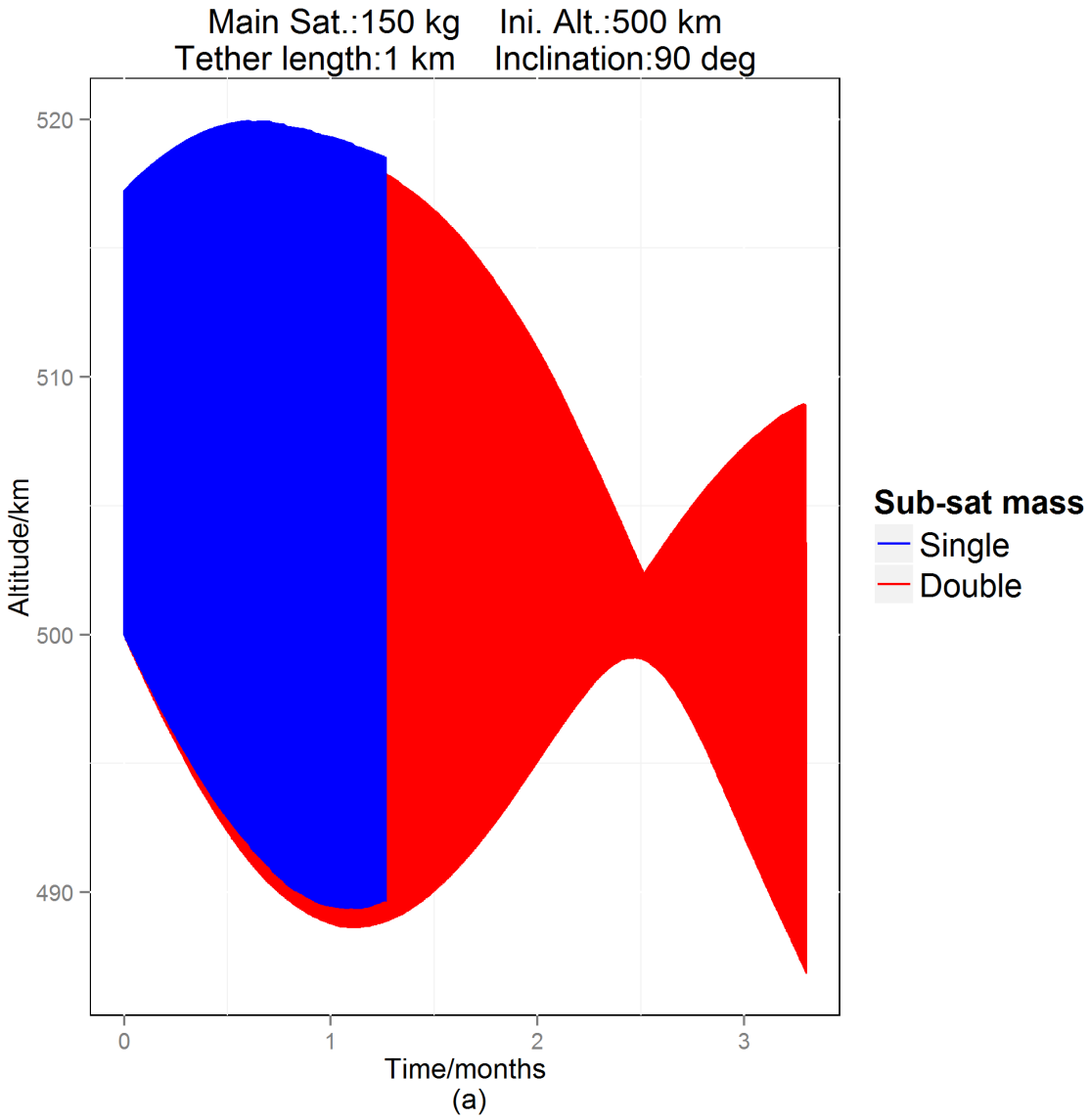
Main Sat.:150 kg Ini. Alt.:500 km
Tether length:1 km Inclination:90 deg
520
510
500
490
Altitude/km
0
1
2
3
Time/months
(a)
Sub-sat mass
Single
Double

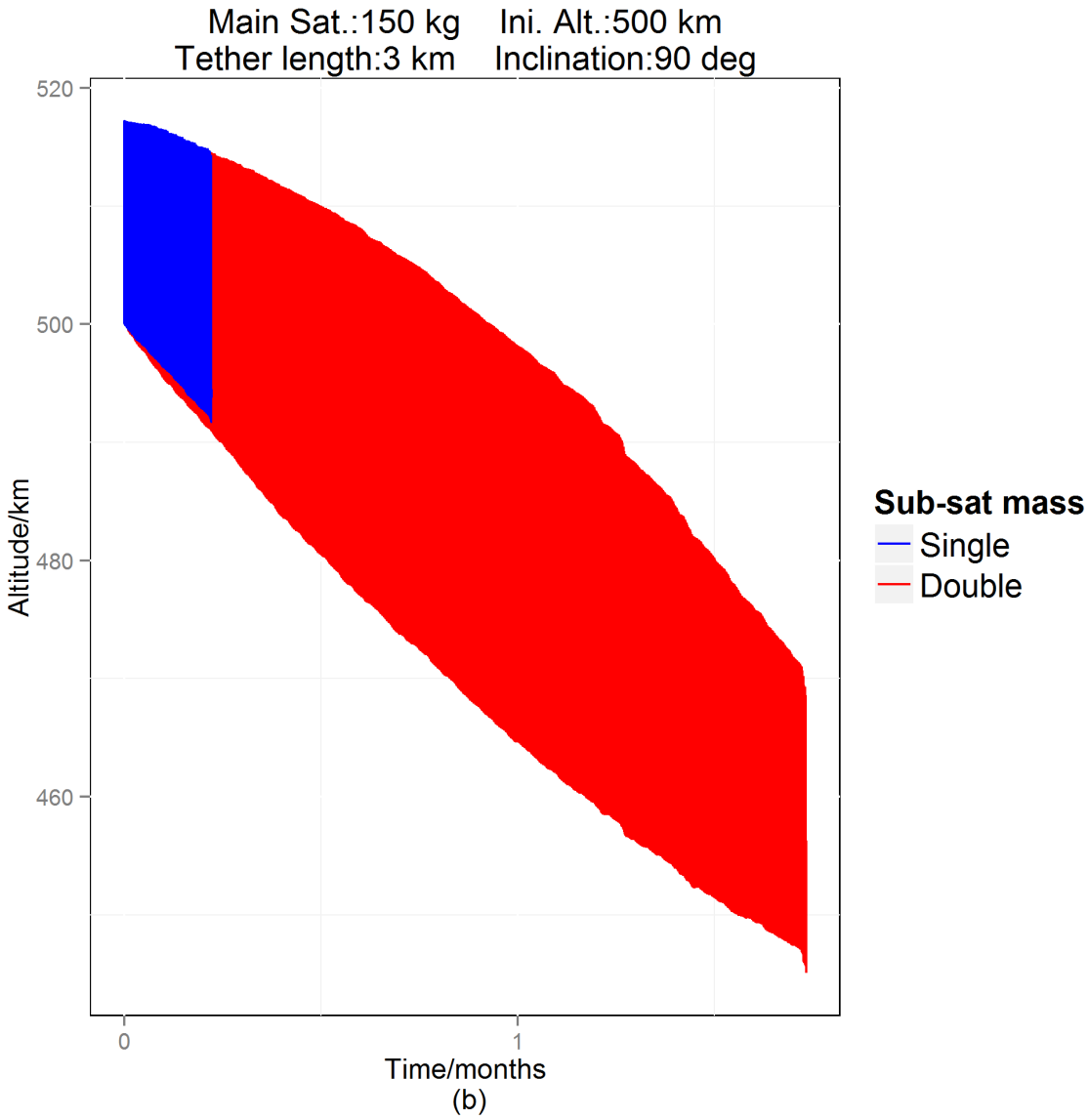
Main Sat.:150 kg Ini. Alt.:500 km
Tether length:3 km Inclination:90 deg
520
500
480
460
Altitude/km
0
1
Time/months
(b)
Sub-sat mass
Single
Double

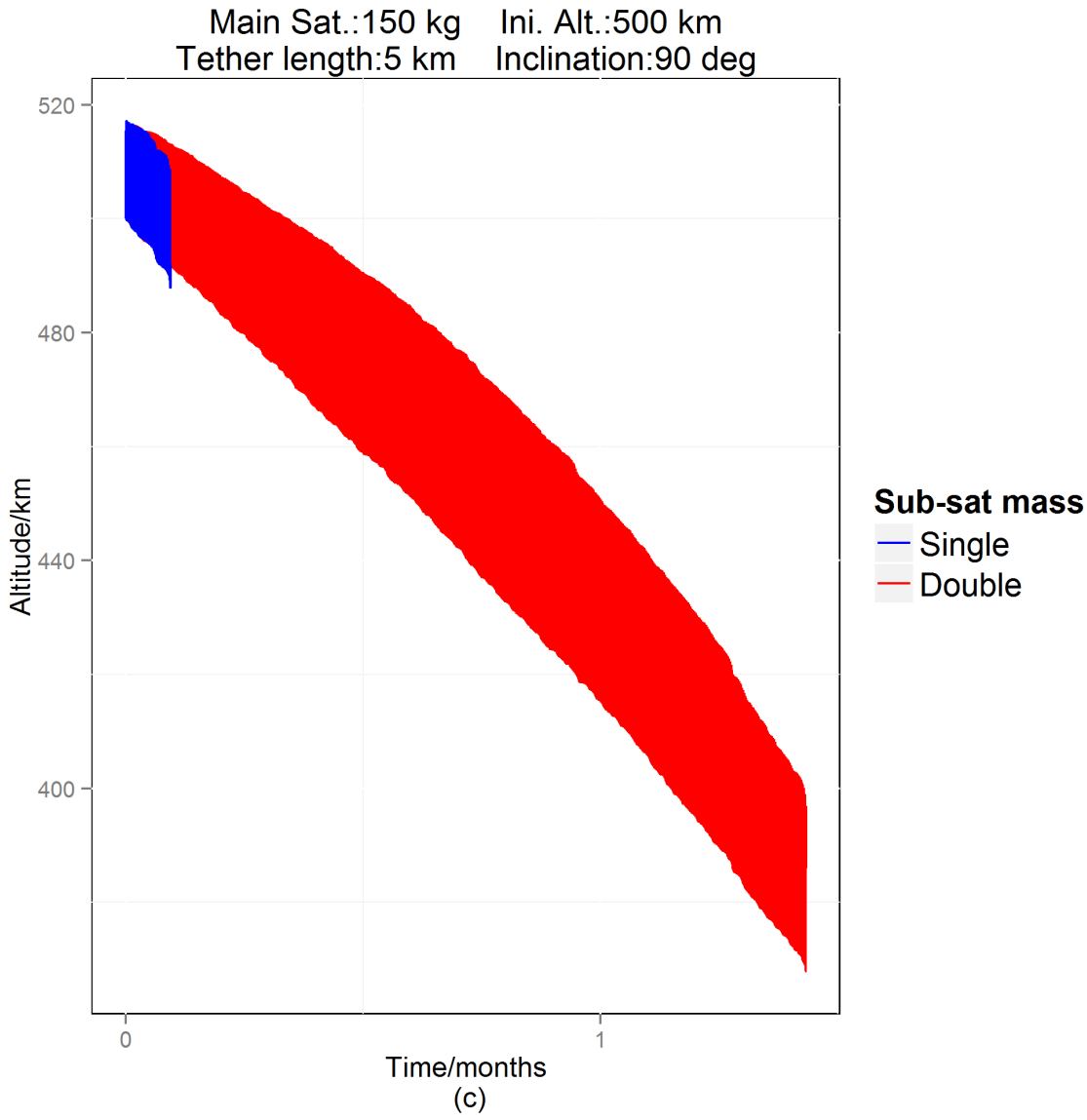

Figure 3.7 Results using the 150 kg main satellite, 500 km initial altitude and 1 km, 3 km and 5 km tether lengths (COMDEV)

We also include a graph showing a sample of the pitch and roll angles for all the simulations performed (see Fig. 3.8). It shows that the libration instability is mainly caused by the pitch motion in the polar orbit. All of the pitch and roll angles for the remaining simulations behaved similar to one of the two cases highlighted here.

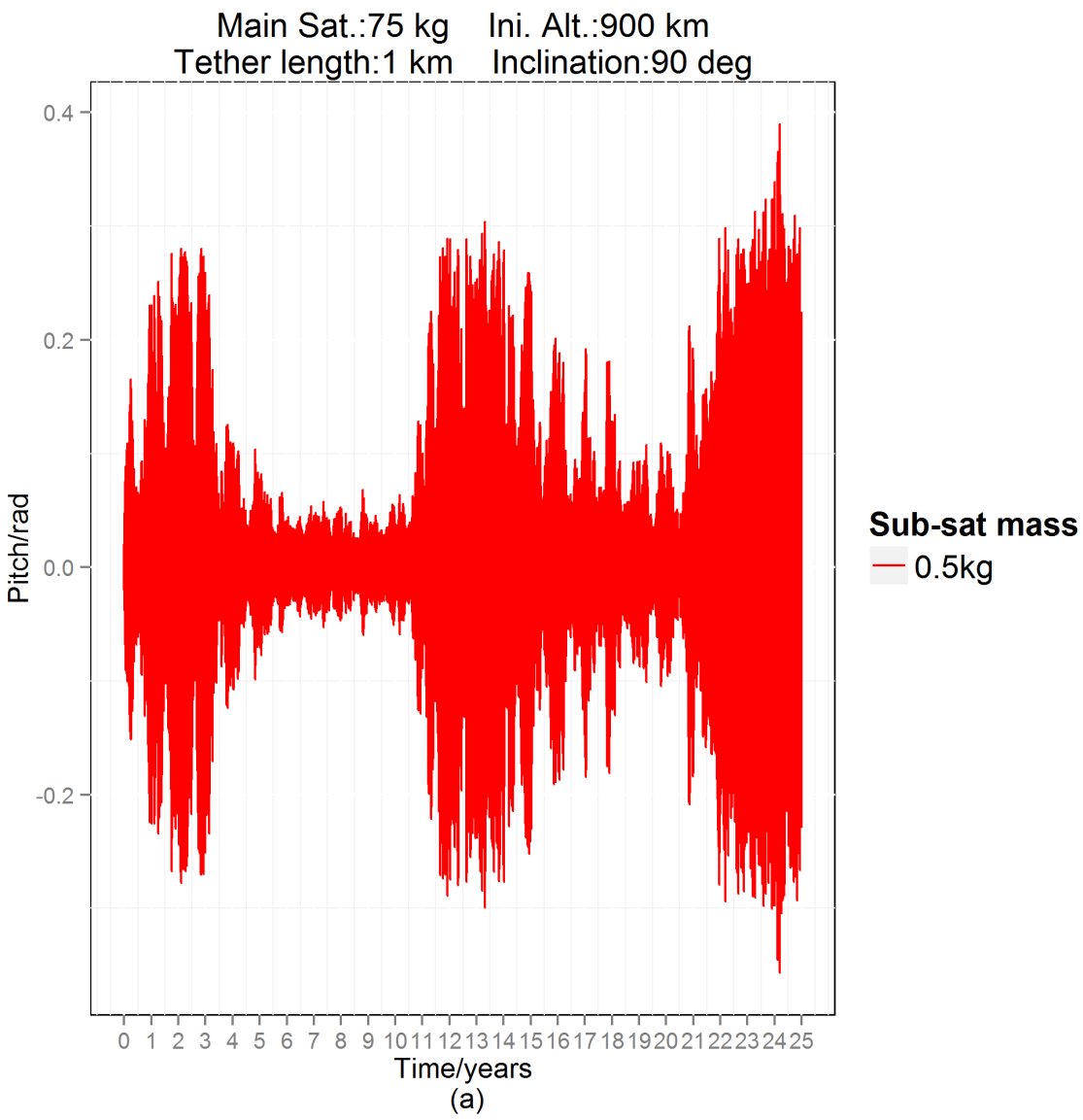
Main Sat.:75 kg Ini. Alt.:900 km
Tether length:1 km Inclination:90 deg
Pitch/rad
0.4
0.2
0.0
-0.2
0 1 2 3 4 5 6 7 8 9 10 11 12 13 14 15 16 17 18 19 20 21 22 23 24 25
Time/years
Sub-sat mass
0.5kg
(a)

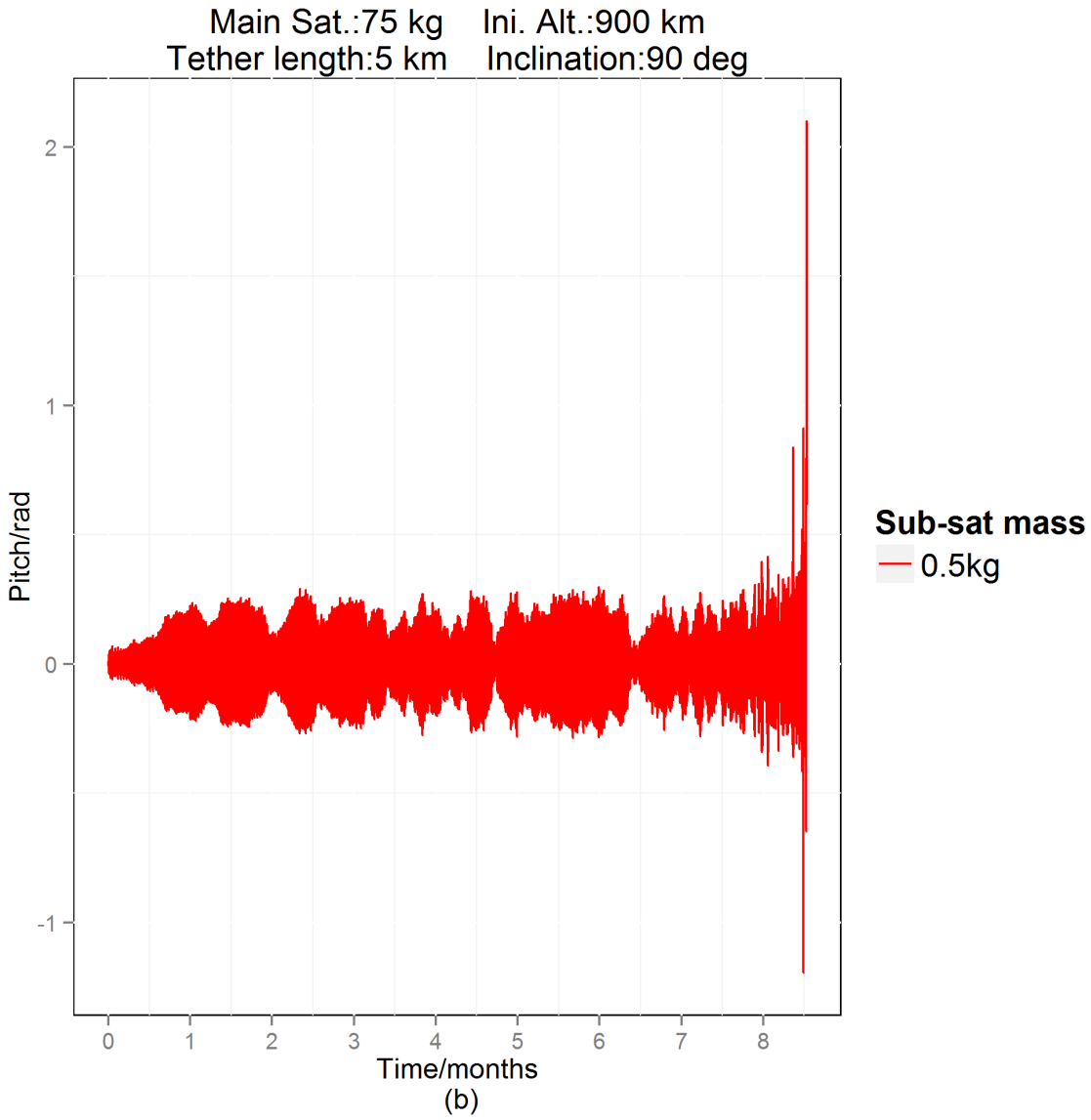
Main Sat.:75 kg Ini. Alt.:900 km
Tether length:5 km Inclination:90 deg
Pitch/rad
2
1
0
-1
0
1
2
3
4
5
6
7
8
Time/months
(b)
Sub-sat mass
0.5kg

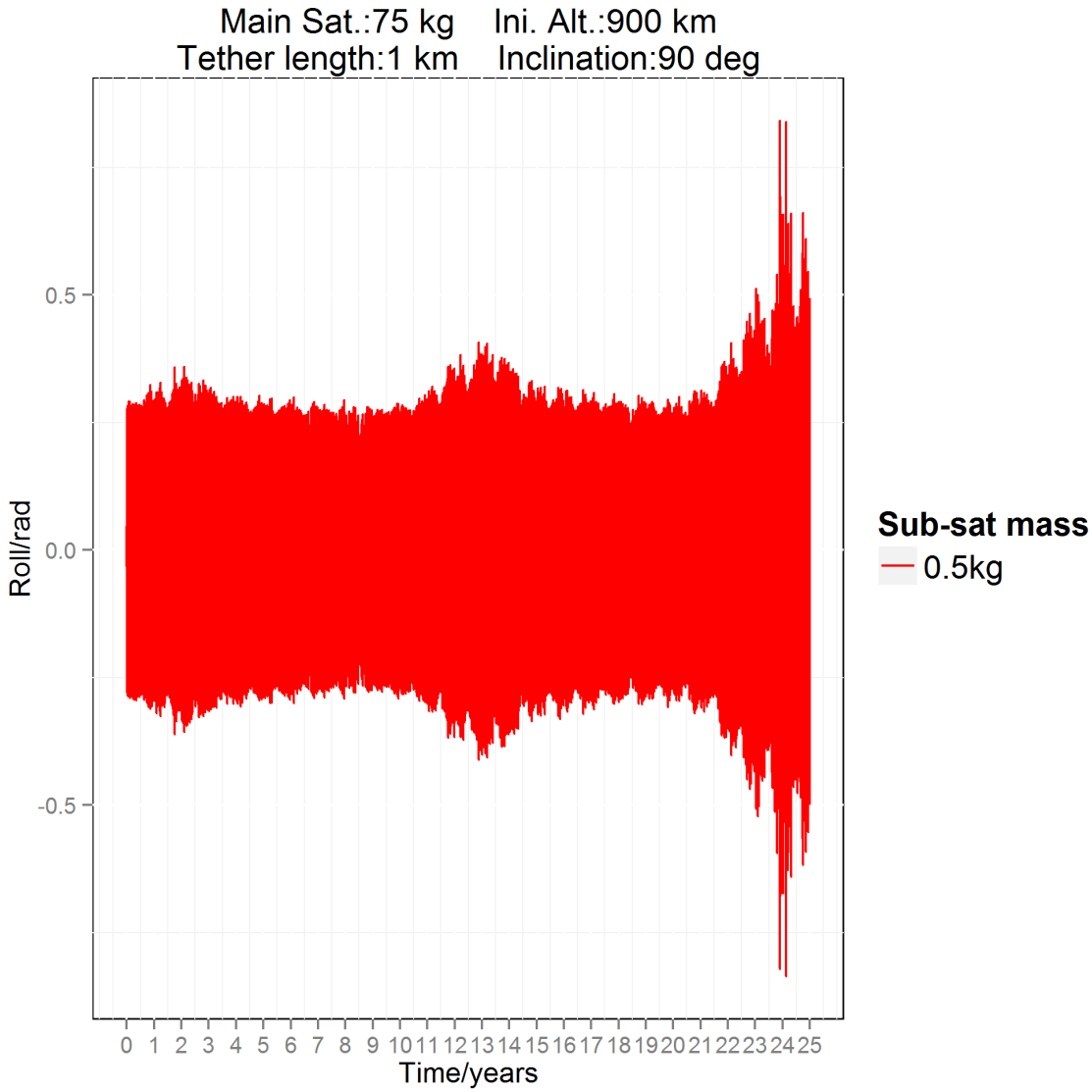
Main Sat.:75 kg Ini. Alt.:900 km
Tether length:1 km Inclination:90 deg
Roll/rad
0.5
0.0
-0.5
0 1 2 3 4 5 6 7 8 9 10 11 12 13 14 15 16 17 18 19 20 21 22 23 24 25
Time/years
Sub-sat mass
0.5kg

(c)

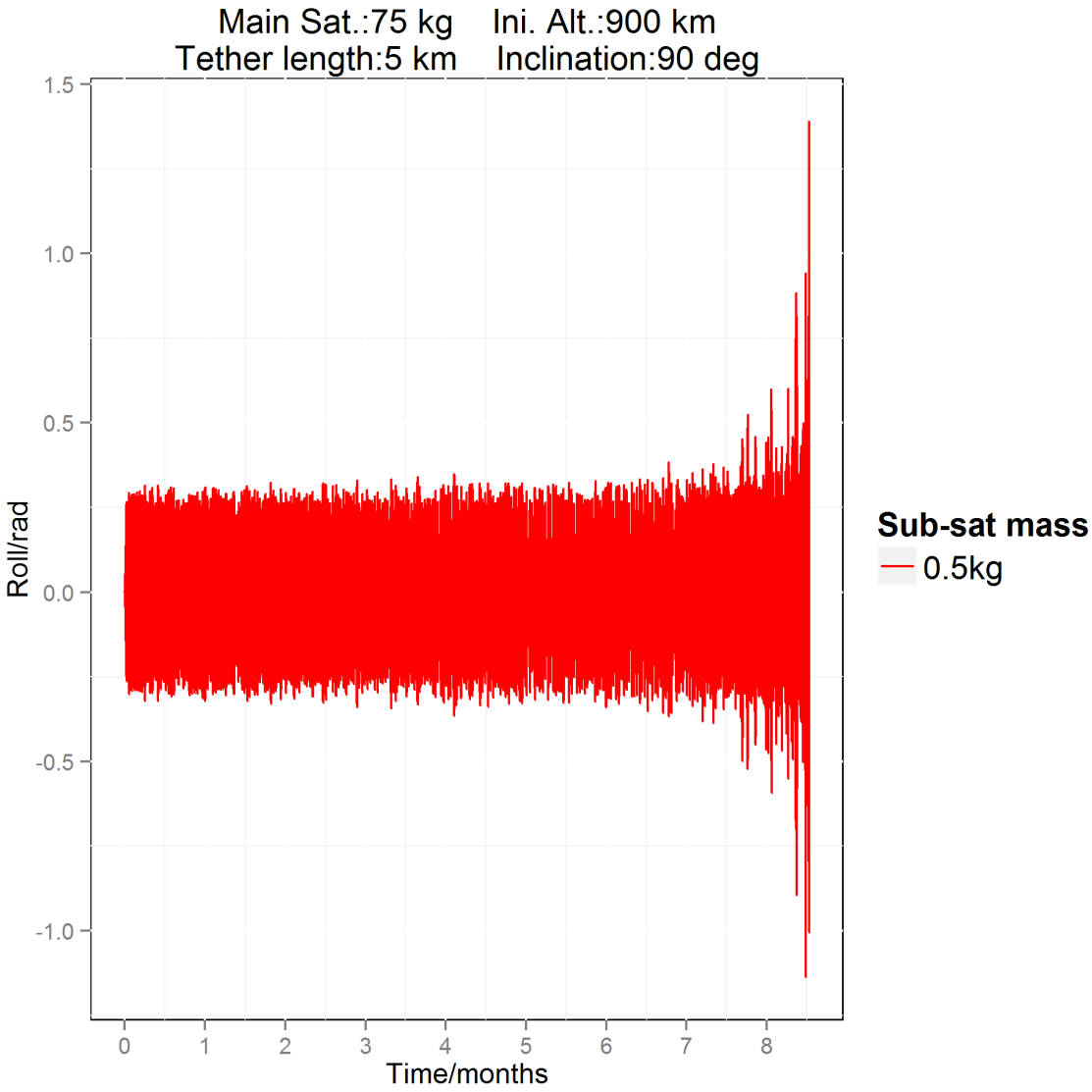

(d)

Figure 3.8 The pitch and roll angles (COMDEV)

Table 3.3 De-orbit from 500km with a light sub-satellite.

Orbit Inclination	90°	Tether Length (km)	1	3	5
		Tether mass (kg)	0.5	1.5	2.5
		Sub-satellite mass (kg)	0.5	1.5	2.5
Masses of main satellite (kg)	75	De-orbit time (days)	33.0	10.0	6.7
		Final altitude (km)	515†	479†	447†
	100	De-orbit time (days)	40.3	3.0	3.7
		Final altitude (km)	489†	494†	506†
	150	De-orbit time (days)	38.7	6.7	2.9
		Final altitude (km)	514†	494†	492†

† -- Simulation stopped when the EDT system starts tumbling.

Table 3.4 De-orbit from 500km with a heavy sub-satellite.

Orbit Inclination	90°	Tether Length (km)	1	3	5
		Tether mass (kg)	0.5	1.5	2.5
		Sub-satellite mass (kg)	1.0	3.0	5.0
Masses of main satellite (kg)	75	De-orbit time (days)	248	48	32
		Final altitude (km)	450†	419†	250†
	100	De-orbit time (days)	266	58	29
		Final altitude (km)	461†	423†	385†
	150	De-orbit time (days)	101	53	44
		Final altitude (km)	504†	445†	386†

† -- Simulation stopped when the EDT system starts tumbling.

3.4 Conclusions from COMDEV Cases

From the results, we conclude:

- Doubling the mass of the sub-satellite caused the space tether system to have longer de-orbit times and to reach a lower de-orbit. This suggests that the extra mass at the sub-satellite end makes the de-orbit more stable.
- The stable de-orbit times from 500 km initial altitude are considerably shorter than those from 900 km initial altitude due the strong electrodynamic force acting on the system.
- In the 900 km initial altitude regime, the tether successfully de-orbits the satellite to an altitude quickly where the air drag would complete the remainder of the de-orbit process for only the 3 km tether and the 5 km tether. For the case of 1km, the EDT is not sufficient to de-orbit the system within 25 years to a region where the air drag dominates.
- In the 500 km initial altitude regime, the tether will become tumbling quickly due to the strong electrodynamic force, without libration control.

3.5 Simple Pitch/Roll Angle Control

3.5.1 Simple Angle Control Strategy

We first discuss the angle control that we implemented in the Simulink model of our space tether system. The EDT system is a simple-input-multiple-output system if there is no thruster on the sub-satellite. The only available control input for the libration control is the electric current in the tether. The crux of the control is that the pitch and roll angles of the tether (measured relative to the vertical the tether would be in after deployment) were

monitored at every time step of the simulation and decisions were made based on their magnitude. If either the pitch or roll angle exceeded 15 degrees, the simulation turned off the electric current in the tether. As the current is switched off, no electrodynamic force is acting on the tether system and it will return to its stable position, the local vertical direction under the gravity effect. In addition, if either the pitch or roll angle reached or exceeded 90 degrees, the simulation would be terminated immediately. At this point, we reasonably assume that the space tether system begins to tumble and the EDT cannot be used anymore.

3.5.2 Results and Discussion

We organise the results in a similar manner to those in the COMDEV's cases. A note about the graphs that follow is that though they appear as filled-in shapes, this is not the reality. Instead, the line simply oscillates frequently for the time scale on the x-axis. Relevant parameters for each case are given atop each graph.

3.5.2.1 Initial Altitude: 500km

The simulation results are shown in Figs. 3.9 ~ 3.11.

The first observation that we can make in this altitude regime is that the space tether system begins to tumble sooner with the old atmospheric model. The newer atmospheric models predict a much longer stable de-orbit period for the space tether system (at least 10 times longer for all cases). This effect is most significantly pronounced with the 1 km tether and with the 3 km tether i.e. in Fig. 3.9 and Fig. 3.10. This indicates that the simulation of de-orbit process is sensitive to the atmospheric model. An accurate and updated atmospheric model, when it becomes available, should always be used in the

simulation.

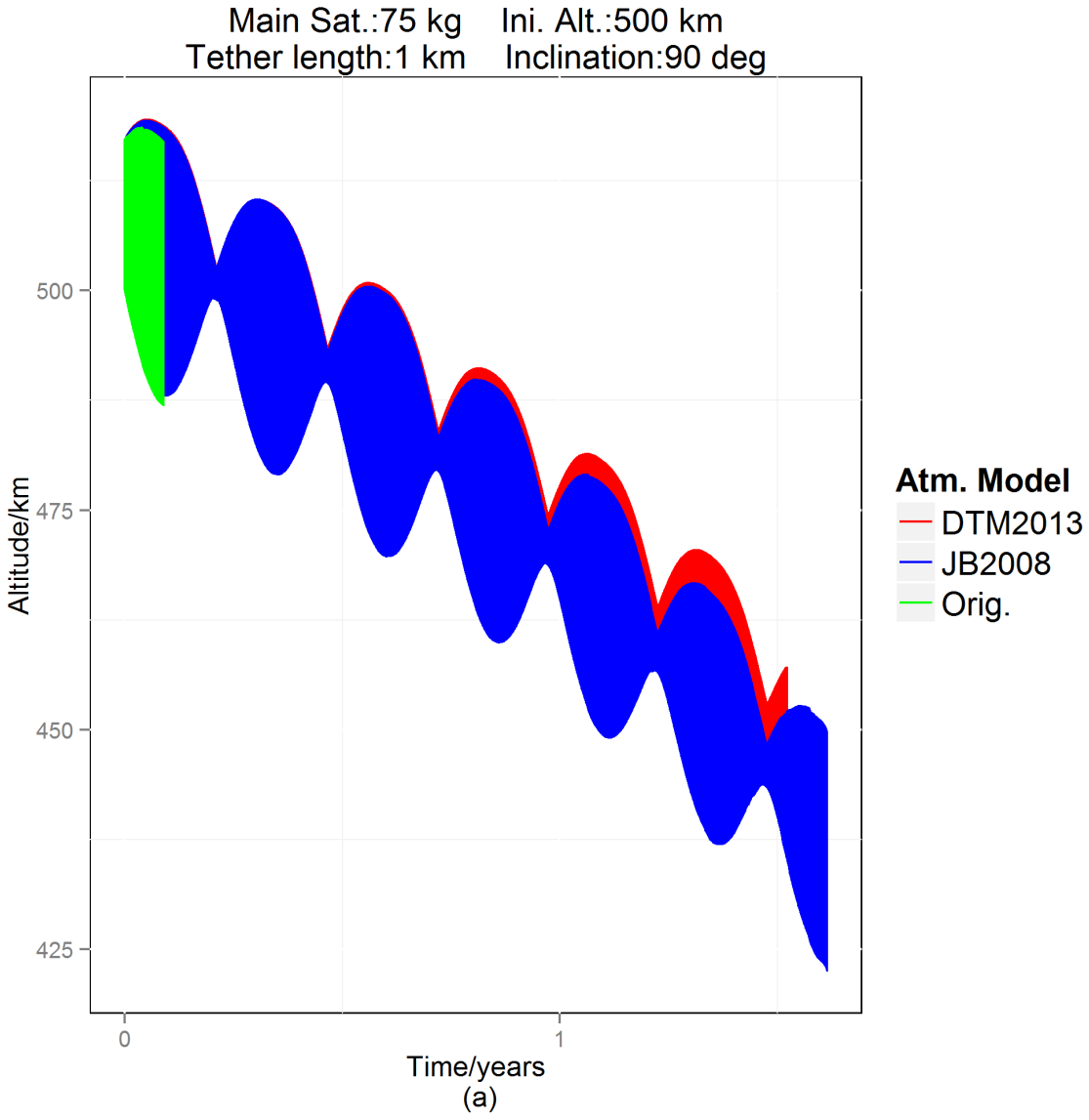
Main Sat.:75 kg Ini. Alt.:500 km
Tether length:1 km Inclination:90 deg
Altitude/km
500
475
450
425
0
1
Time/years
(a)
Atm. Model
DTM2013
JB2008
Orig.

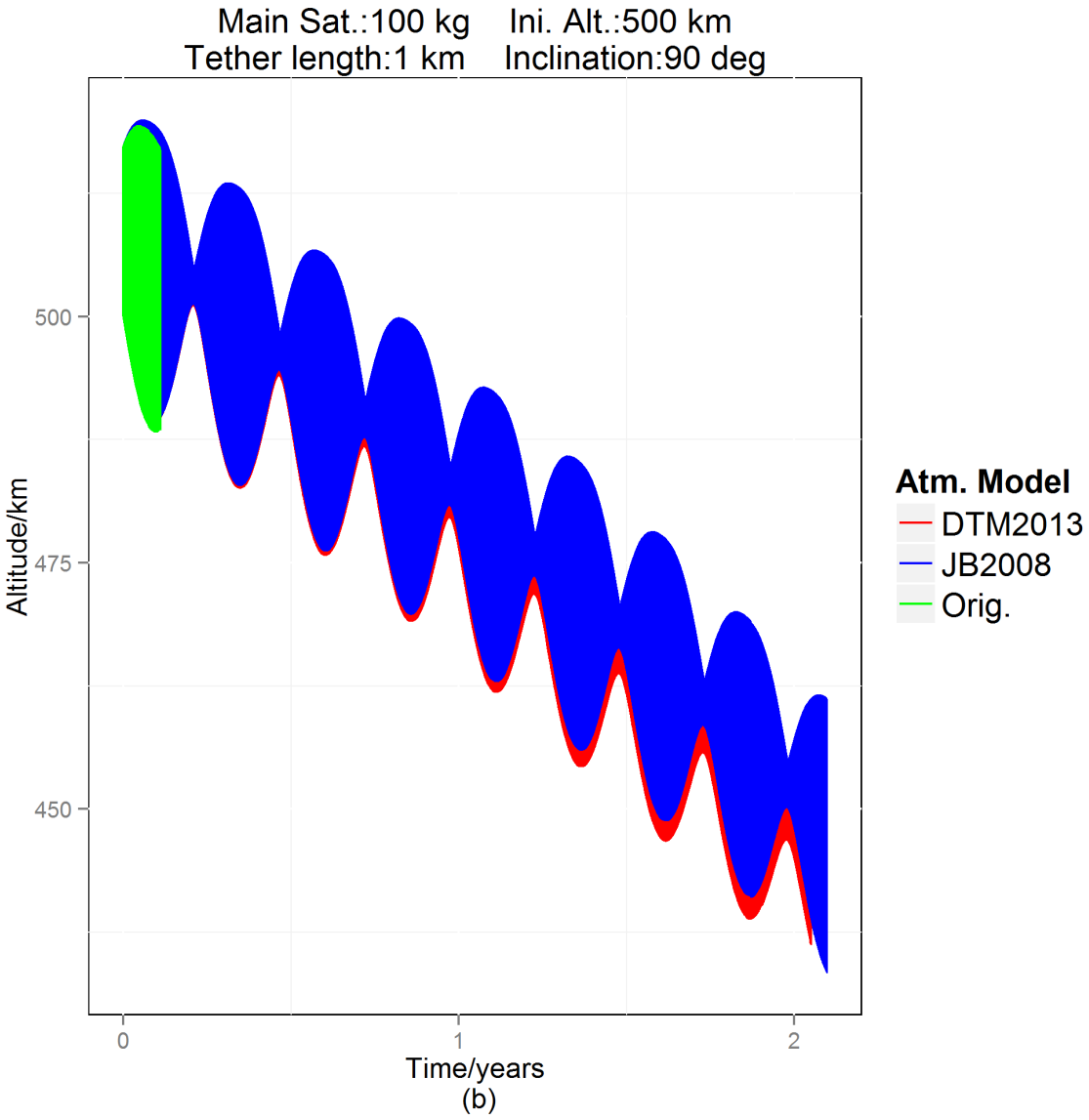
Main Sat.:100 kg Ini. Alt.:500 km
Tether length:1 km Inclination:90 deg
Altitude/km
500
475
450
0
1
2
Time/years
(b)
Atm. Model
DTM2013
JB2008
Orig.

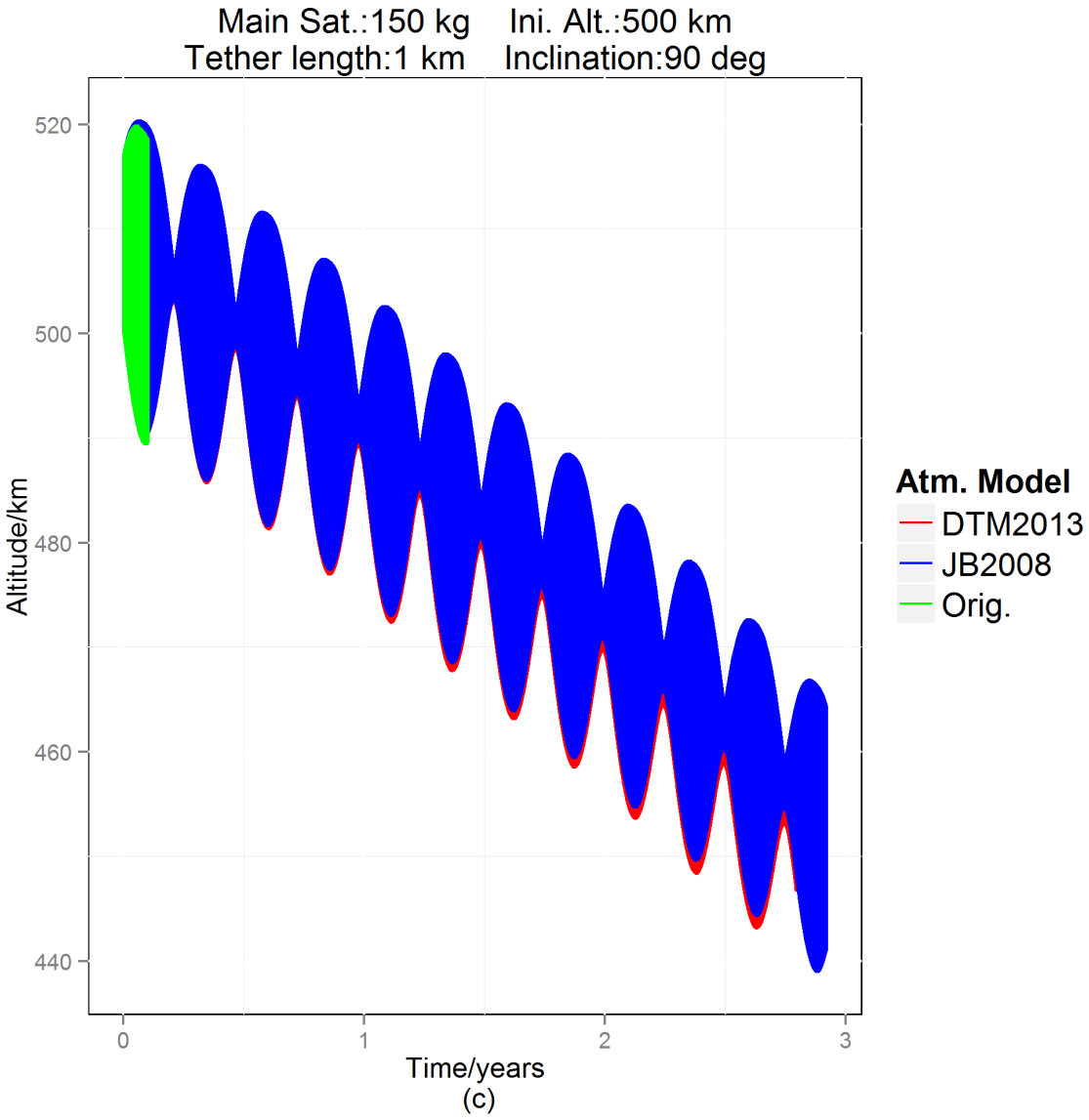

Figure 3.9 Results using the 1 km tether, initial altitude 500 km and main satellite masses of 75 kg, 100 kg, 150 kg (Angle control)

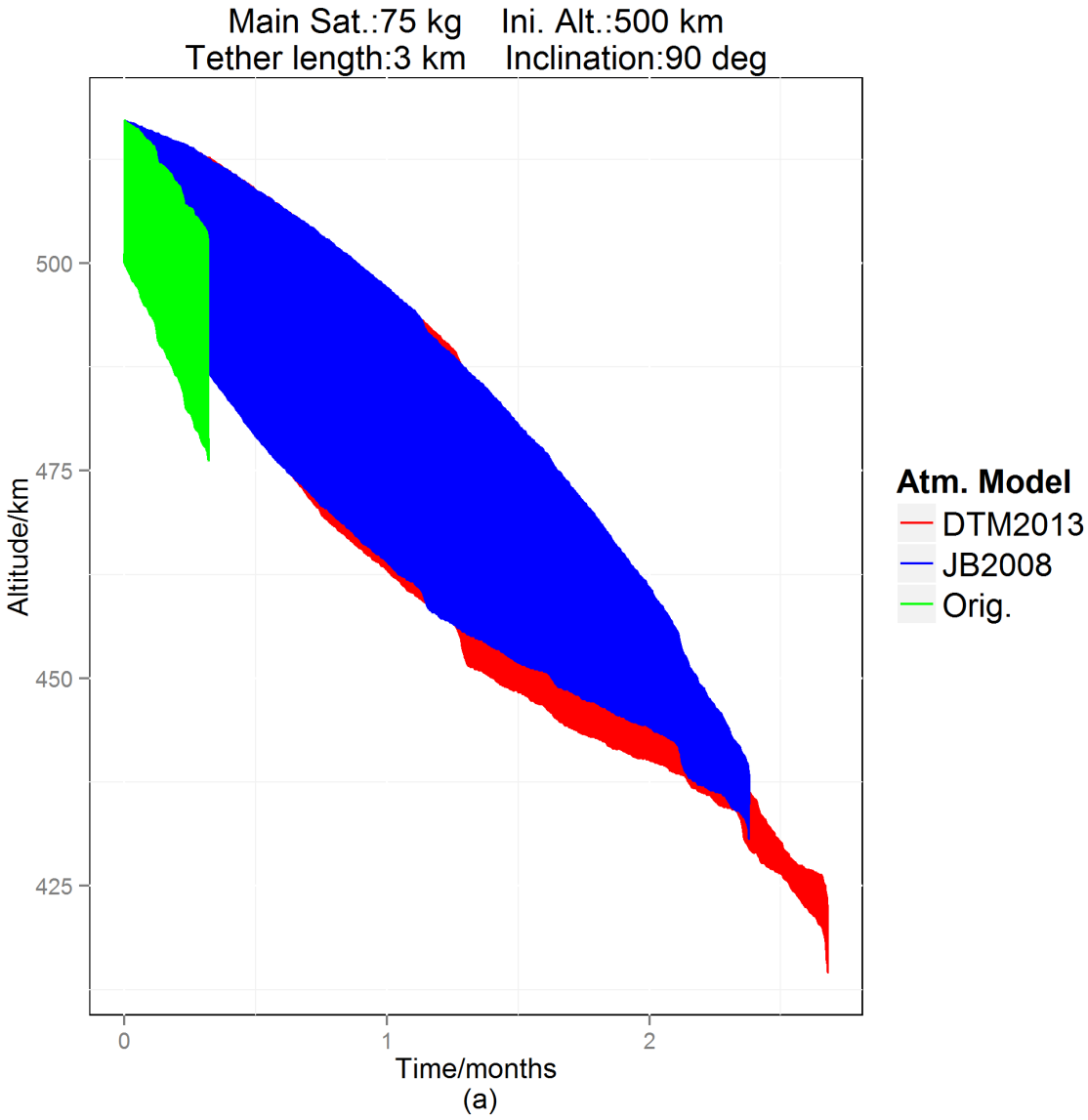
Main Sat.:75 kg Ini. Alt.:500 km
Tether length:3 km Inclination:90 deg
Altitude/km
500
475
450
425
0
1
2
Time/months
(a)
Atm. Model
DTM2013
JB2008
Orig.

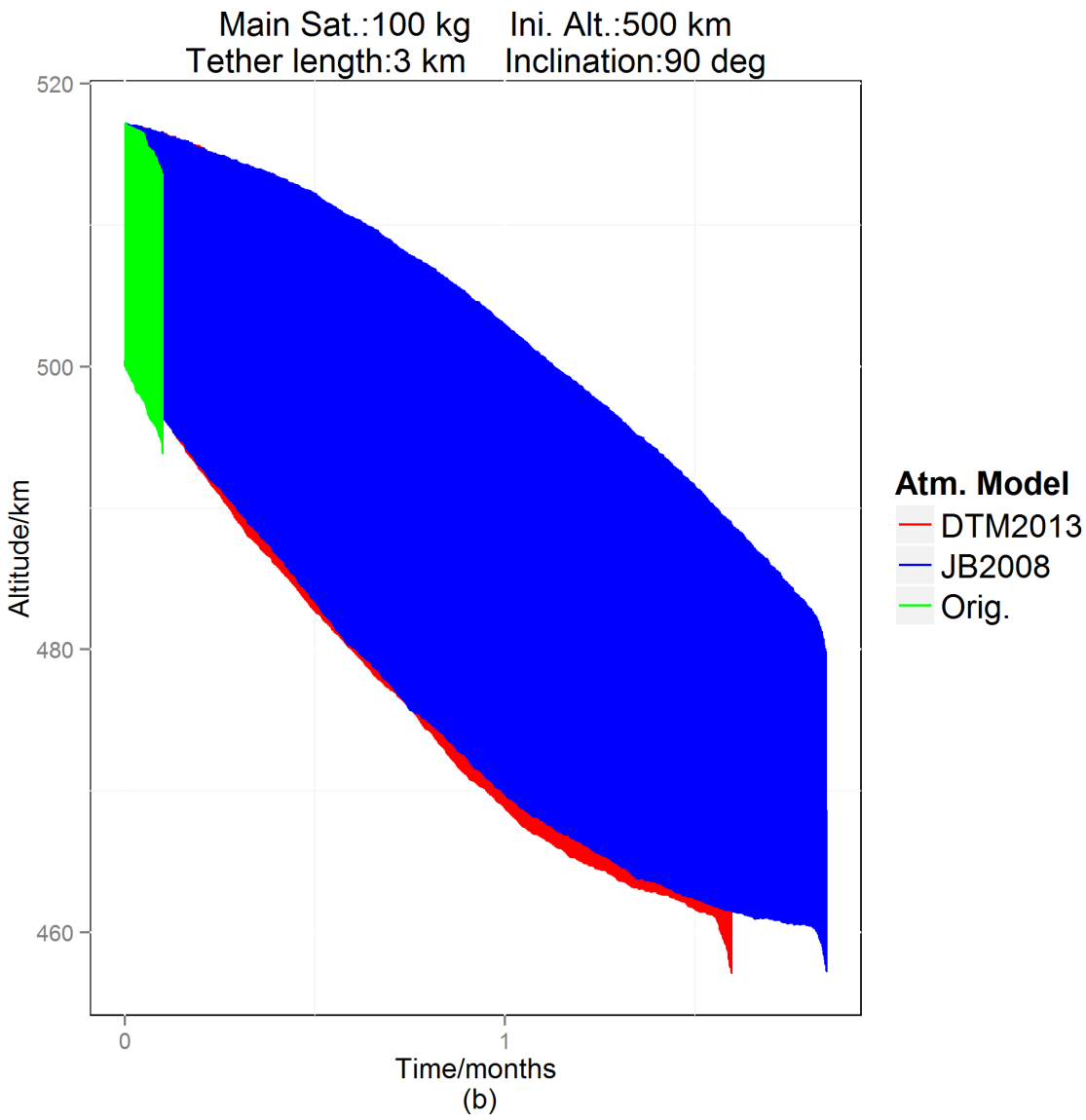
Main Sat.:100 kg Ini. Alt.:500 km
Tether length:3 km Inclination:90 deg
520
500
480
460
Altitude/km
0
1
Time/months
(b)
Atm. Model
DTM2013
JB2008
Orig.

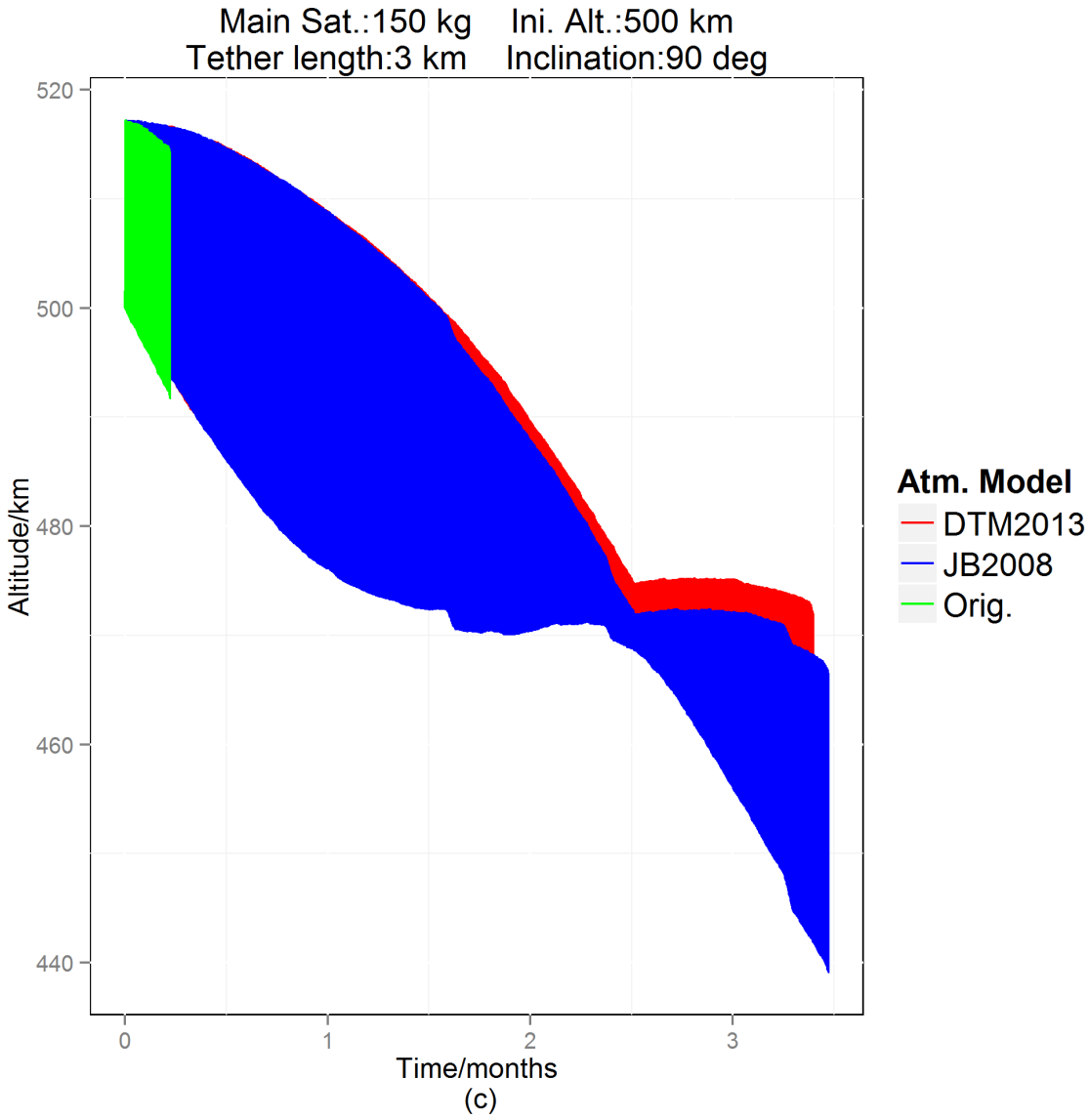

Figure 3.10 Results using the 3 km tether, initial altitude 500 km and main satellite masses of 75 kg, 100 kg, 150 kg (Angle control)

Another observation is that the results from the new atmospheric models are generally in agreement with each other throughout the de-orbit process. Only two cases appear to deviate from this trend and both involve the 5 km tether as seen in Fig. 3.11 (a) and (b). With the longest tether, the Lorentz force generated is the largest thus making the tether more difficult to control by the simple angle control strategy. Consequently, we get much

shorter stable de-orbit times for this tether length since the space tether system will begin to tumble faster. Therefore, whatever difference there is in the two new atmospheric models may appear magnified in a shorter period. Additionally, this may be why we do not see a significantly longer stable de-orbit period with the newer atmospheric models using the 5 km tether (Fig. 3.11). With this tether length, the tether becomes most energetic as more energy being pumped into the tether system and naturally more prone to causing the space tether system to tumble.

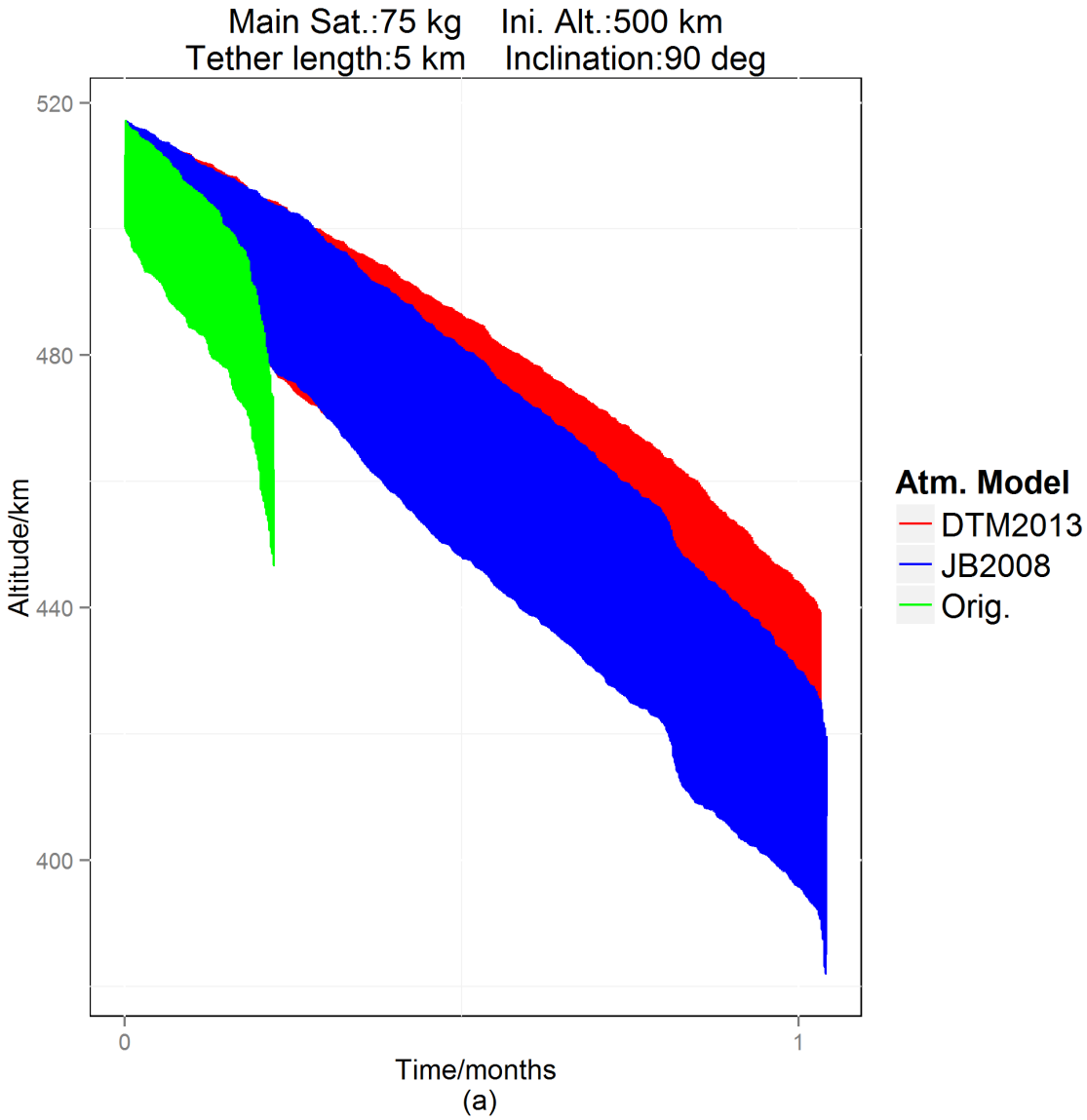

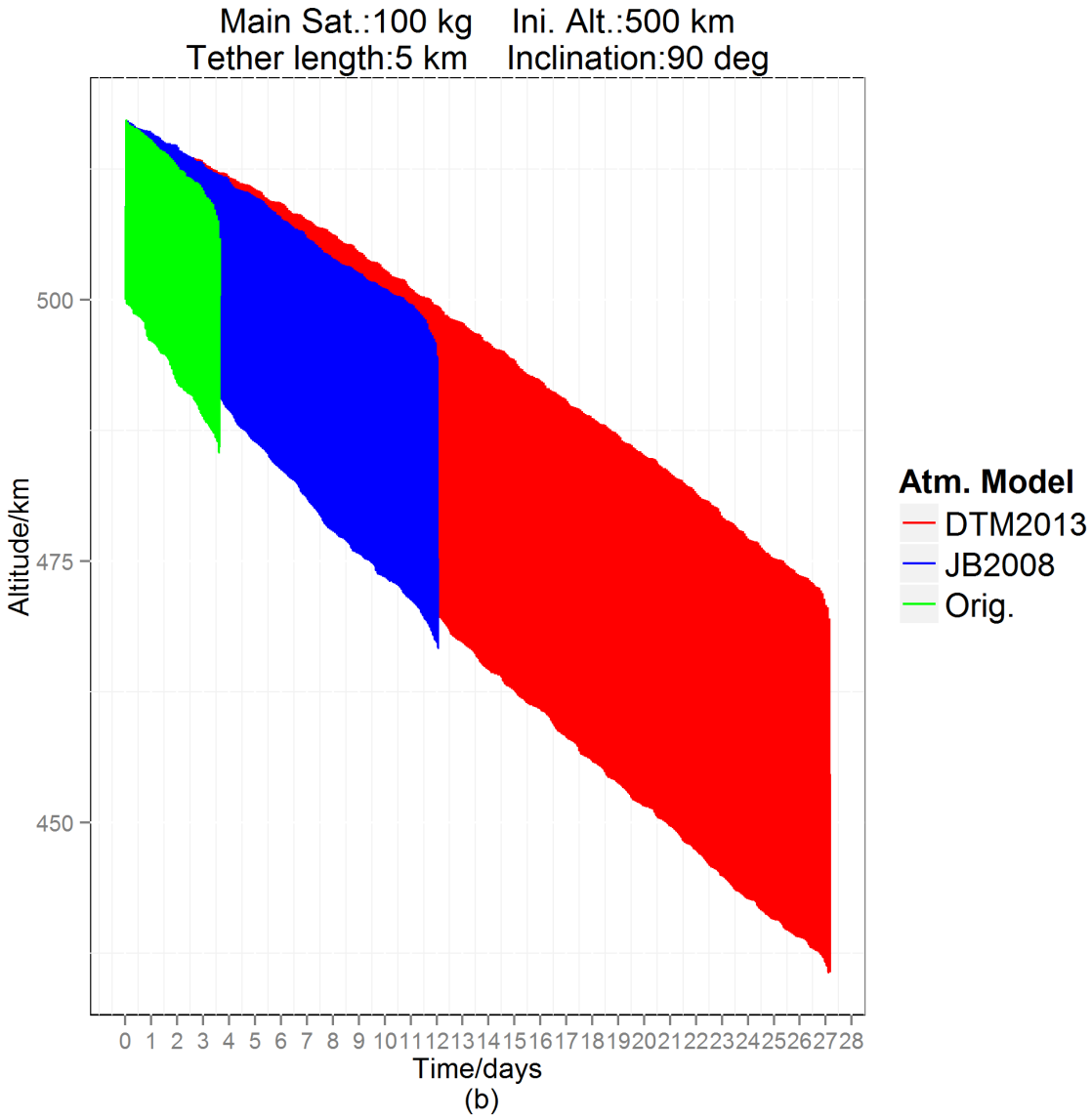
Main Sat.:100 kg Ini. Alt.:500 km
Tether length:5 km Inclination:90 deg
Altitude/km
500
475
450
0 1 2 3 4 5 6 7 8 9 10 11 12 13 14 15 16 17 18 19 20 21 22 23 24 25 26 27 28
Time/days
Atm. Model
DTM2013
JB2008
Orig.
(b)

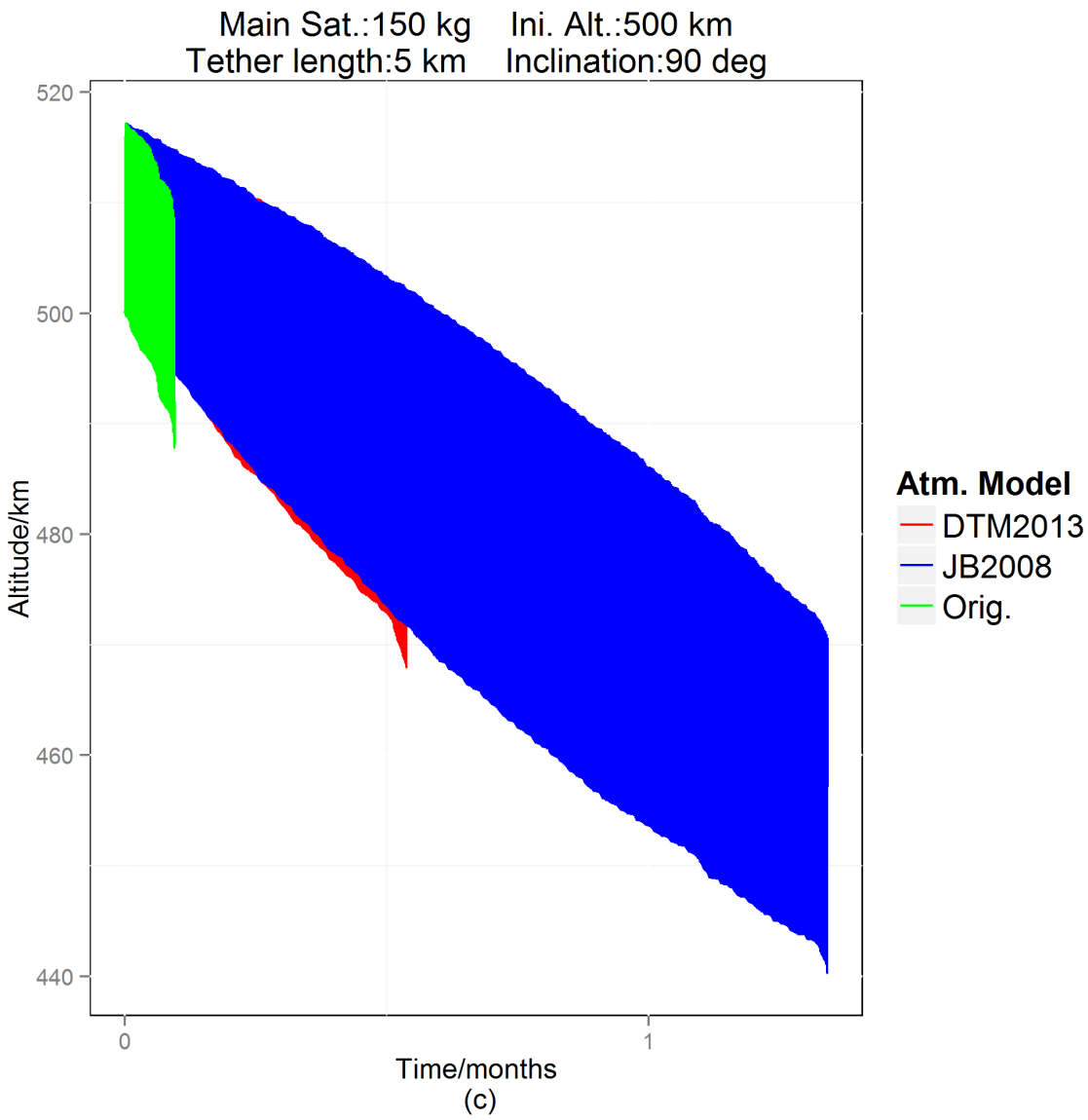

Figure 3.11 Results using the 5 km tether, initial altitude 500 km and main satellite masses of 75 kg, 100 kg, 150 kg (Angle control)

A third observation is that the space tether system did not de-orbit to its target altitude of 250 km in any of these cases. The electrodynamic force is proportional to the plasma density. The plasma density increases as the altitude reduces and peaks around 400km. As mentioned early, the instability of the tether system is due to the EDT pumps energy into the system. The strong electrodynamic force in this altitude regime makes the simple

angle control strategy not suitable. This suggests that it is better to control the libration energy than the libration angles, which will be studied in the next Chapter.

In summary, the effect of simple angle control is very limited when the electrodynamic force is strong and the control of libration energy should be investigated.

3.5.2.2 Initial Altitude: 900 km

The simulation results are shown in Figs. 3.12 ~ 3.15.

This altitude regime shows some similarities to the previous one. For the 3 km and 5 km tether cases (seen in Fig. 3.13 and Fig. 3.14), we notice a trend where the new atmospheric models are in close agreement with each other. Further, the new atmospheric models predict that the space tether system will de-orbit stably for a much longer period and, also, to a lower altitude.

Another observation that is well pronounced in this altitude regime is the impact of the mass of the main satellite on the de-orbit time of the space tether system. Specifically, we see that the heavier main satellites have a longer de-orbit time and a higher final altitude for the same tether length (3 km and 5 km) due to larger orbital kinetic energy (Figs. 3.13 (b), (c) and 3.14 (b), (c)). For the cases of sub-satellite, the heavier sub-satellites provide larger restoring moment due to the gravity to stabilize the tether system, leading to a longer stable de-orbiting period. The phenomenon can be explained by considering the ratio of the masses of the main satellite and the sub-satellite. A large ratio between these two quantities seems to lead to a less efficient de-orbit. From the Simulink model, we found that this ratio has a positive correlation to the perturbation due to oblateness on the tether segment. This means that a larger ratio of the two masses causes a larger perturbation in the tether segment (due to oblateness). Consequently, the tether

will breach the 15 degree threshold imposed by the simulation more frequently. During these times, the de-orbit is only caused by atmospheric drag that is orders of magnitude less than the electrodynamic force. Additionally, stronger perturbations on the tether will make the space tether system tumbling more easily. Thus, for heavier tmain satellites, we have a less efficient de-orbit in terms of both time and final altitude.

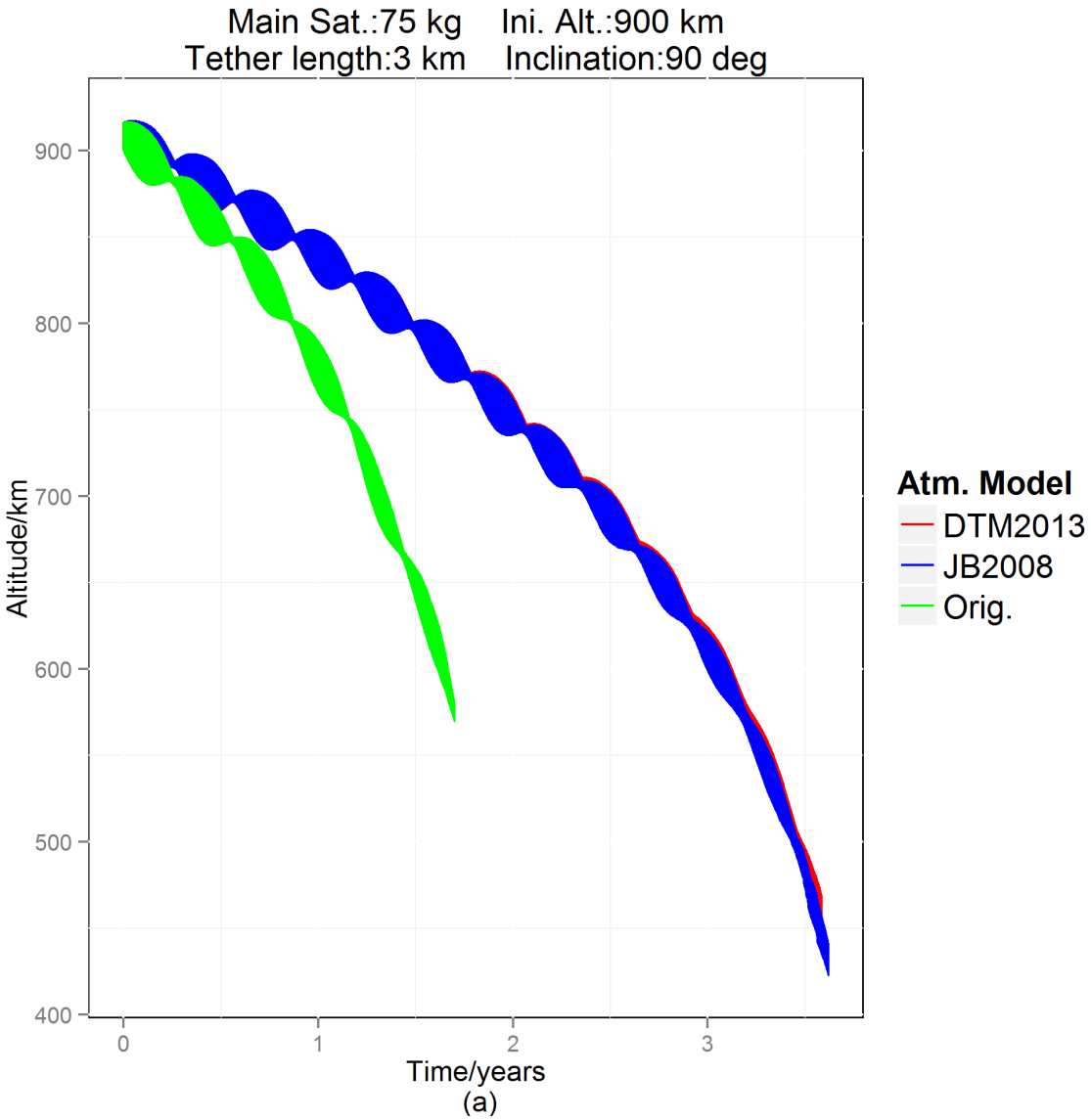

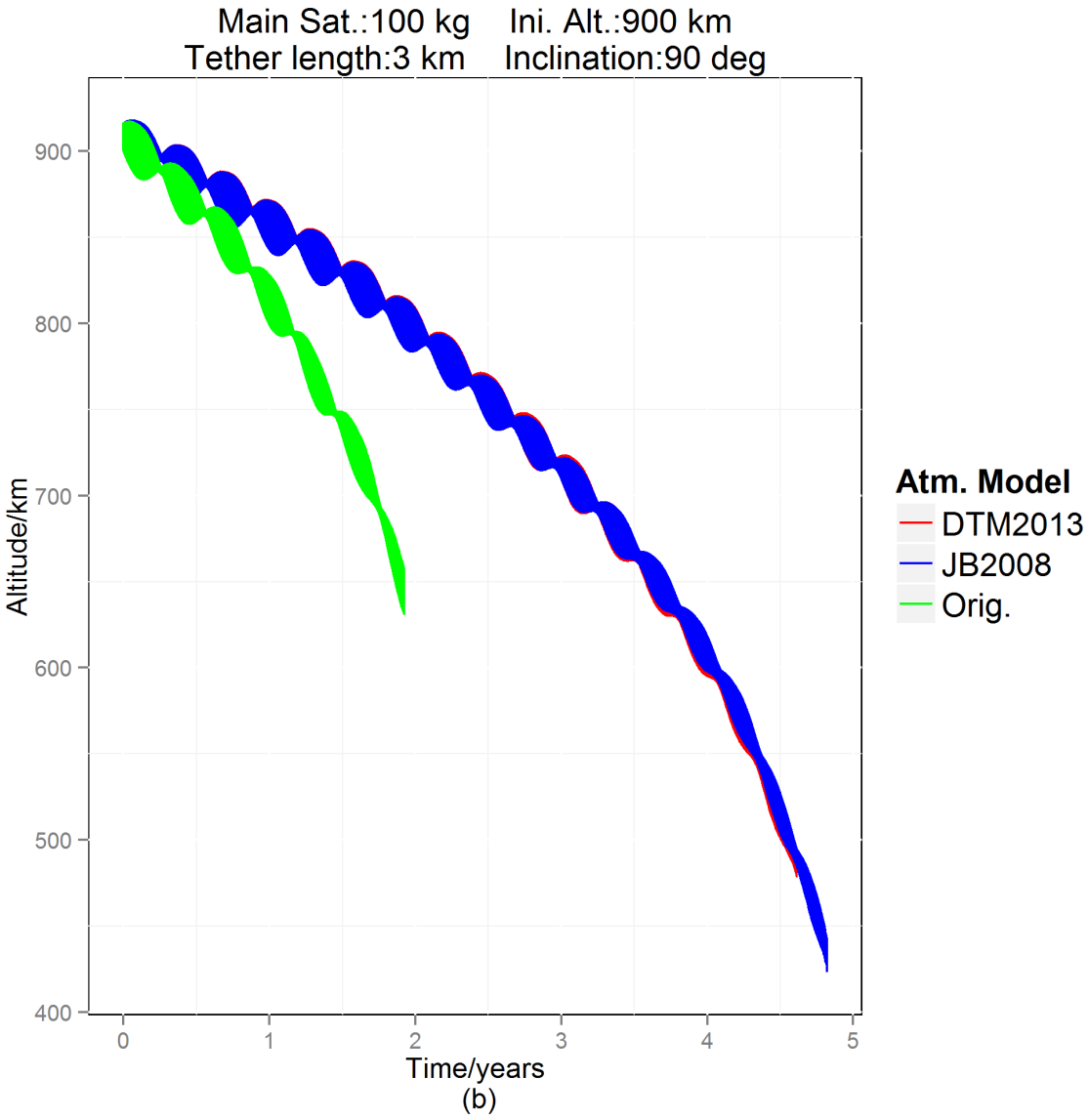
Main Sat.:100 kg Ini. Alt.:900 km
Tether length:3 km Inclination:90 deg
Altitude/km
900
800
700
600
500
400
0
1
2
3
4
5
Time/years
Atm. Model
DTM2013
JB2008
Orig.
(b)

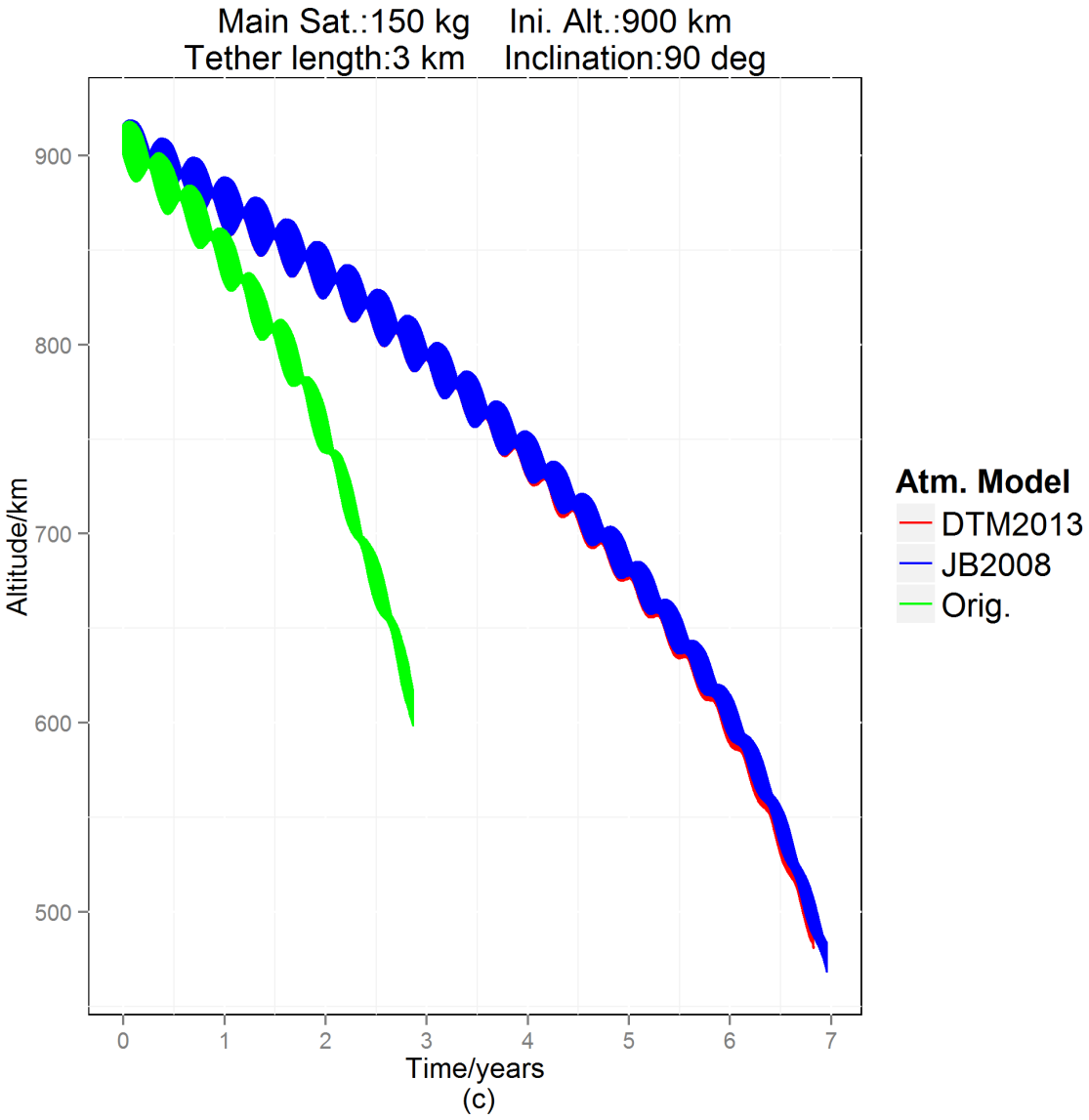

Figure 3.12 Results using the 3 km tether, initial altitude 900 km and main satellite masses of 75 kg, 100 kg, 150 kg (Angle control)

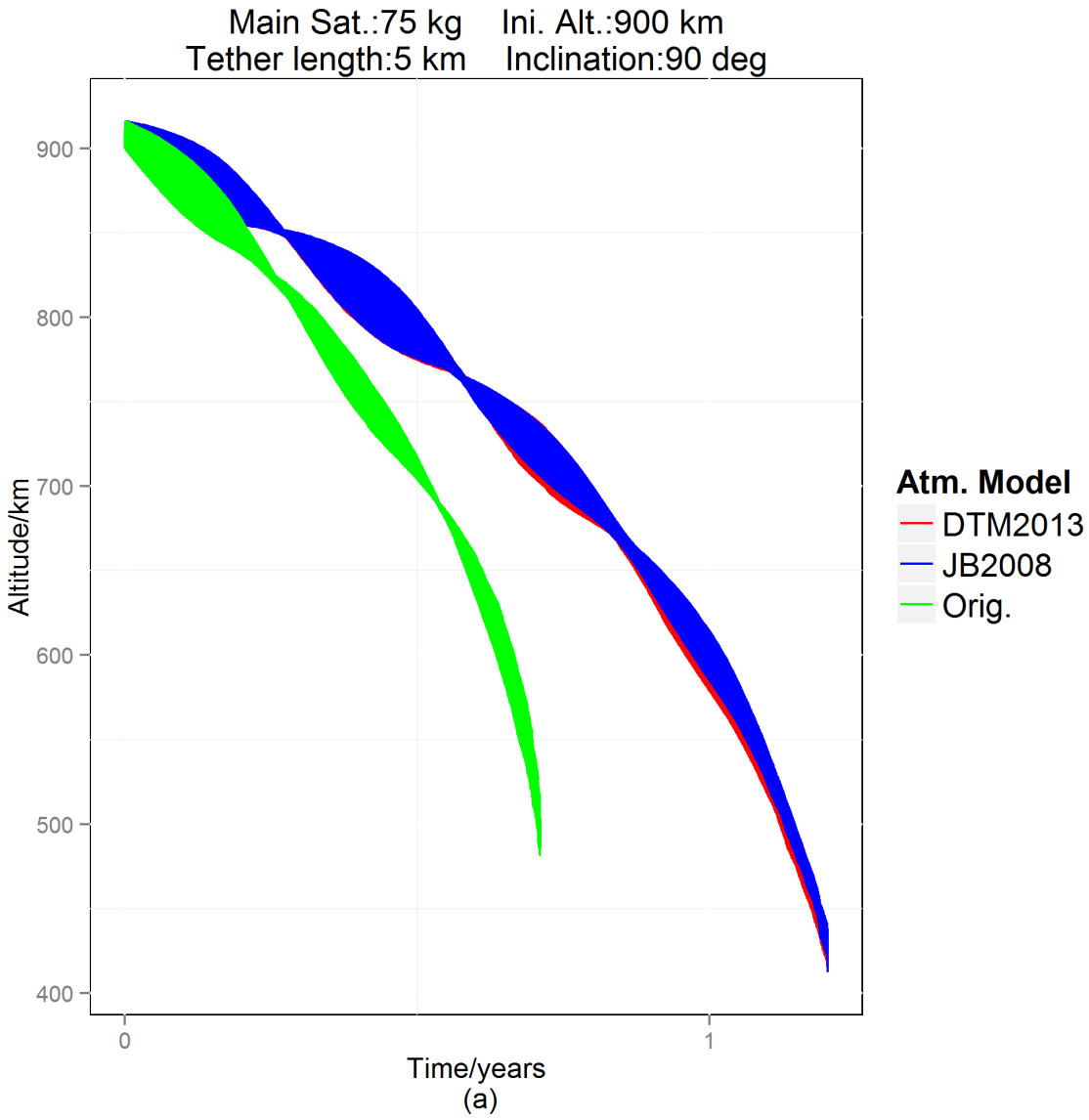
Main Sat.:75 kg Ini. Alt.:900 km
Tether length:5 km Inclination:90 deg
900
800
700
600
500
400
Altitude/km
0
1
Time/years
(a)
Atm. Model
DTM2013
JB2008
Orig.

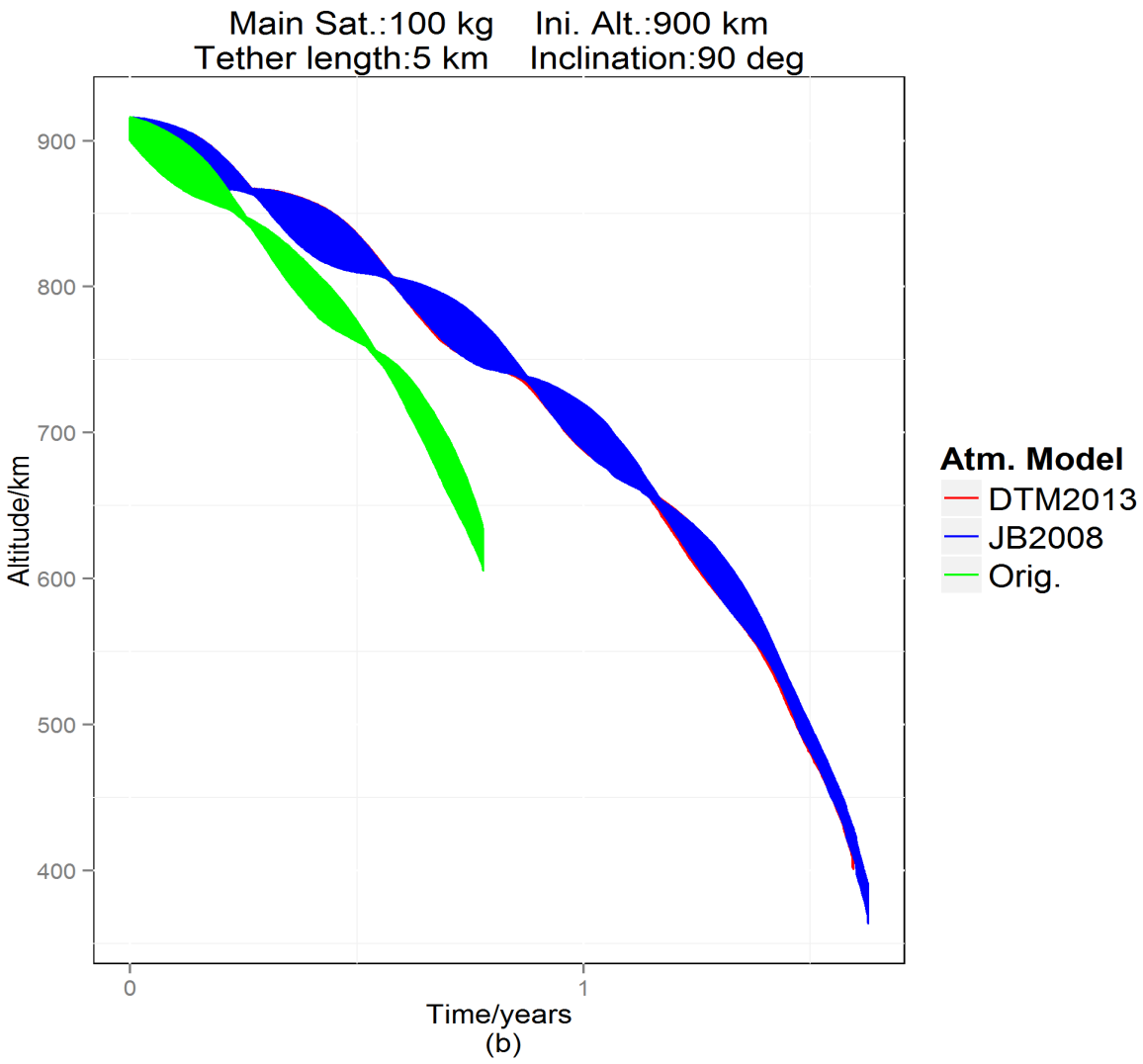
Main Sat.:100 kg Ini. Alt.:900 km
Tether length:5 km Inclination:90 deg
900
800
700
600
500
400
Altitude/km
0
1
Time/years
(b)
Atm. Model
DTM2013
JB2008
Orig.

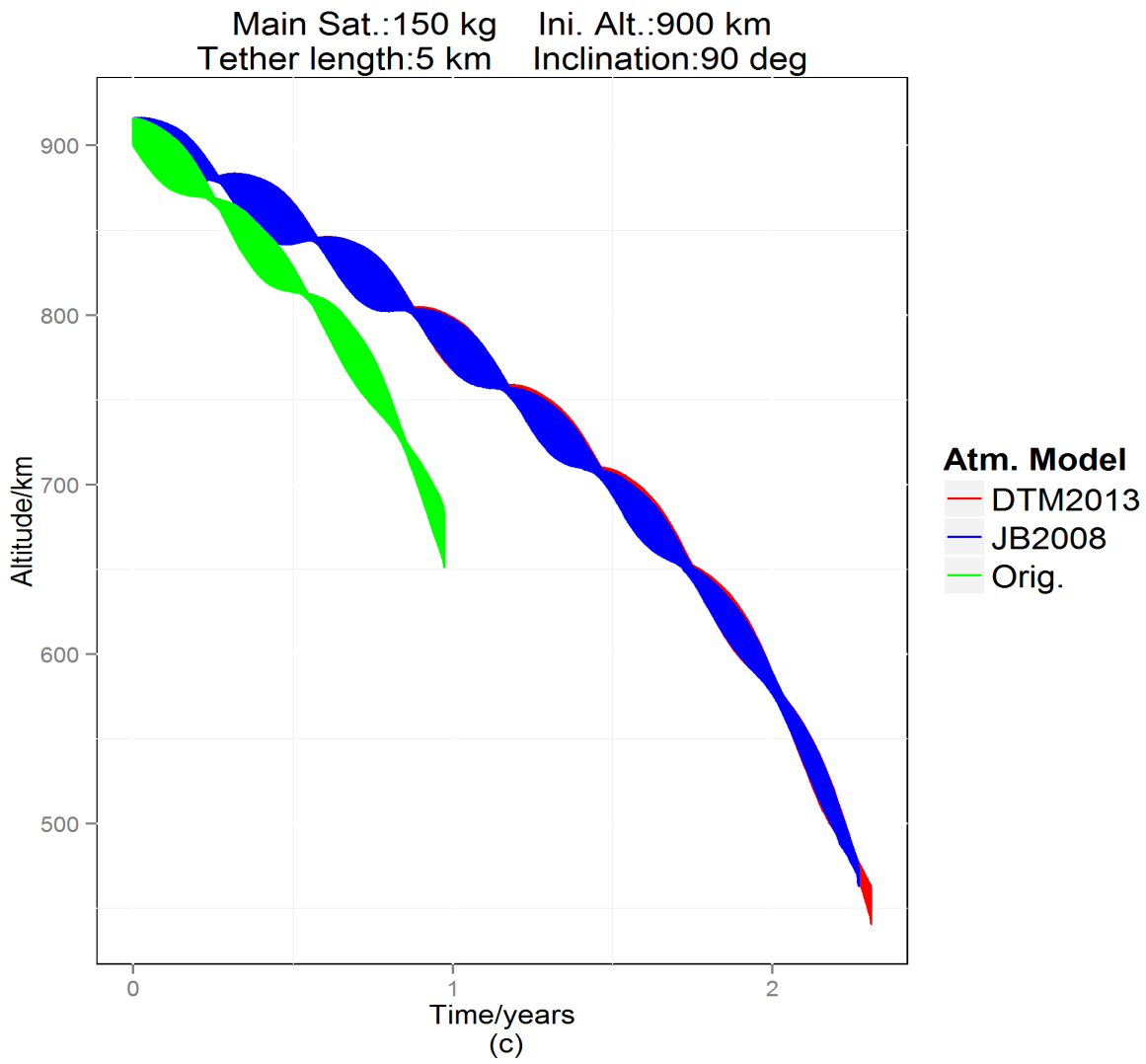

Figure 3.13 Results using the 5 km tether, initial altitude 900 km and main satellite masses of 75 kg, 100 kg, 150 kg (Angle control)

There is some deviation from this trend for the 1 km tether cases as seen in Fig. 3.12. Here, we see a significant difference in the behaviour of the new atmospheric models especially in Fig. 3.12 (b) and (c). However, both still predict a longer stable de-orbit period than the old atmospheric model. Note that, in these cases, the simulation reached its maximum time limit of 25 years. The space tether system did not tumble until this time and could remain stable for some time after.

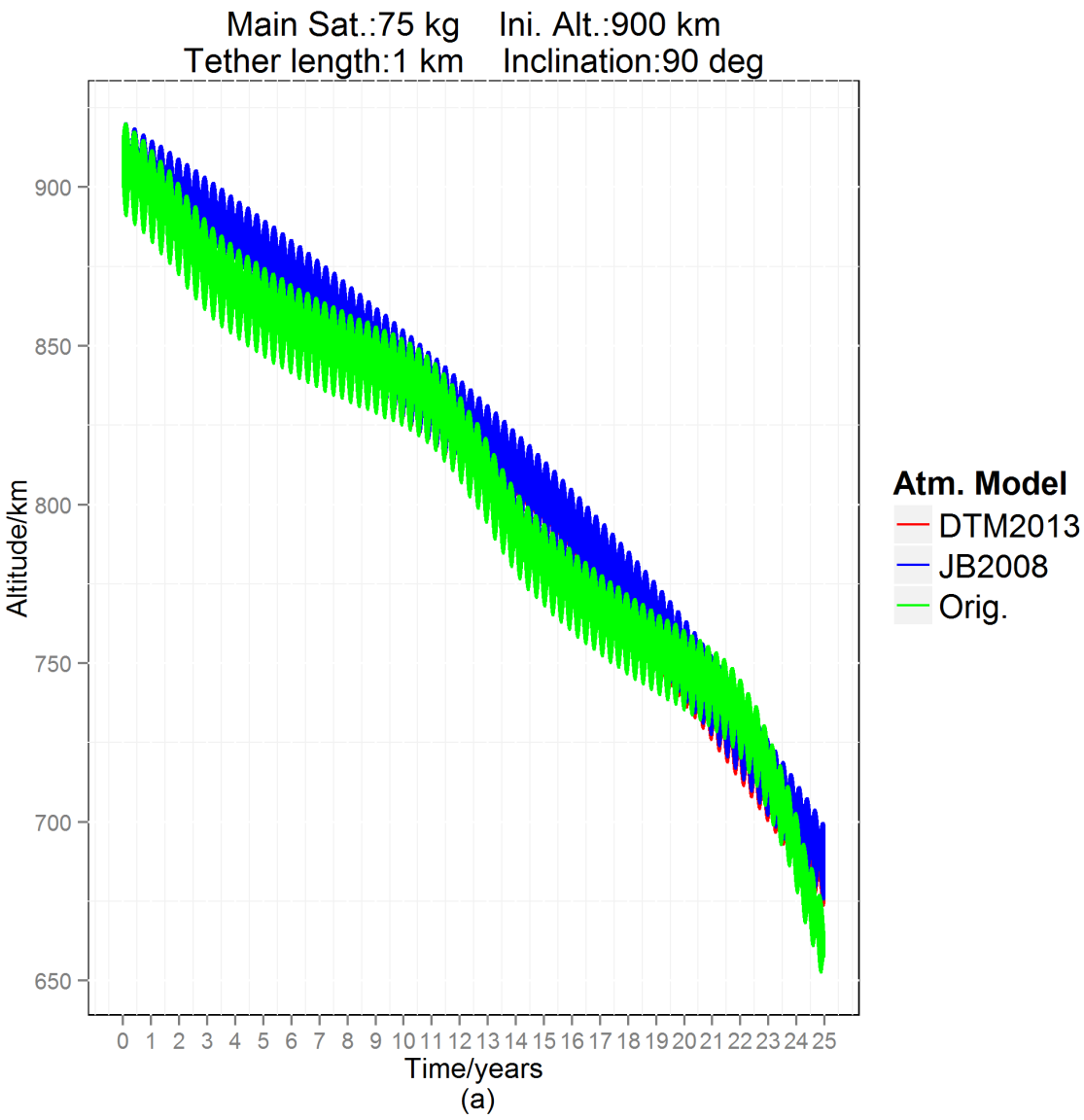
Main Sat.:75 kg Ini. Alt.:900 km
Tether length:1 km Inclination:90 deg
Altitude/km
900
850
800
750
700
650
0 1 2 3 4 5 6 7 8 9 10 11 12 13 14 15 16 17 18 19 20 21 22 23 24 25
Time/years
(a)
Atm. Model
DTM2013
JB2008
Orig.

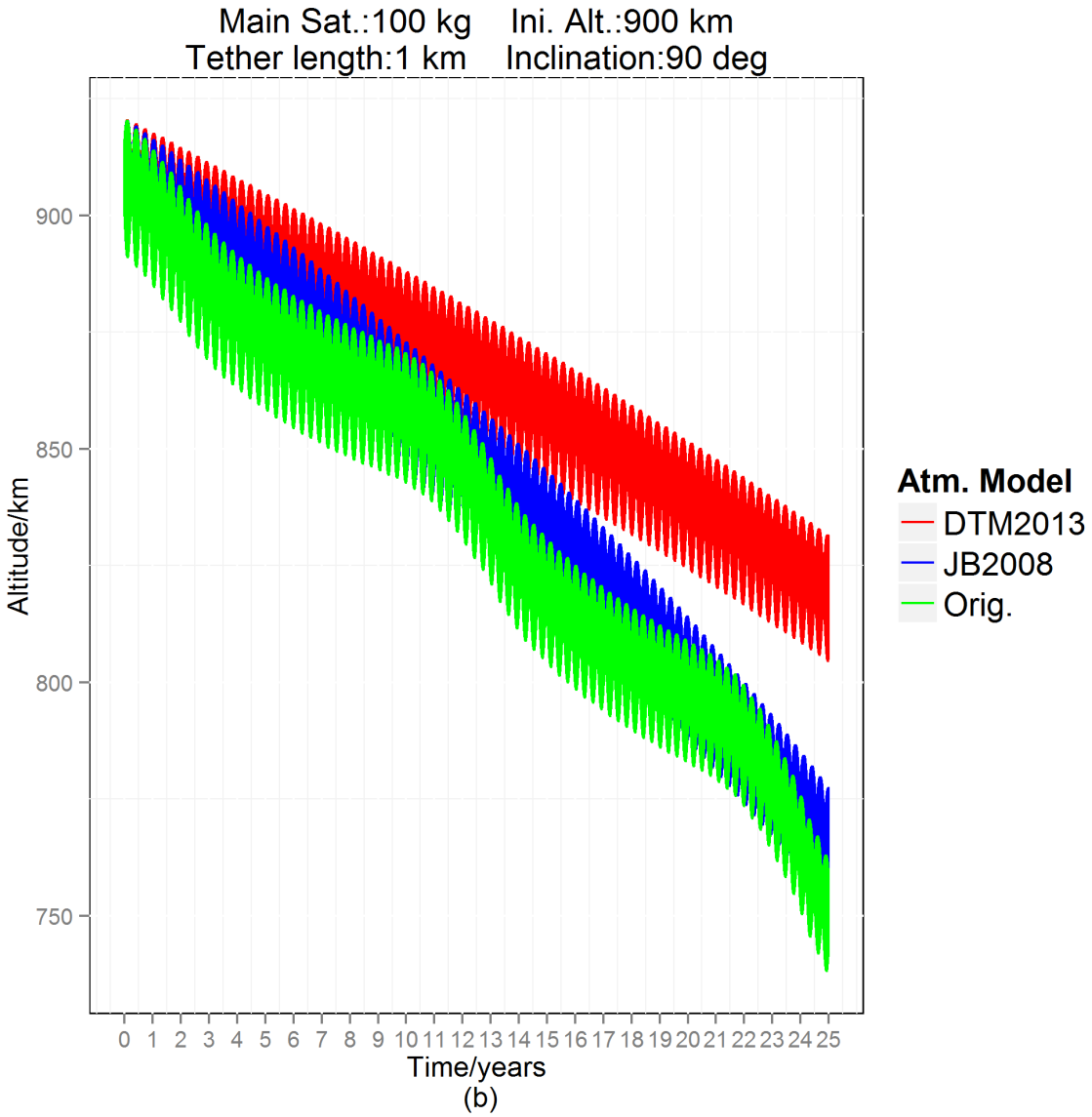
Main Sat.:100 kg Ini. Alt.:900 km
Tether length:1 km Inclination:90 deg
Altitude/km
900
850
800
750
0 1 2 3 4 5 6 7 8 9 10 11 12 13 14 15 16 17 18 19 20 21 22 23 24 25
Time/years
Atm. Model
DTM2013
JB2008
Orig.
(b)

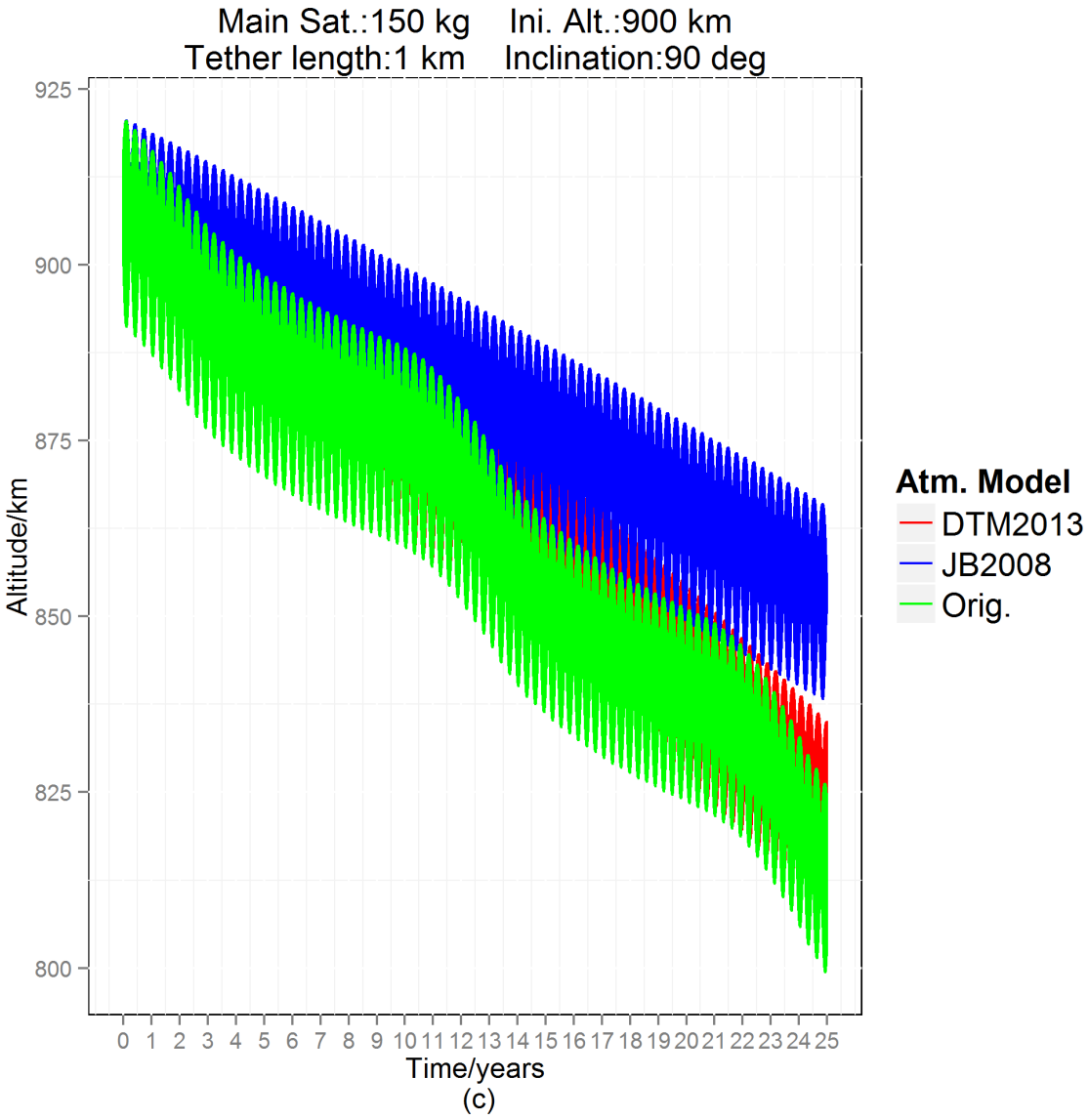

Figure 3.14 Results using the 1 km tether, initial altitude 900 km and main satellite masses of 75 kg, 100 kg, 150 kg (Angle control)

We now consider Figure 3.15 that gives us a cross section of the pitch and roll angles for all of the cases run. Though these graphs appear as filled-in shapes, this is not the case; the angles are simply oscillating rapidly with respect to the time scale. If we consider Fig. 3.15 (a) and (c), we immediately notice that the roll was consistently larger than the pitch throughout the 25 years. For approximately the first 21 years of de-orbit

process, the roll was consistently near the imposed threshold of 15 degrees (0.26 rad) while the pitch was only occasionally near the threshold; the pitch was often well below the threshold. This faster destabilisation of the roll in inclined orbits is expected and is due to the out-of-plane disturbance [22]. For the final 4 years of the de-orbit, the pitch and roll begin to escalate beyond the 15 degrees threshold. This is because the effect of the air drag becomes more prominent at lower altitudes causing more perturbations to the tether. Figures 3.15 (b) and (d) show how the pitch and roll angles behave when the space tether system begins to tumble. When the system begins to tumble, the angles quickly increase to the simulation's termination value of 90 degrees.

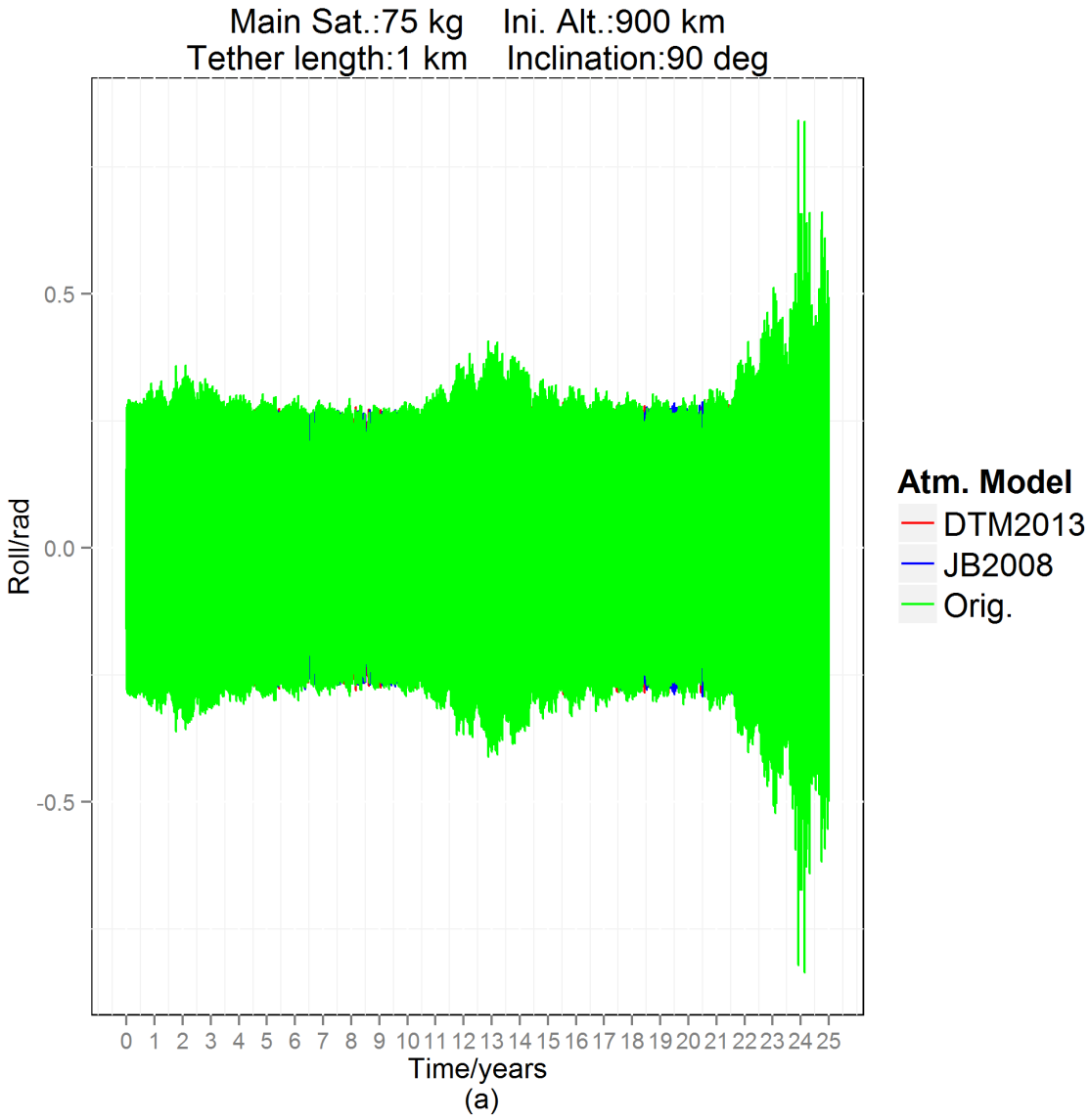
Main Sat.:75 kg Ini. Alt.:900 km
Tether length:1 km Inclination:90 deg
Roll/rad
0.5
0.0
-0.5
0 1 2 3 4 5 6 7 8 9 10 11 12 13 14 15 16 17 18 19 20 21 22 23 24 25
Time/years
(a)
Atm. Model
DTM2013
JB2008
Orig.

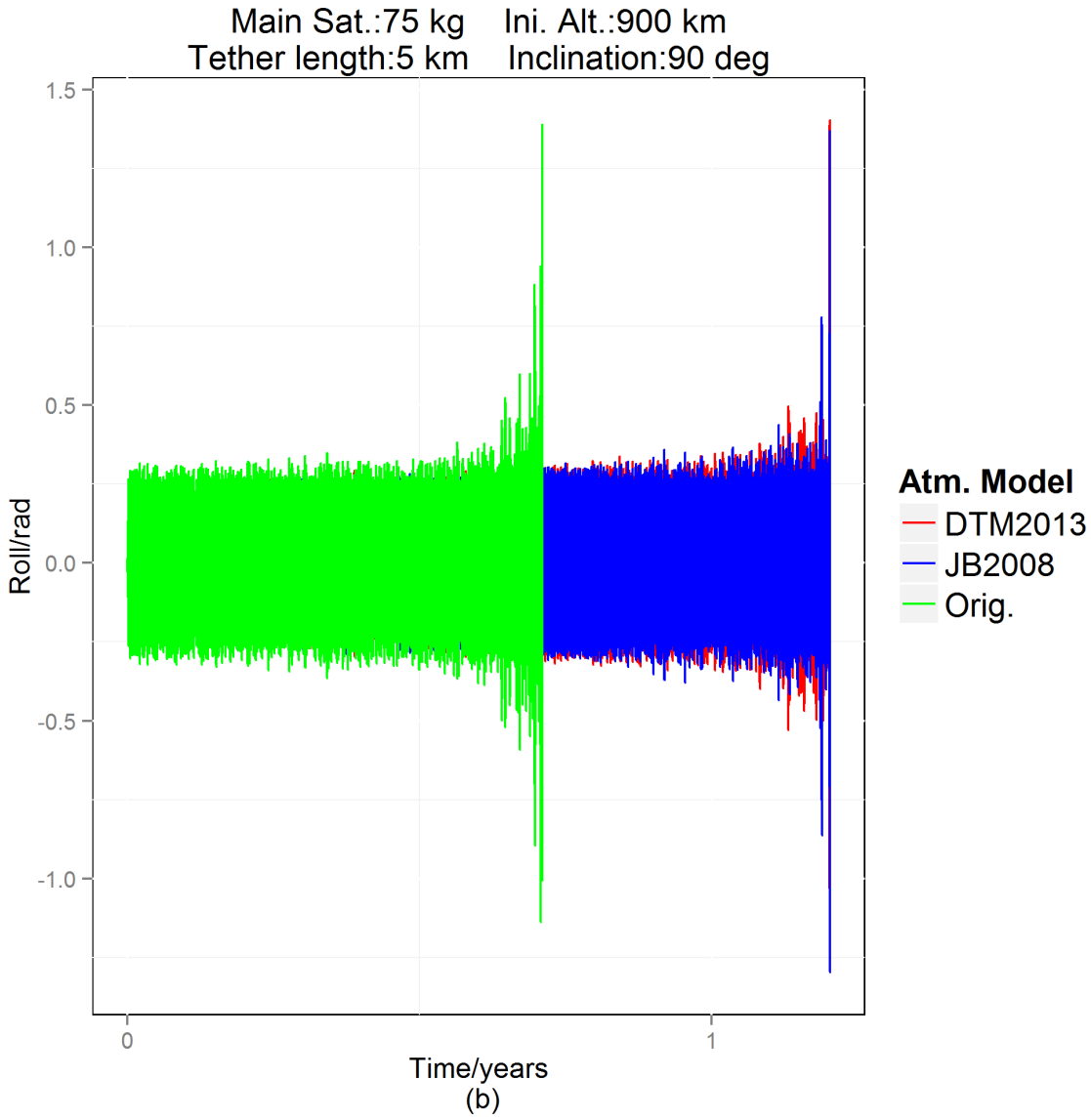
Main Sat.:75 kg Ini. Alt.:900 km
Tether length:5 km Inclination:90 deg
1.5
1.0
0.5
0.0
-0.5
-1.0
Roll/rad
0
1
Time/years
(b)
Atm. Model
DTM2013
JB2008
Orig.

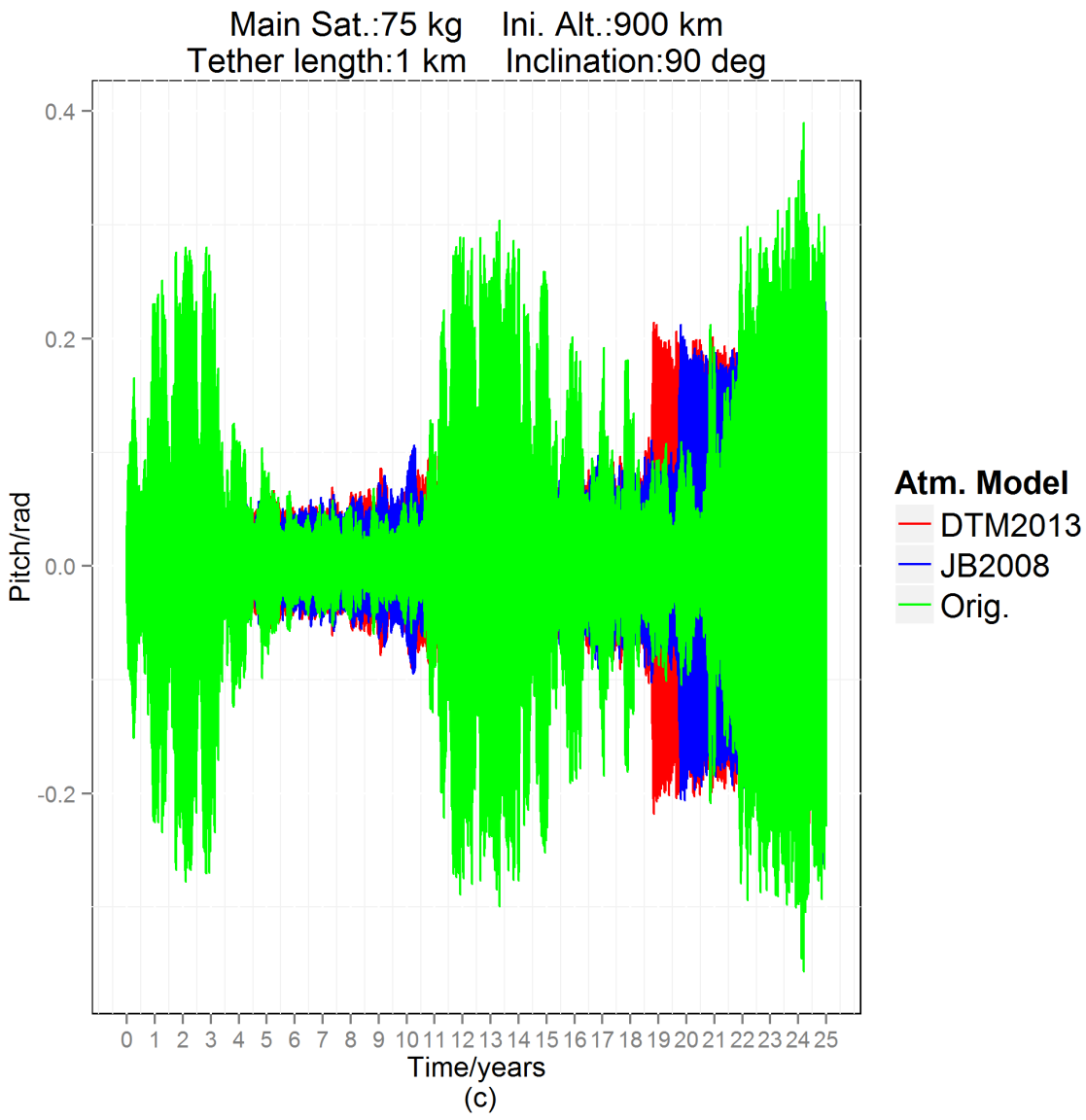
Main Sat.:75 kg Ini. Alt.:900 km
Tether length:1 km Inclination:90 deg
Pitch/rad
0.4
0.2
0.0
-0.2
0 1 2 3 4 5 6 7 8 9 10 11 12 13 14 15 16 17 18 19 20 21 22 23 24 25
Time/years
(c)
Atm. Model
DTM2013
JB2008
Orig.

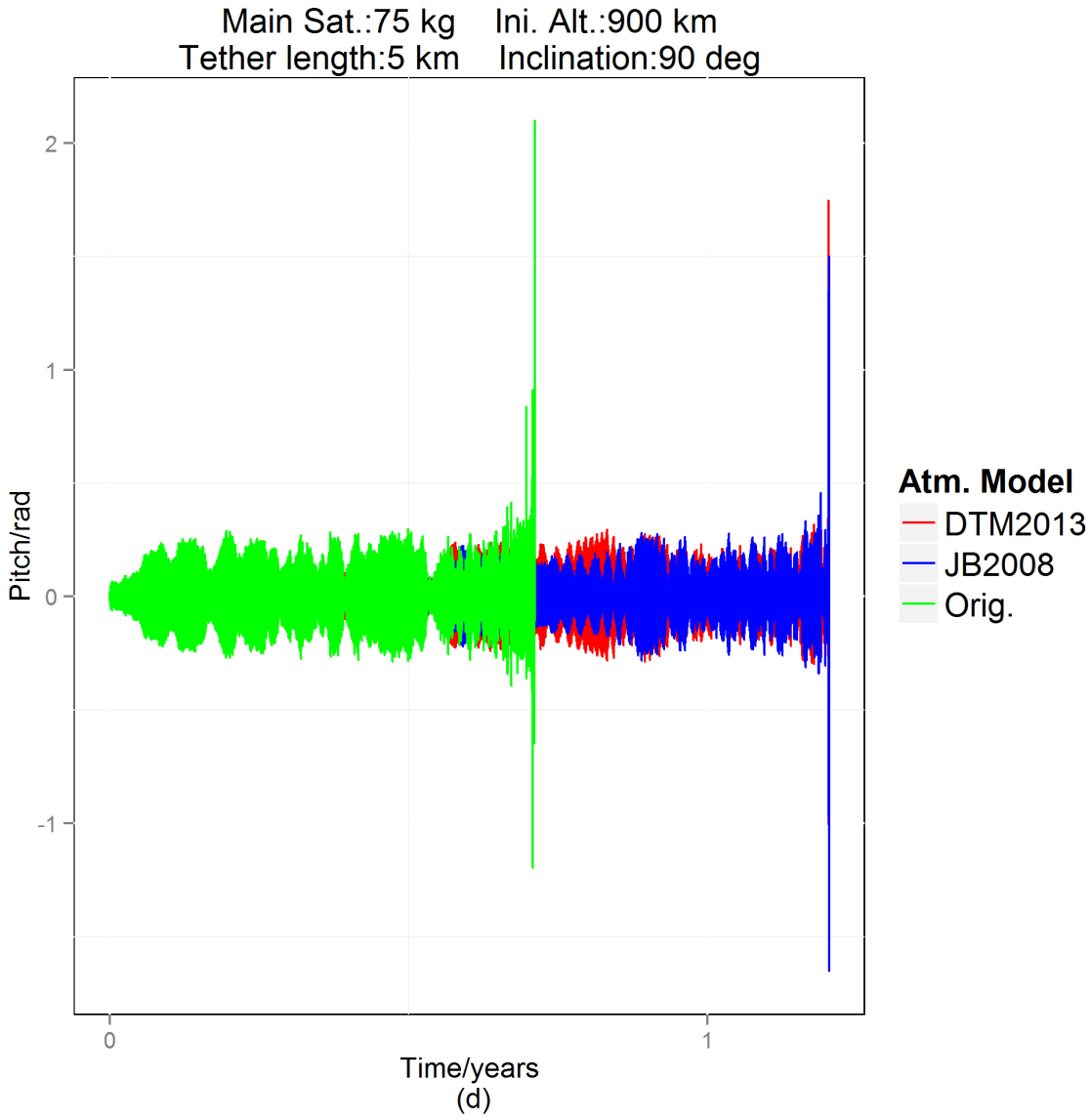

Figure 3.15 The pitch and roll angles (Angle control)

3.5.2.3 Impact of Atmospheric Models

We now strive to explain why the lower densities given by the new atmospheric model give rise to these longer de-orbit times. The air drag contributes to one of the perturbation forces experienced by the space tether (and the involved satellites) as outlined by Zhong and Zhu [22]. In their paper, it was shown that there were perturbative torques that influenced the pitch and roll respectively. Below are the equations for each perturbative

torque (pitch, $Q_{Air,\alpha}$, and roll, $Q_{Air,\beta}$ respectively) due to the air drag.

$$Q_{Air,\alpha} = \frac{1}{4} C_D \rho D L (L - 2\gamma_{dist})(\sqrt{\mu r^{-1}} - \omega_E r \cos i)^2 \tag{3.1}$$

$$Q_{Air,\beta} = -\frac{1}{4} C_D \rho D L (L - 2\gamma_{dist})(\omega_E r \cos u \sin i)^2 \tag{3.2}$$

Both equations show us that the perturbative torque due to the air drag on each angle is proportional to the density of the surrounding atmosphere. From our comparison of the atmospheric models used in the simulations above, we noted that the newer models (the JB2008 and the DTM2013 models) predicted a lower density for the atmosphere than the old model (the US 1976 Standard Atmosphere). As such, we should expect that the perturbative torque on each angle will be less in the simulations that used the newer atmospheric models. This means that the pitch and roll angles should be more stable; these angles will less often exceed the 15 degree bound that the simulation imposed. Figure 3.14 above shows that pitch and roll angle calculated using the old atmospheric model is larger than that from the new atmospheric model. Though we presented only two examples above, they serve as a cross-section of the pitch and roll angles for the other cases in both altitude regimes.

As such, we should expect the space tether system to de-orbit to lower altitudes if the tether is more controlled because it is less likely to tumble. This is what we observe in the graphs above: The JB2008 and DTM2013 models predict a longer stable de-orbit period (and, thus, lower final de-orbit altitude) for the space tether system than the US 1976 Standard Atmosphere. Eventually, however, the space tether system began to tumble for all atmospheric models; it simply took longer for the space tether system to do so when

passing through the atmosphere predicted by the JB2008 model and the DTM2013 model.

Note that the above paragraph only applies for tether lengths of 3 km and 5 km at the initial altitude (900 km). For the 1 km tether, all three cases completed 25 years of simulation time without tumbling or complete de-orbit.

Chapter 4 LIBRATION ENERGY CONTROL STRATEGY

4.1 Libration Energy Control Strategy

Before we look at the results from the Simulink model using libration energy control, we will give a more detailed description of the libration energy control that we used. Takeichi [76] states that it is possible to control the in-plane and out-of-plane libration simultaneously by turning on the electric current only when the Lorentz force decelerates both the in-plane libration and out-of-plane libration. Libration energy control makes use of the Hamiltonian of the tethered system. Takeichi strived to define a function that avoided unnecessary libration control to maximise the time the current flowed through the tether. He started by considering the well-established Hamiltonian for a tethered system presented below.

$$H = \frac{1}{2} M_r l^2 \left[\frac{\mu_g}{r^3} \left(1 - 3\cos^2\phi\cos^2\theta\right) + \cos^2\phi\left(\dot{\theta}^2 - \dot{\upsilon}^2\right) + \dot{\phi}^2 \right] \tag{4.1}$$

Equation 4.1 contains the reduced mass of the space tether system, M_r, gravitational constant of the Earth, μ_g, the out-of-plane angle, ϕ, the in-plane angle, θ, the orbital radius, r and the orbital angular velocity, υ. For a tethered system in a circular orbit, we can introduce a conservative Hamiltonian by using the mean orbital motion, n.

$$H_c = \frac{1}{2} M_r l^2 [n^2 \left(1 - 3\cos^2\phi\cos^2\theta\right) + \cos^2\phi\left(\dot{\theta}^2 - n^2\right) + \dot{\phi}^2 \tag{4.2}$$

However, for elliptical orbits, the orbital radius, r, and the angular velocity, υ, vary which causes the Hamiltonian to be non-conservative. However, it is possible to create a conservative function of mechanical energy if the mean orbital motion and the libration are considered. Takeichi [76] also states that the minimum mechanical energy is achieved when the tether librates with the same period as the space tether system. Knowing this, Takeichi [76] sought to manipulate the Hamiltonian accordingly and suggested

$$H_e = \frac{1}{2} M_r l^2 \left\{n^2 \left[1 - 3\cos^2\phi\cos^2\left(\theta - \theta_p\right)\right] + \cos^2\phi\left[\left(\dot{\theta} - \theta_p\right)^2 - n^2\right] + \dot{\phi}^2\right\} \tag{4.3}$$

Equation (4.3) contains the approximate periodic solutions, θ_p and ϕ_p, such that

$$\begin{aligned} \theta_p &= e\sin\upsilon - \frac{1}{2}e^2\sin 2\upsilon \\ \dot{\theta}_p &= n\left(e\cos\upsilon - e^2\cos 2\upsilon\right) \\ \phi_p, \dot{\phi}_p &= 0 \end{aligned} \tag{4.4}$$

Using Eq. (4.3), we can obtain a function in terms of mechanical energy as shown below.

$$V_e = 4 - 3\cos^2\phi\cos^2\left(\theta - \theta_p\right) + \frac{1}{n^2}\left\{\cos^2\phi\left[\left(\dot{\theta} - \dot{\theta}_p\right)^2 - n^2\right] + \dot{\phi}^2\right\} \tag{4.5}$$

For a circular orbit, as we consider in our work, Eq. 4.5 can be re-written as,

$$V_c = 4 - 3\cos^2\phi\cos^2\left(\theta - \theta_p\right) + \frac{1}{n^2}\left\{\cos^2\phi\left[\left(\dot{\theta} - \dot{\theta}_p\right)^2 - n^2\right] + \dot{\phi}^2\right\} \tag{4.6}$$

This is the stability function that we adopt in our libration energy control method.

This control method seeks to suppress both the in-plane and out-of-plane libration simultaneously by using the total libration energy. This is different from our angle control used before because it would often only target either the in-plane or the out-of-plane libration.

We specify a threshold beyond which the libration energy, V_c, should not exceed. In general, V_c should be between 0 and 3. The lower bound corresponds to keeping the tether pointing vertically downwards at all times while the upper bound corresponds to having the tether swing to a maximum of 90 degrees from the vertical. In our simulations, we chose a threshold of V_c = 1.0, which allows the pitch to reach a maximum of 35 degrees. The roll was always less than the pitch in these experiments because the pitch is the driver leading to the instability in the polar orbit as shown before. When the threshold is breached by the space tether system, the current flowing through the tether is switched off until the excess energy dissipates.

4.2 Results and Discussion

Similar to the previous Chapter, we consider two initial altitudes (500km and 900km) for de-orbit analysis. In our results, we present the altitude of the space tether system as it de-orbits for each case. In addition, we also present sample cases of the pitch, roll and the libration energy for each altitude regime. The graphs of these quantities all bore resemblance and to avoid redundancy and for brevity and clarity, we included only samples cases of these quantities. These sample cases were chosen to reflect, as best as possible, the behaviour of these quantities in all of the cases.

4.2.1 Initial Altitude: 500 km

In this altitude regime, we see similar results to the angle control section. In all cases, the new atmospheric models predicted a longer de-orbit time than the old atmospheric model. The difference between the two sets of models is largest with the 1 km tether as seen in Figs. 4.1 (a), 4.2 (a), 4.3 (a). As the tether length increases, the results begin to get more similar. With the 5 km tether (4.1 (c), 4.2 (c), 4.3 (c)), the results have little difference between them. However, the 5 km tether also causes the space tether system to de-orbit much faster than the shorter tethers. As such, since the time frame is shorter for the cases with the 5 km tether, there is little time for the atmospheric models to distinguish themselves. Indeed, if we more closely observe the graphs of the cases with the 1 km and the 3 km tether in Fig. 4.1 and Fig. 4.2 below, we see that the three graphs start off very similarly and then begin to diverge as time further increases. So, the similarity we see between the results for the 5 km case is pronounced because of the shortened time frame.

This brings us to another salient point about space tether systems. The longer tether is always more energetic and will result in a larger electrodynamic force and, thus, a larger electrodynamic drag. Consequently, space tether systems with longer tethers will de-orbit faster than those with shorter tethers. This observation can be made for the cases using libration energy control and angle control.

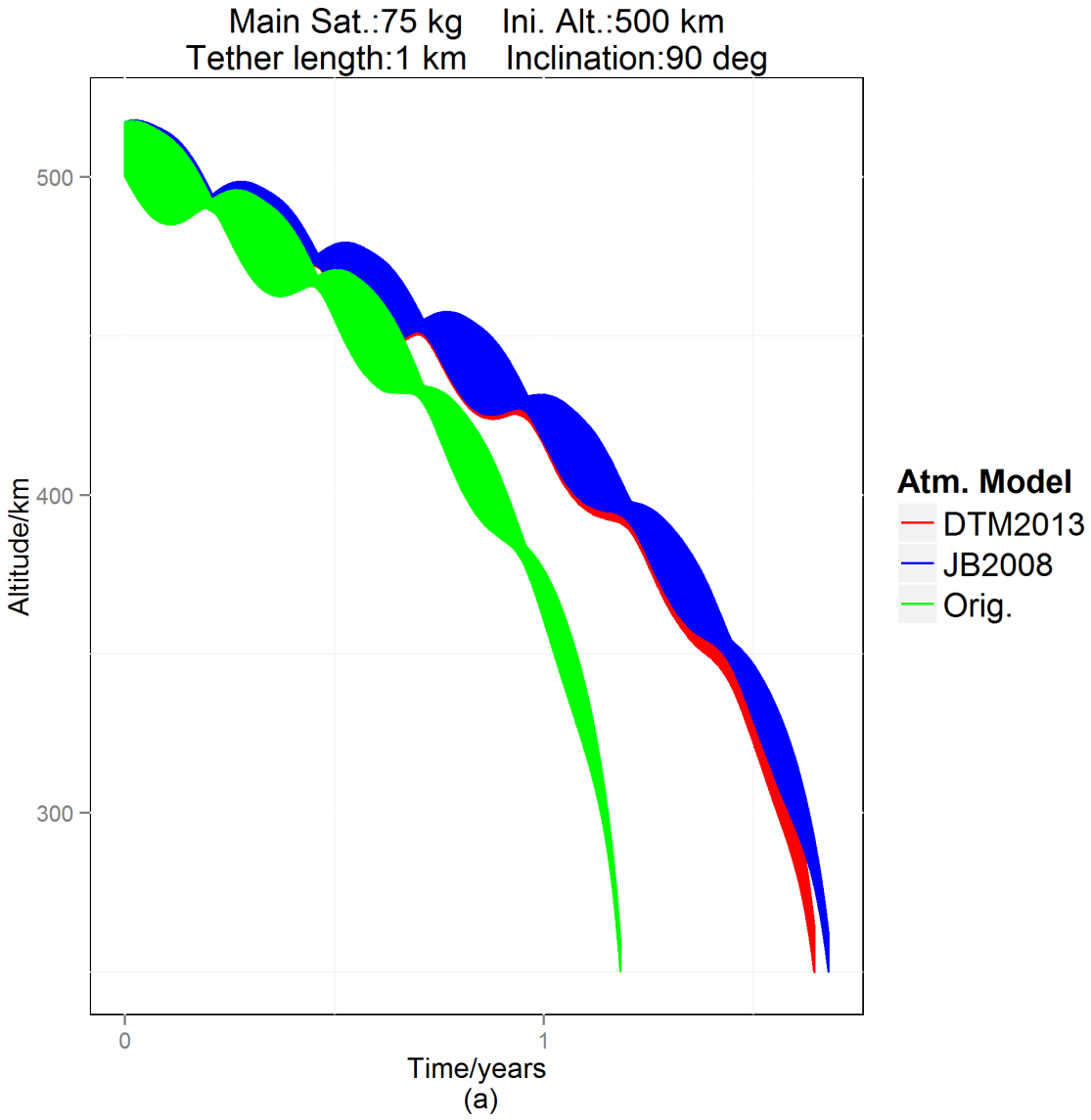
Main Sat.:75 kg Ini. Alt.:500 km
Tether length:1 km Inclination:90 deg
500
400
300
Altitude/km
0
1
Time/years
(a)
Atm. Model
DTM2013
JB2008
Orig.

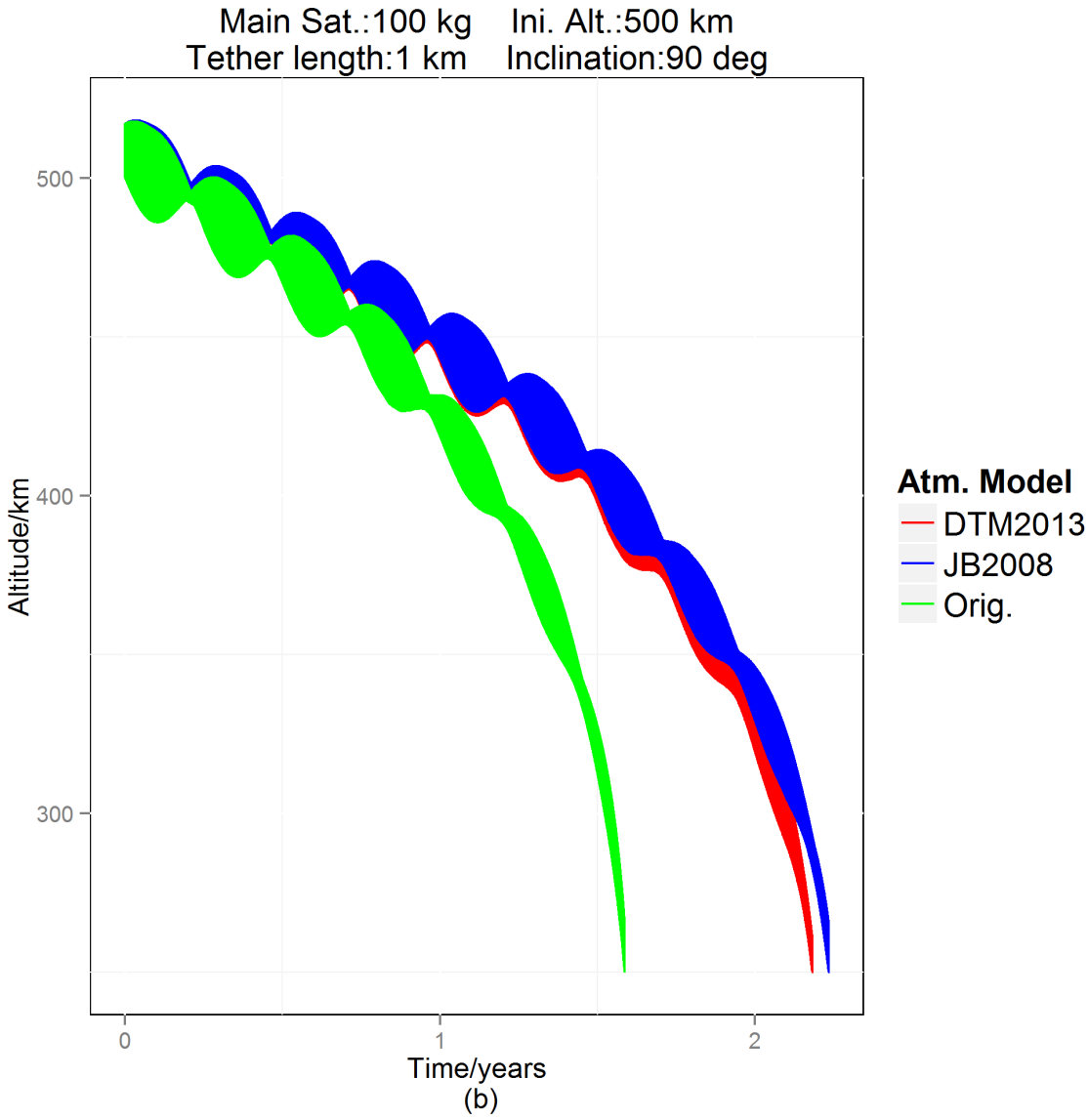
Main Sat.:100 kg Ini. Alt.:500 km
Tether length:1 km Inclination:90 deg
500
400
300
Altitude/km
0
1
2
Time/years
(b)
Atm. Model
DTM2013
JB2008
Orig.

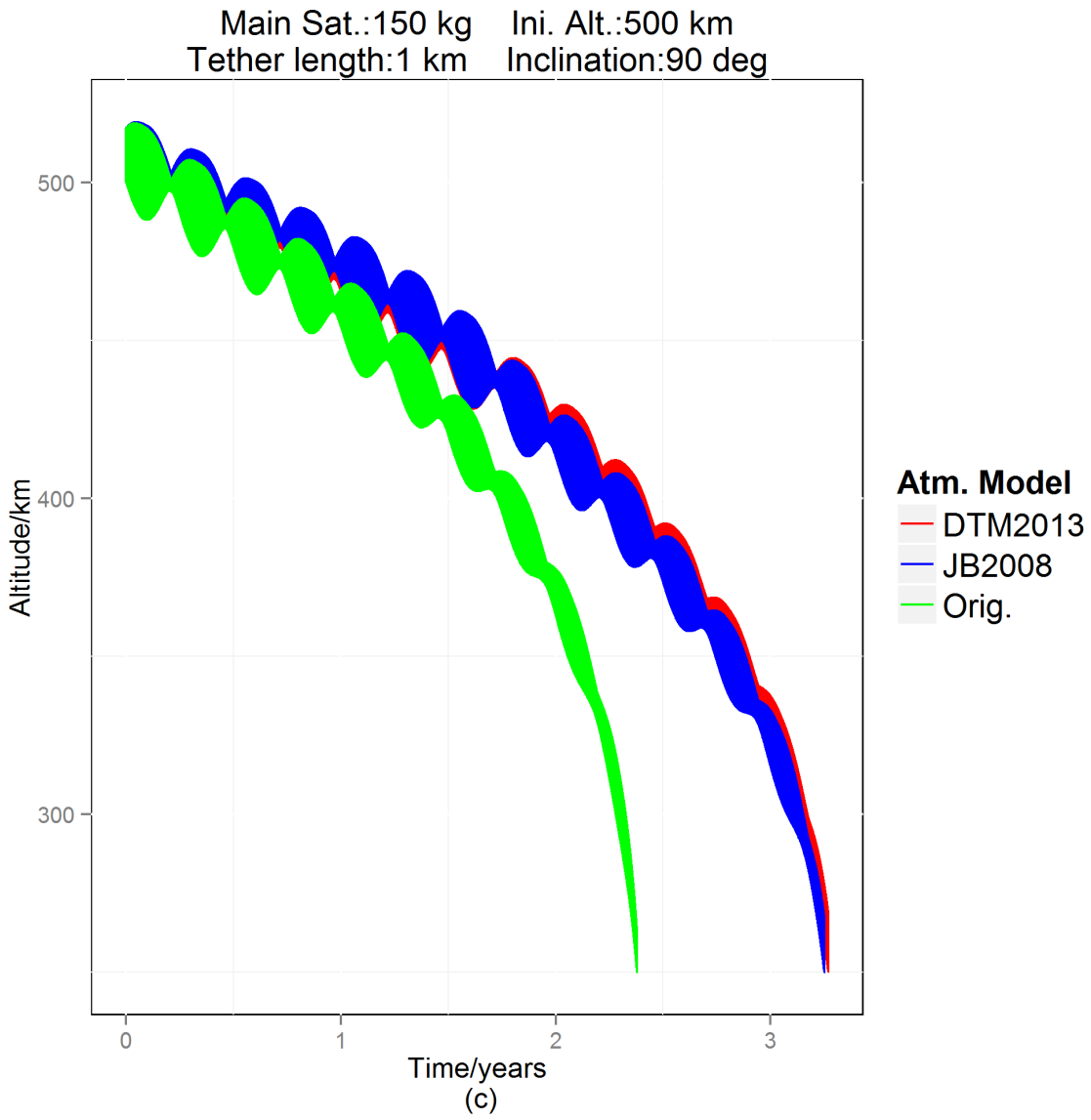

Figure 4.1 Results of the 1 km tether, initial altitude 500 km and main satellite masses of 75 kg, 100 kg, 150 kg (Energy control).

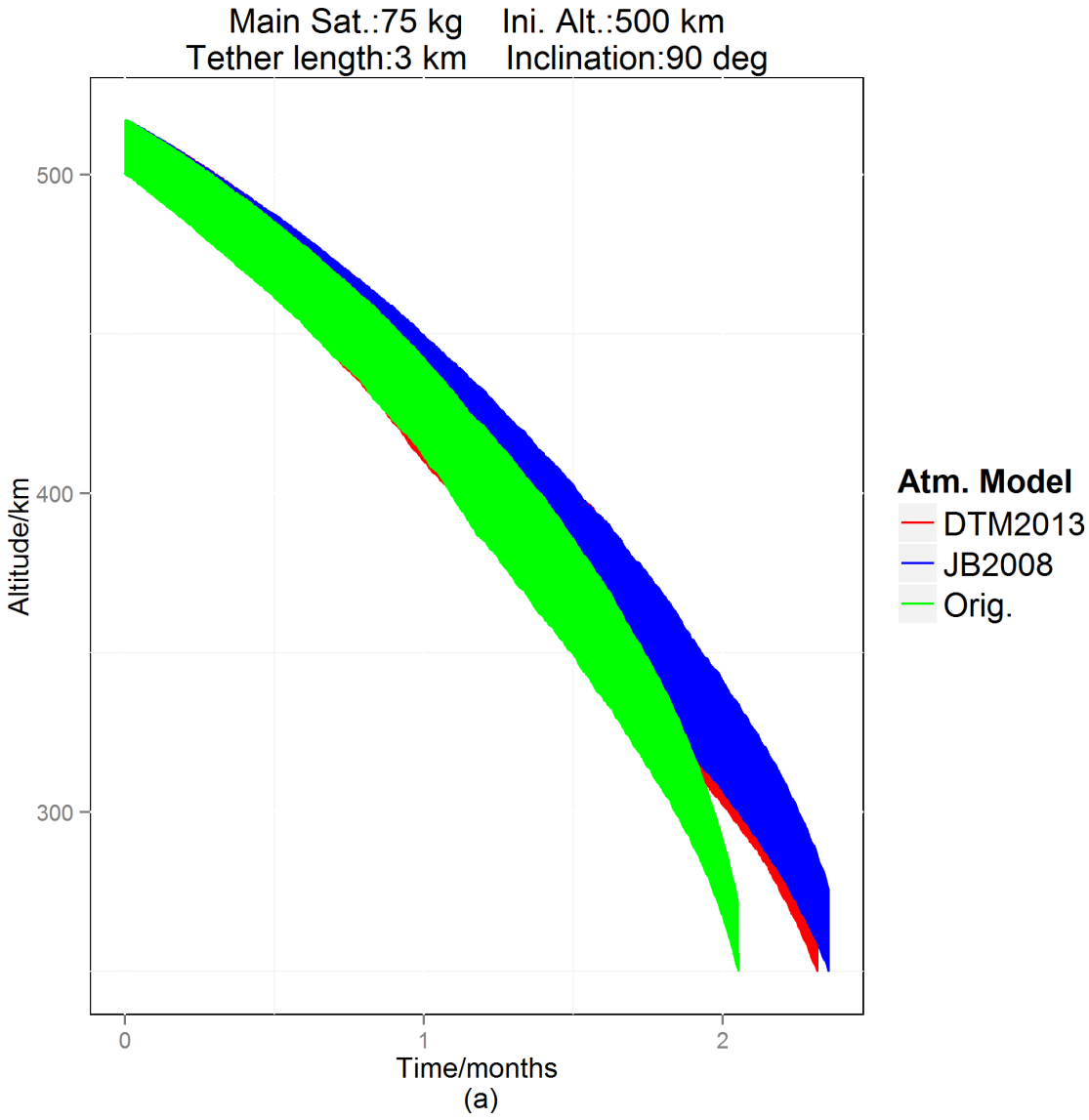
Main Sat.:75 kg Ini. Alt.:500 km
Tether length:3 km Inclination:90 deg
500
400
300
Altitude/km
0
1
2
Time/months
(a)
Atm. Model
DTM2013
JB2008
Orig.

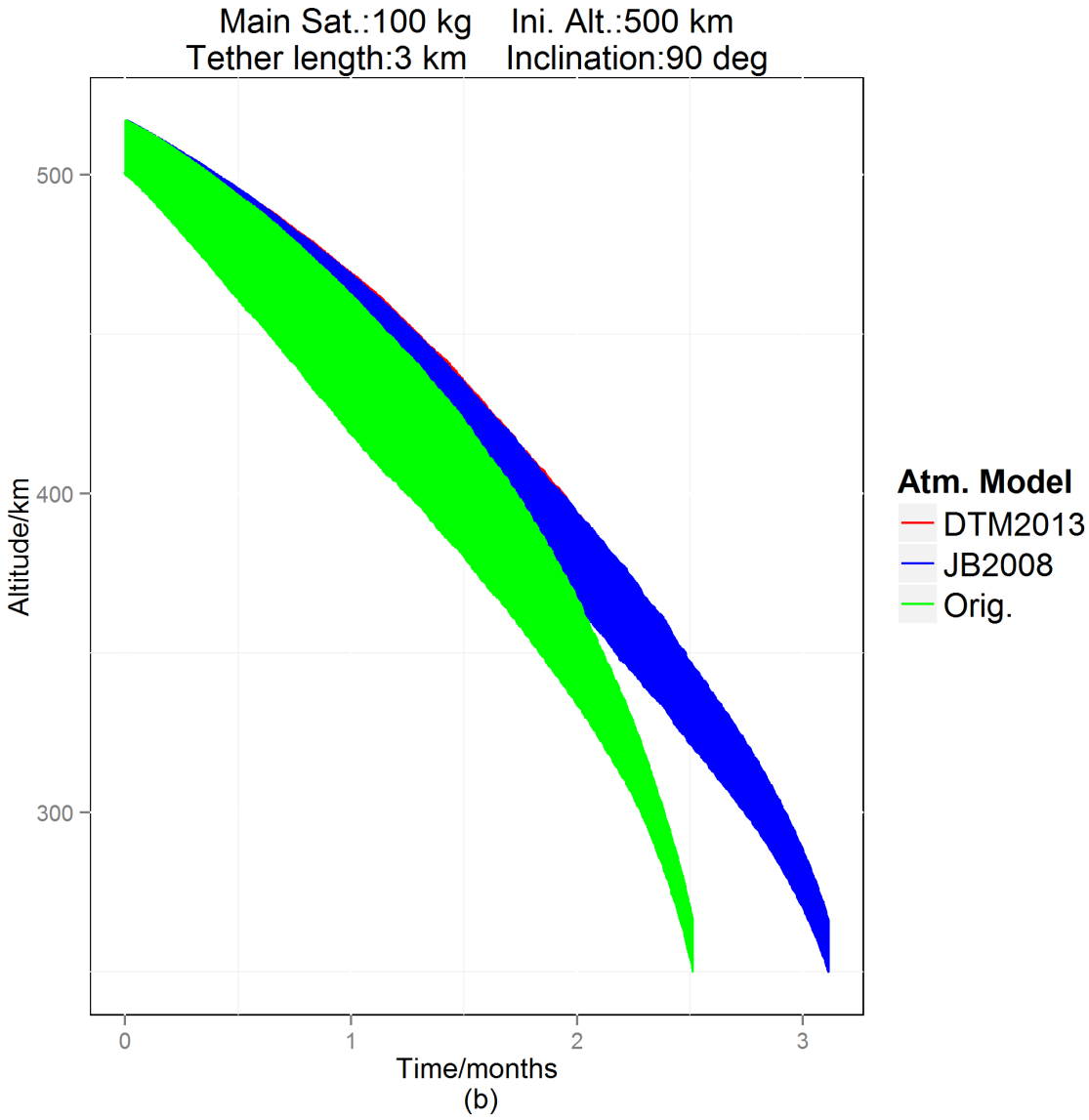
Main Sat.:100 kg Ini. Alt.:500 km
Tether length:3 km Inclination:90 deg
500
400
300
Altitude/km
0
1
2
3
Time/months
(b)
Atm. Model
DTM2013
JB2008
Orig.

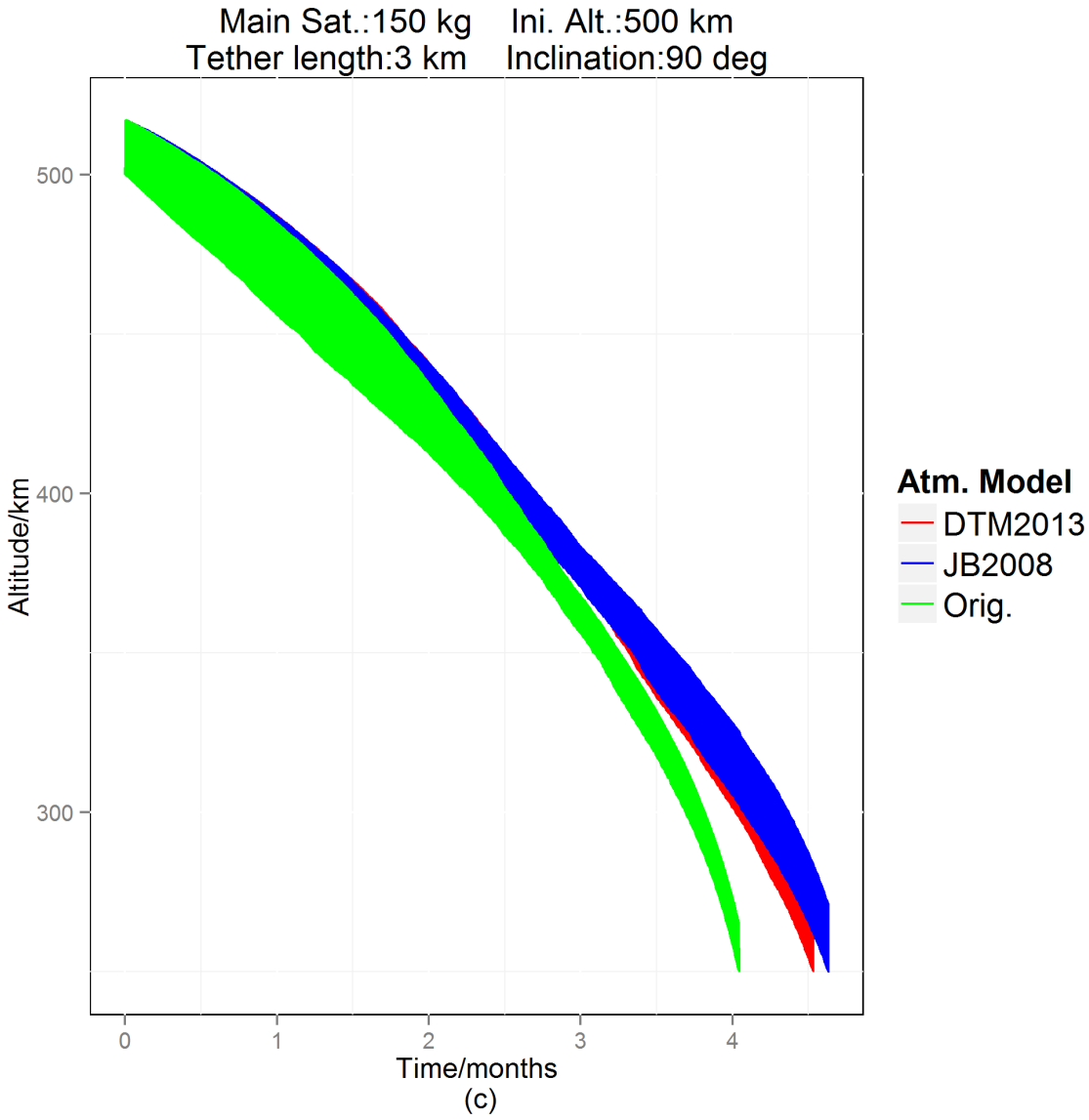

Figure 4.2 Results of the 3 km tether, initial altitude 500 km and main satellite masses of 75 kg, 100 kg, 150 kg (Energy control).

Another point worth noting here is that, in all of the cases, the space tether system completely de-orbited to the simulation's final altitude of 250 km. Using angle control, none of the cases fully de-orbited; they began to tumble before the final altitude.

We can compare the de-orbit results using libration energy control from this section to their counterparts that used angle control in the previous chapter. For the 3 km and 5

km cases (see Figs. 4.2, 4.3), the space tether systems de-orbits faster under libration energy control and to its final altitude of 250 km. For the 1 km case (see Fig. 4.1), the results indicate an adherence to this trend although not all the cases allow for a direct comparison because they both reached the final simulation time of 25 years. We can infer from this comparison that controlling the libration energy allows the tether to de-orbit the system more efficiently and successfully.

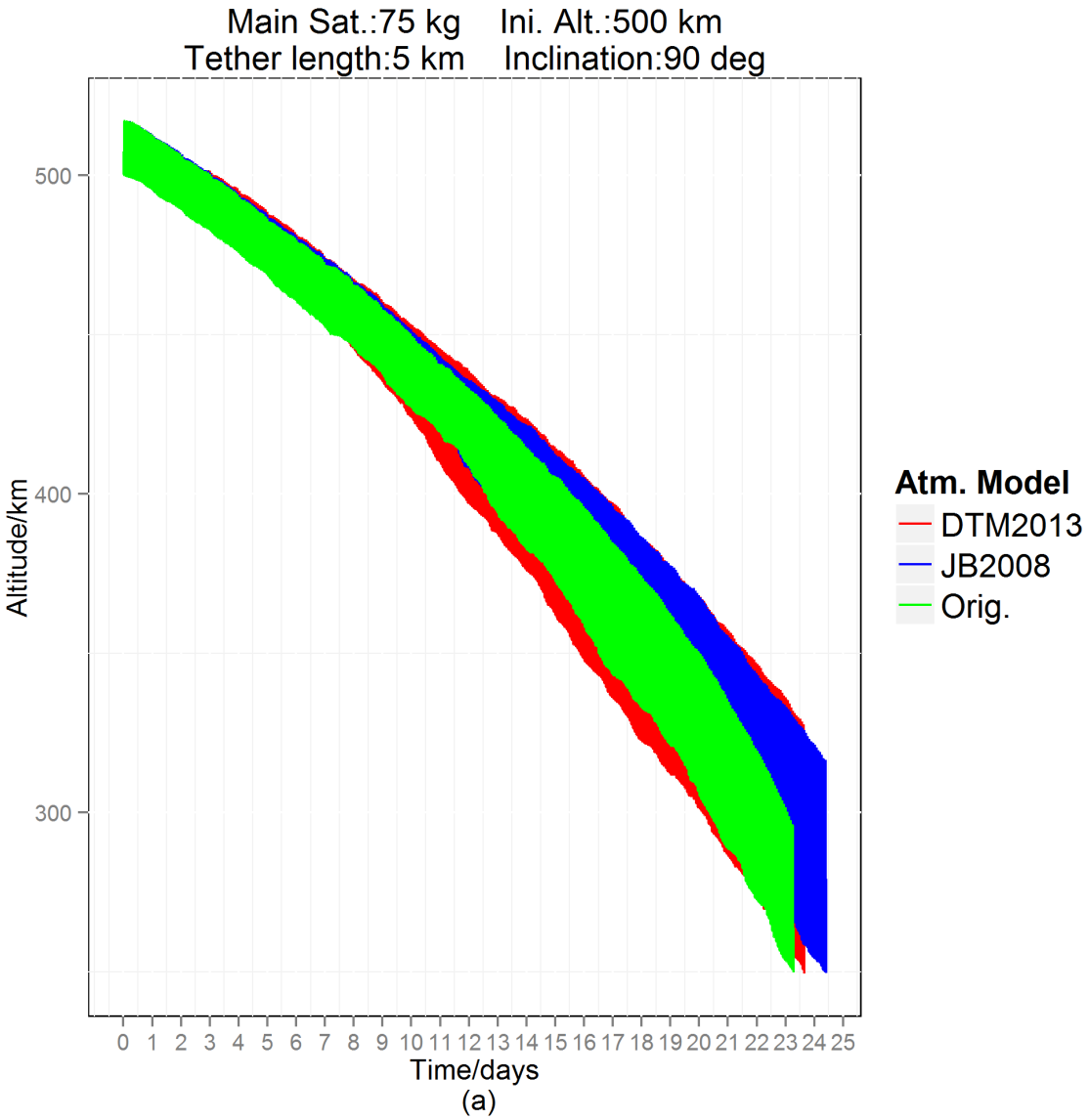

(a)

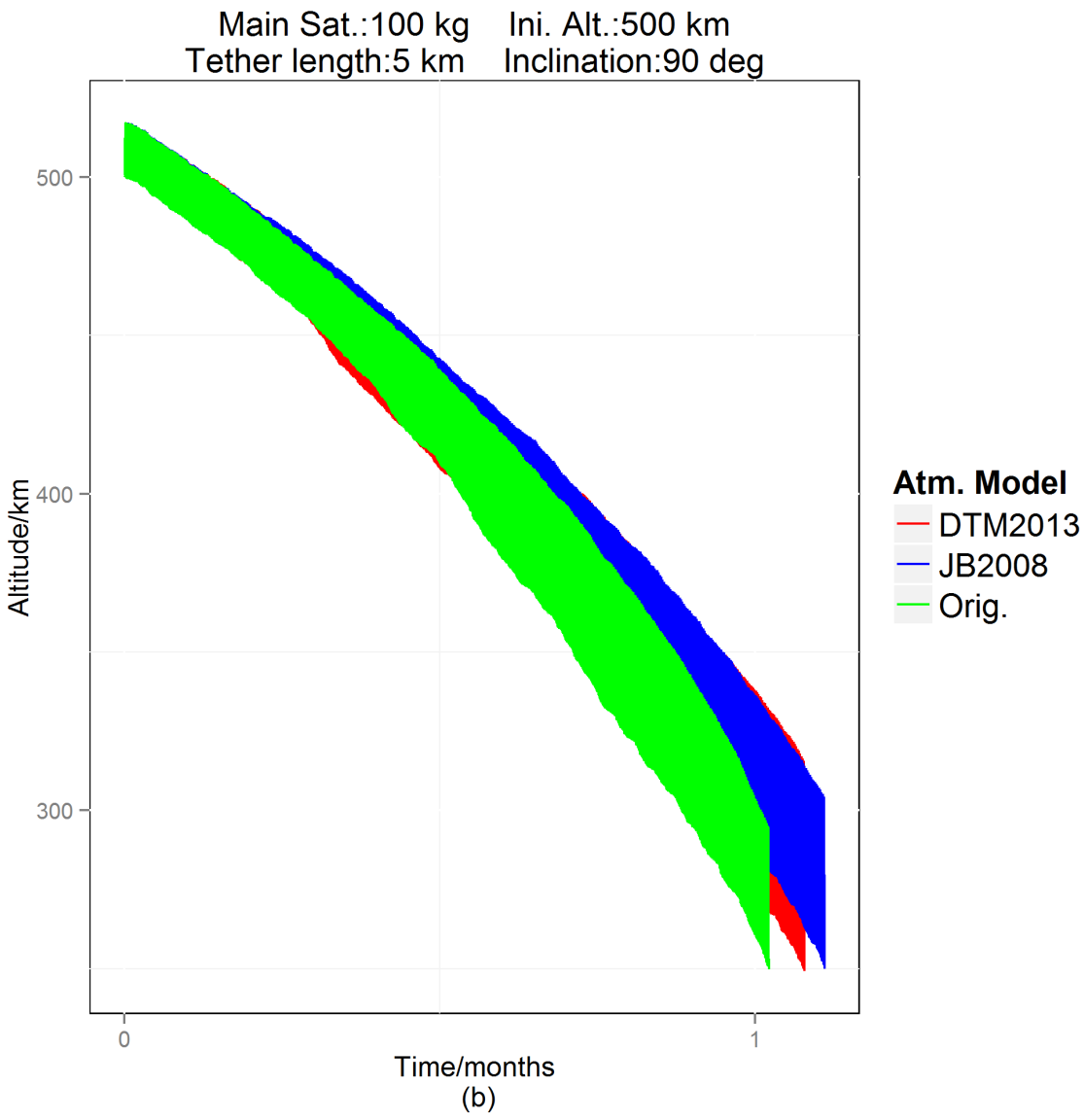
Main Sat.:100 kg Ini. Alt.:500 km
Tether length:5 km Inclination:90 deg
500
400
300
Altitude/km
0
1
Time/months
(b)
Atm. Model
DTM2013
JB2008
Orig.

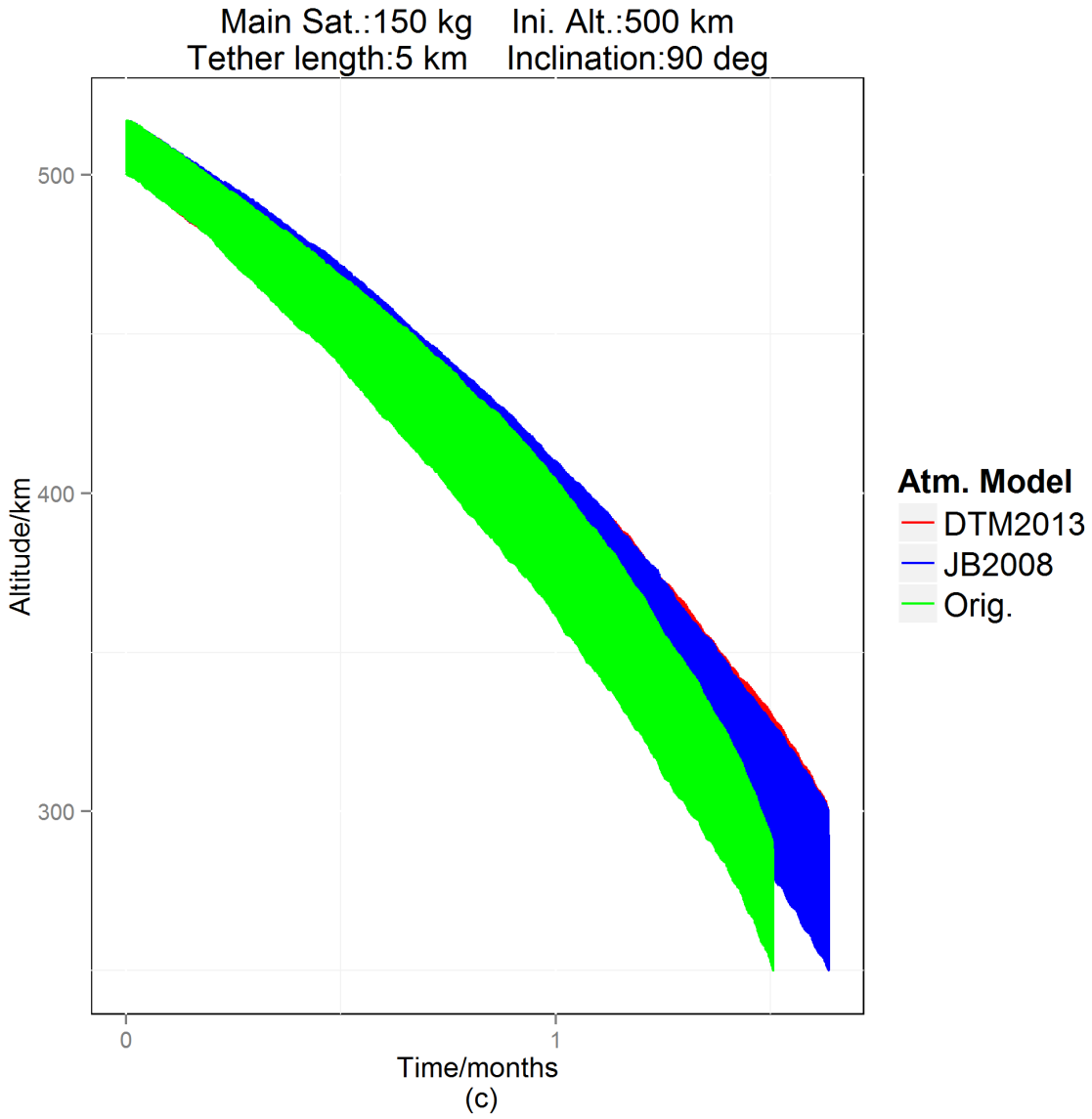

Figure 4.3 Results of 5 km tether initial altitude 500 km and main satellite masses of 75 kg, 100 kg, 150 kg (Energy control).

Another observation we can make from the libration energy graphs (see Fig. 4.7) is that the space tether system quickly gathers libration energy equal to the threshold libration energy. In a more robust control method, we should expect to see the libration energy remain constant at the threshold value until the end of simulation. However, in our method of libration energy control, there is a noticeable difference to the ideal case. The

libration energy slowly increases once it has reached the threshold and continues to do so until the end of the simulation.

This occurs because the method of control is not so robust to maintain the libration energy at the threshold level as the space tether system de-orbits. However, this does not mean that our method of control is ineffective; it still keeps the libration energy of the system near the threshold, which is a manageable level for the space tether system. Recall that the energy threshold corresponds to a particular libration angle. In theory, once the libration angle is not in excess of 90 degrees (which would initiate tumbling), the space tether system can still use electrodynamic drag to de-orbit provided the system is properly controlled. Thus, the incremental increase of libration energy as the de-orbit progresses is of little concern especially considering that the space tether system successfully de-orbits to its target altitude in nearly all cases.

Near the end of the simulation, we start to see some more significant departure from the threshold. However, this is short-lived and only occurs near the end of the simulation. As mentioned earlier, all the simulations predicted that the space tether system will de-orbit to 250 km in this height regime. Consequently, by the time our control method appears to be ineffective, the space tether system, has already de-orbited to 250 km and can complete the rest of its de-orbit using only air drag; there is no need to control the tether past this altitude. Finally, this observation is true for both altitude regimes.

From Zhong and Zhu [22], we know that the tether experiences a perturbative torque from the air drag. This perturbative torque influences both the pitch and roll angles of the tether and is proportional to the air density. If we recall, the air density given by the US 1976 Standard Atmosphere is greater than that given by both the JB2008 model and the

DTM2013 model.

Thus, the tether experiences a larger perturbative torque under the old atmospheric model. This larger torque will cause the pitch of the tether to experience greater deviations from the vertical. As such, we can expect a larger pitch as well as a greater rate of change in both angles. However, from the graphs above, we see that the roll behaves nearly the same in all three atmospheric models.

Since the pitch, as well as its rates of change, is greater with the US 1976 Standard Atmosphere, the cosine of all these values will be smaller. In addition, we see that the old atmosphere model predicts a larger squared mean orbital motion, n^2, from the graphs above. With this information, we can deduce that the libration energy found by the old atmospheric model was, overall, less (albeit only slightly so) than that found by the newer atmospheric models (this is confirmed by the results produced by the simulation) using the equation for libration energy given in this section. However, numerical computation and the robustness of the libration energy control can produce results contrary to theory especially as time increases.

4.2.2 Initial Altitude: 900 km

For the 1 km tether, we notice that the lighter main satellites (75 kg and 100 kg) (see Fig 4.4 (a), (b)) experience a similar behaviour. The DTM-2013 model shows the longest de-orbit time, followed by the JB2008 model. For the lightest main satellite, all three graphs show that the space tether system completely de-orbits. For the 100 kg main satellite (see Fig. 4.4 (b)), only the DTM-2013 model predicts that the space tether system will not de-orbit in the given 25 years. For the heaviest main-satellite in Fig. 4.4 (c), we see that all three atmospheric models predict similar results and none of them predict that the space

tether system will completely de-orbit.

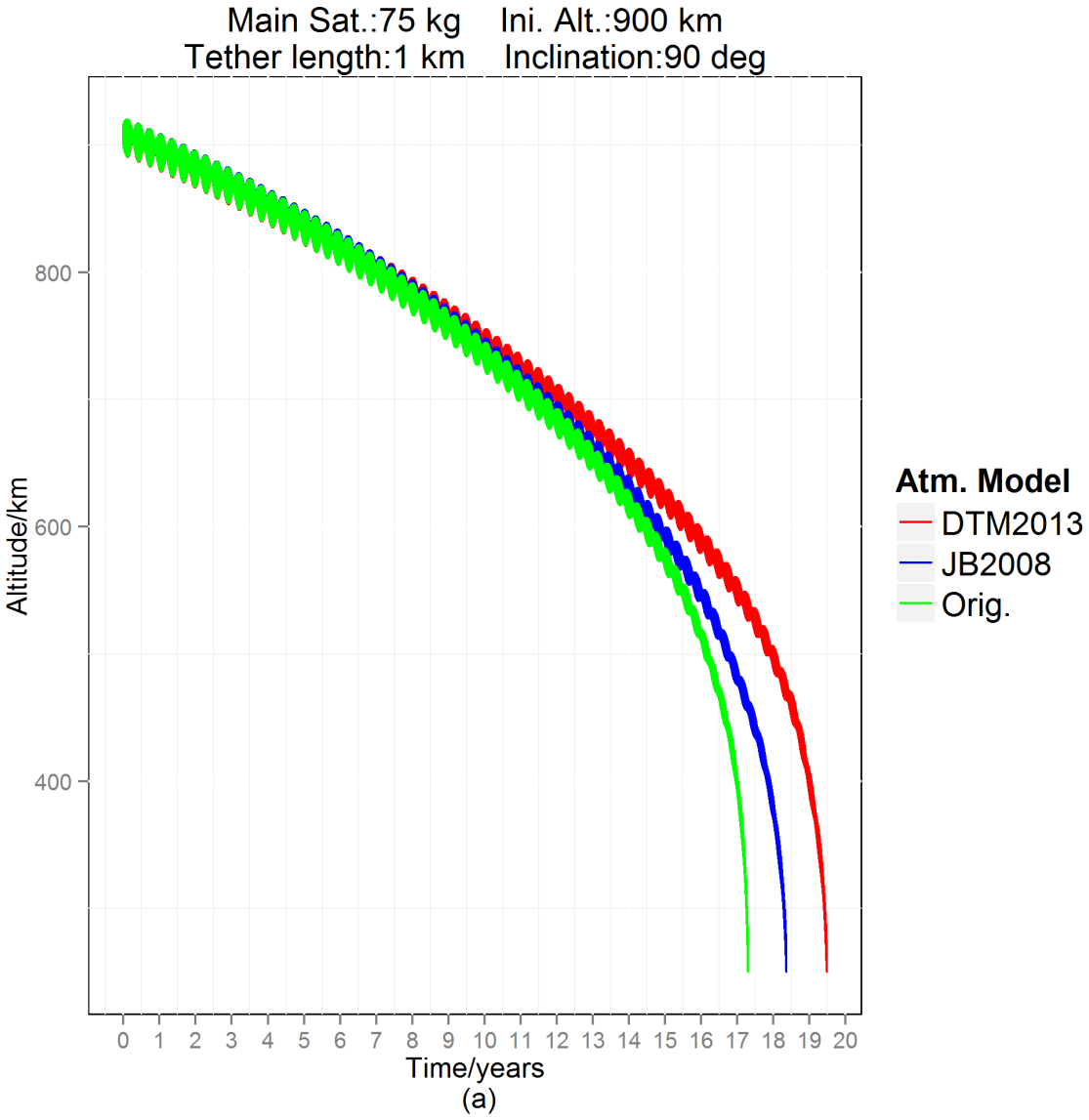

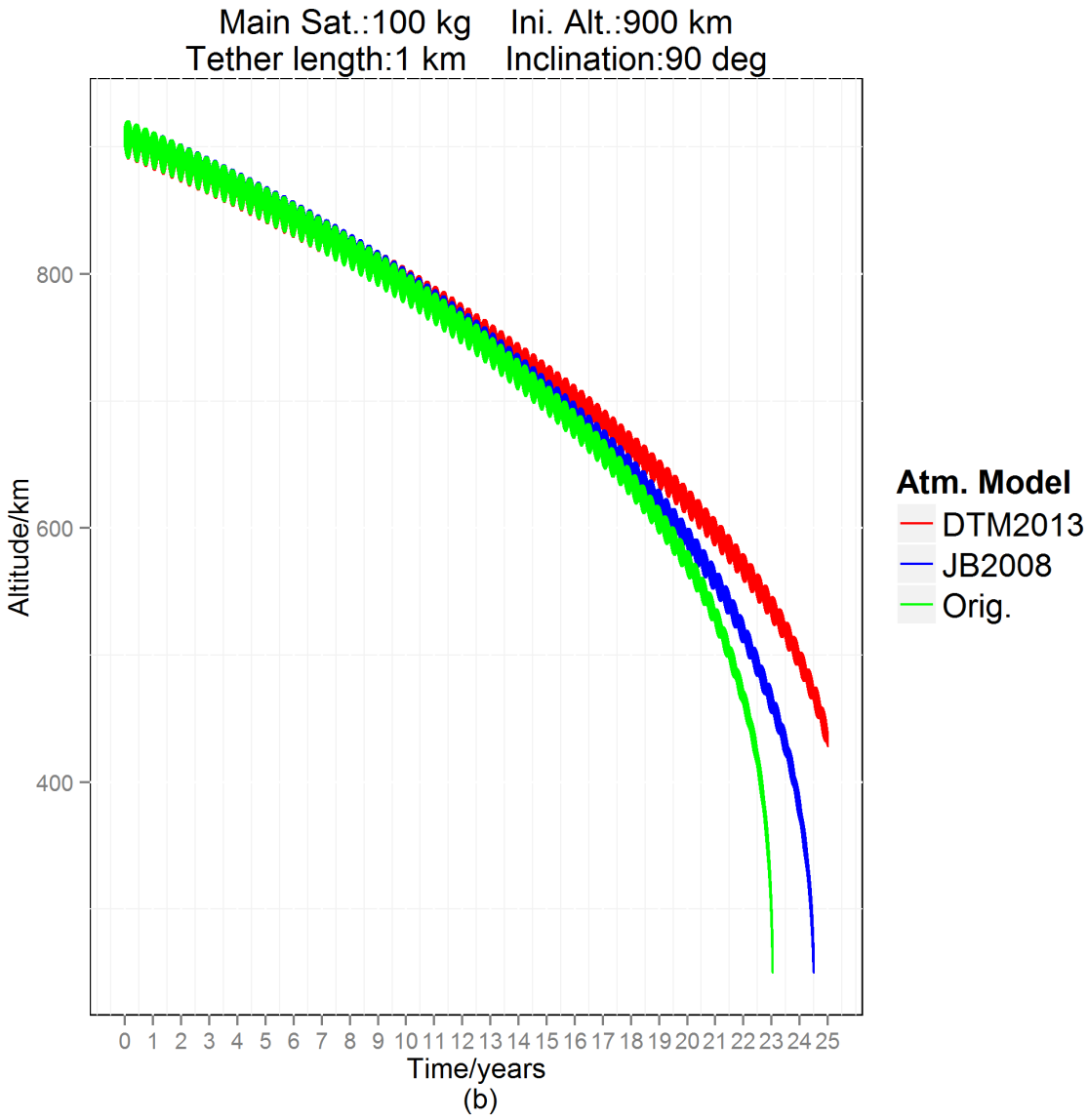
Main Sat.:100 kg Ini. Alt.:900 km
Tether length:1 km Inclination:90 deg
Altitude/km
800
600
400
0 1 2 3 4 5 6 7 8 9 10 11 12 13 14 15 16 17 18 19 20 21 22 23 24 25
Time/years
Atm. Model
DTM2013
JB2008
Orig.
(b)

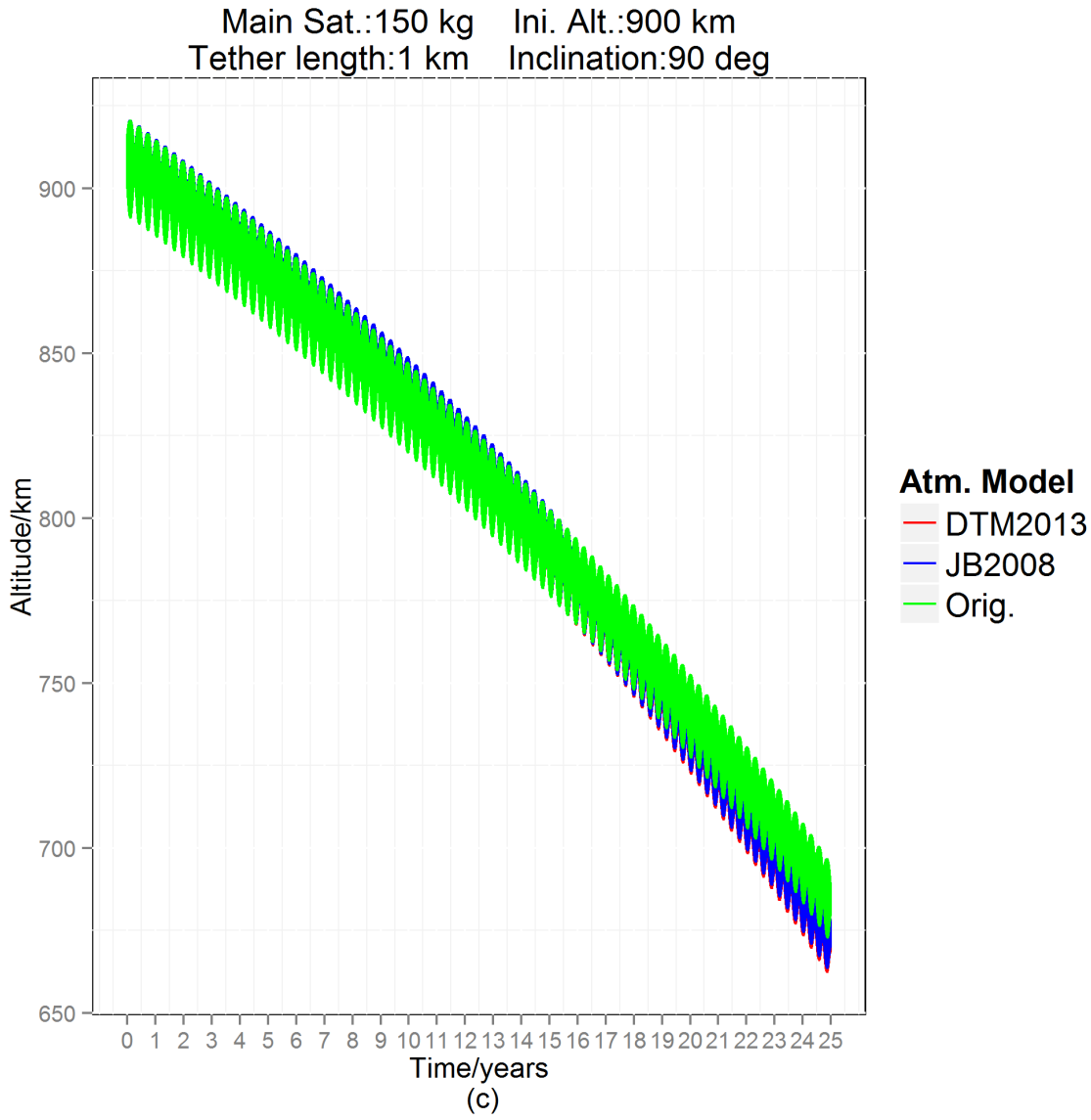

Figure 4.4 Results of the 1 km tether, initial altitude 900 km and main satellite masses of 75 kg, 100 kg, 150 kg (Energy control).

The results of libration energy of the tether system are shown in Fig. 4.7. For the 3 km and 5 km (see Fig. 4.5 and 4.6) tether in this altitude regime, we see that there is little difference between the results from the old atmospheric model and the new atmospheric models. In spite of the similarity, we still notice that the old atmospheric model generally has a slightly shorter de-orbit time than the newer atmospheric models. The same

explanation given above explaining the reason for the shorter de-orbit still applies.

However, we see a greater similarity between the results in this altitude regime than in the 500 km regime. The air density at 900 km is significantly less (by three orders of magnitude) than at 500 km. Consequently, the perturbative torques due to air drag will be the weakest at this altitude. This means that the de-orbit of the space tether system under each of the atmospheric models will differ only slightly from this altitude. However, as the altitude decreased through de-orbit, the air density increases making the perturbative torques from air drag increase. Using the results from the 500 km regime as evidence, we see that the deviation in the altitude becomes more pronounced with lower altitudes.

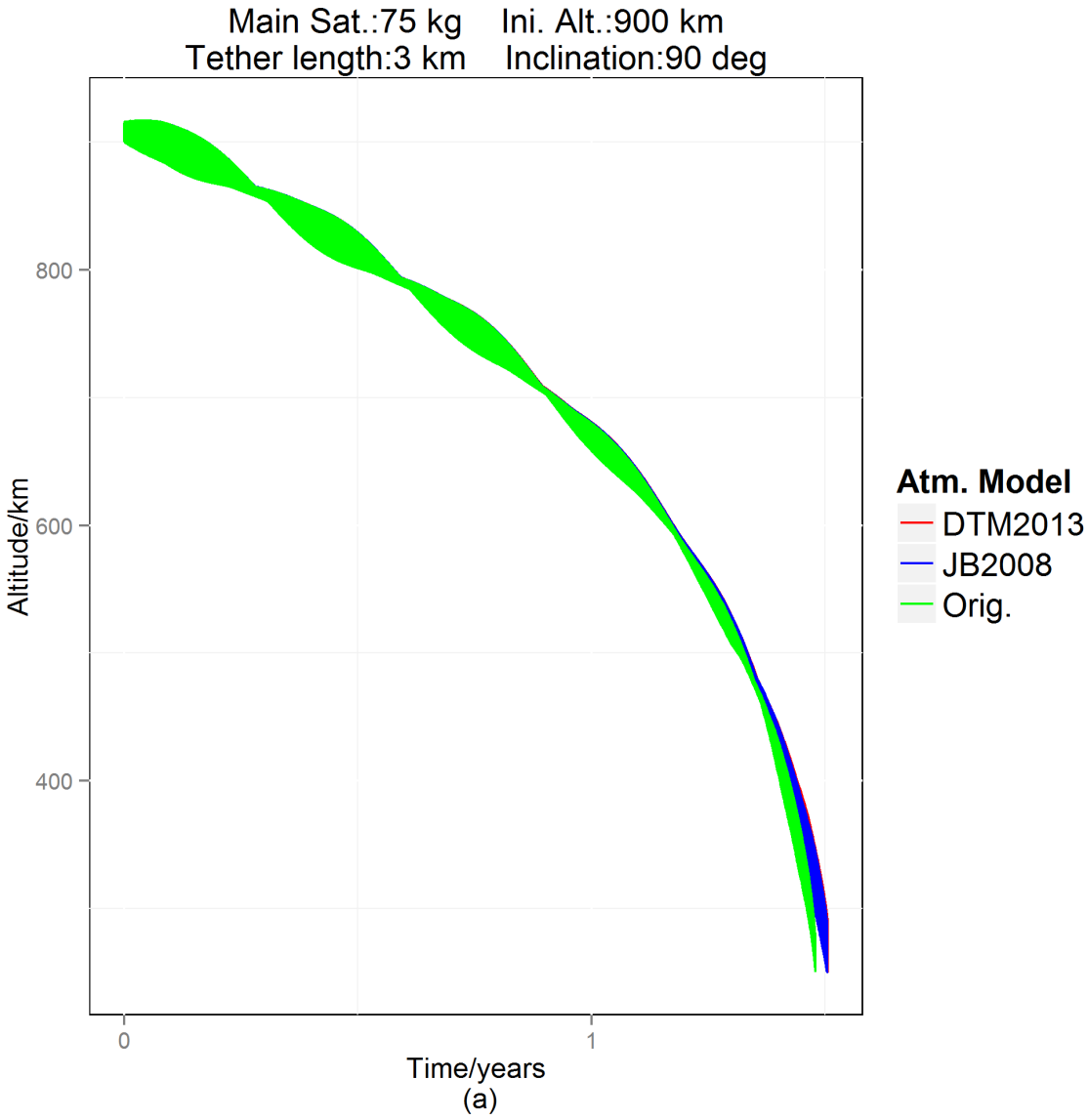
Main Sat.:75 kg Ini. Alt.:900 km
Tether length:3 km Inclination:90 deg
800
600
400
Altitude/km
0
1
Time/years
(a)
Atm. Model
DTM2013
JB2008
Orig.

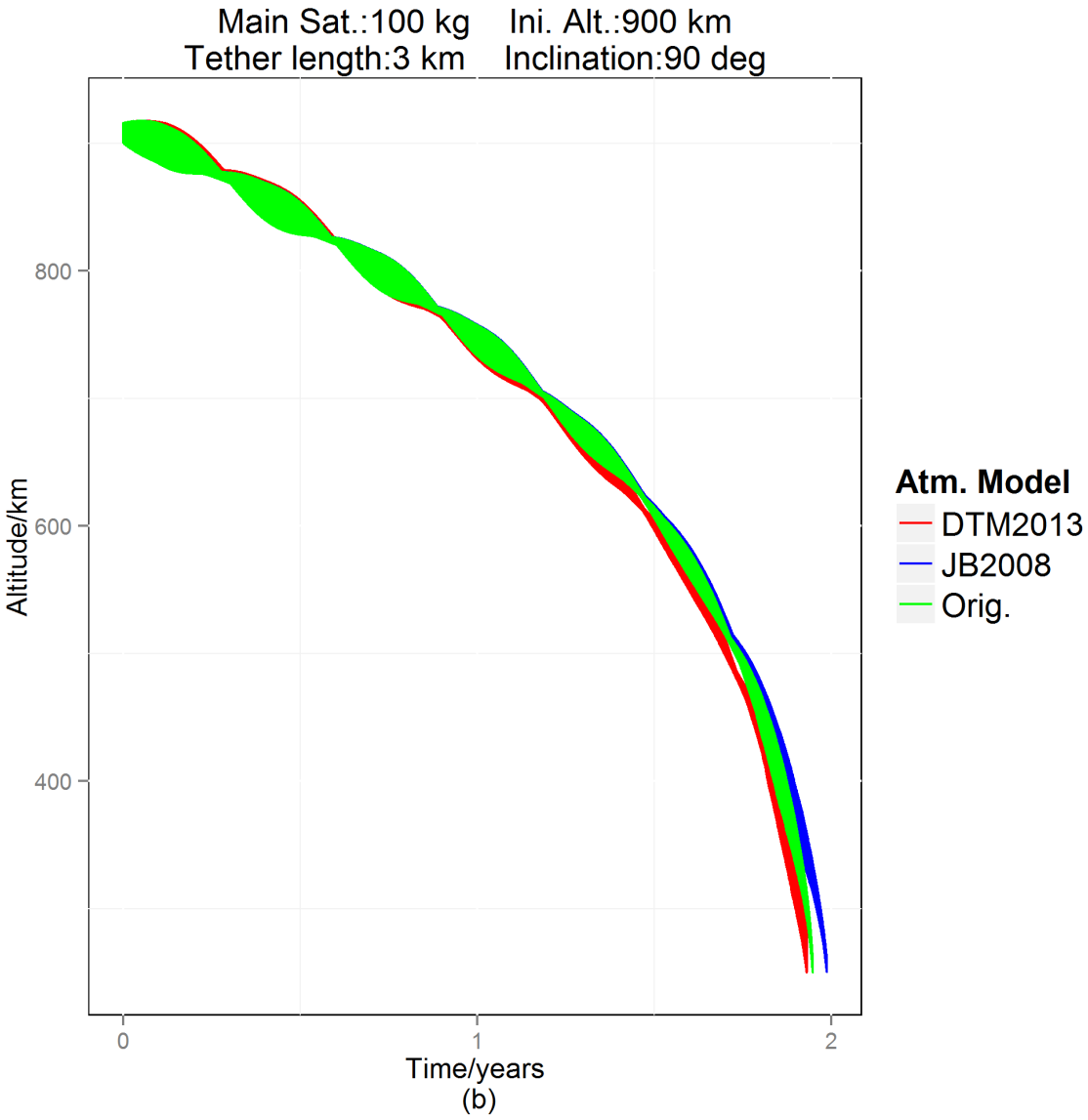
Main Sat.:100 kg Ini. Alt.:900 km
Tether length:3 km Inclination:90 deg
800
600
400
Altitude/km
0
1
2
Time/years
(b)
Atm. Model
DTM2013
JB2008
Orig.

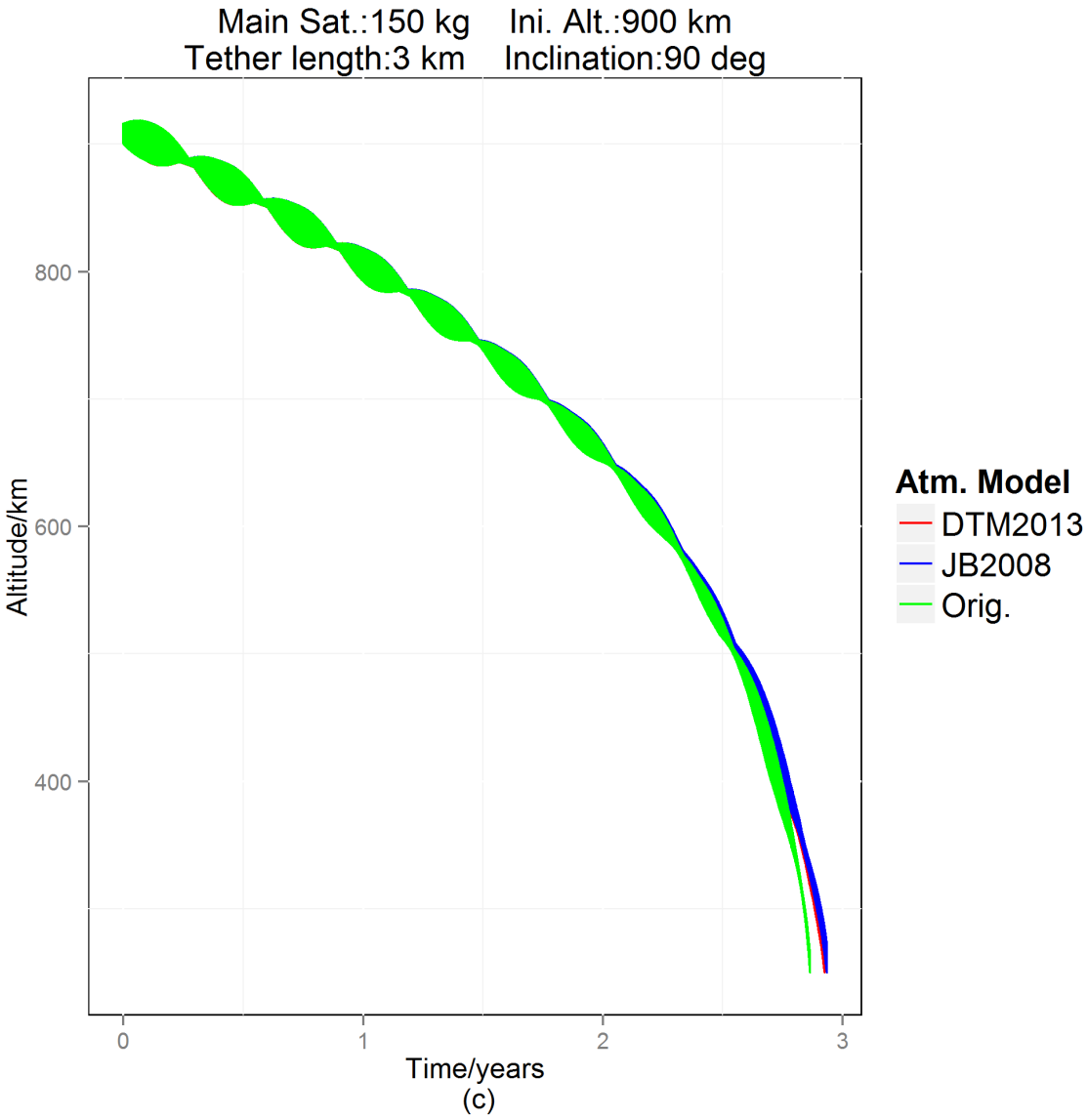

Figure 4.5 Results of the 3 km tether, initial altitude 900 km and main satellite masses of 75 kg, 100 kg, 150 kg (Energy control).

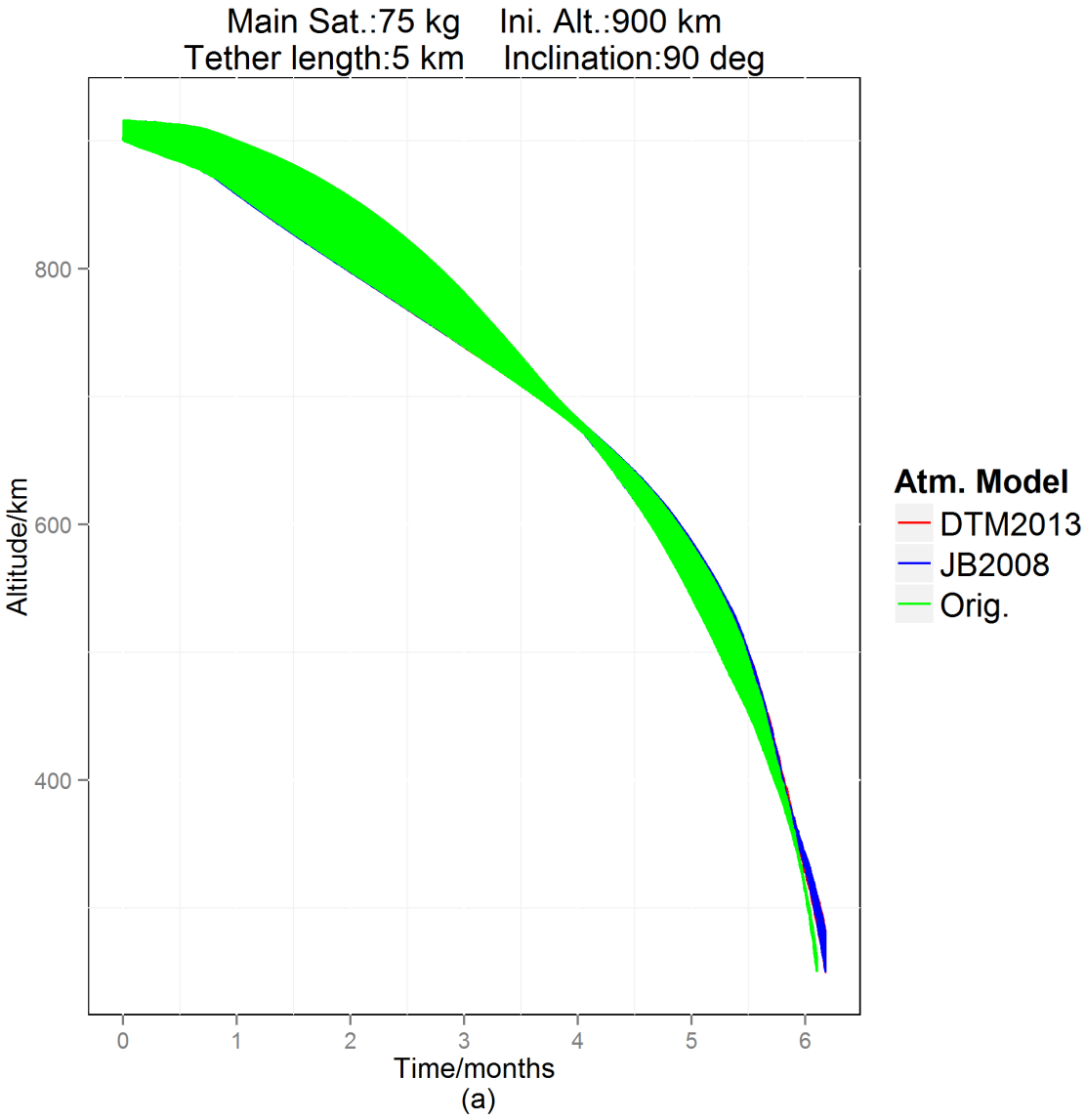
Main Sat.:75 kg Ini. Alt.:900 km
Tether length:5 km Inclination:90 deg
Altitude/km
800
600
400
0
1
2
3
4
5
6
Time/months
(a)
Atm. Model
DTM2013
JB2008
Orig.

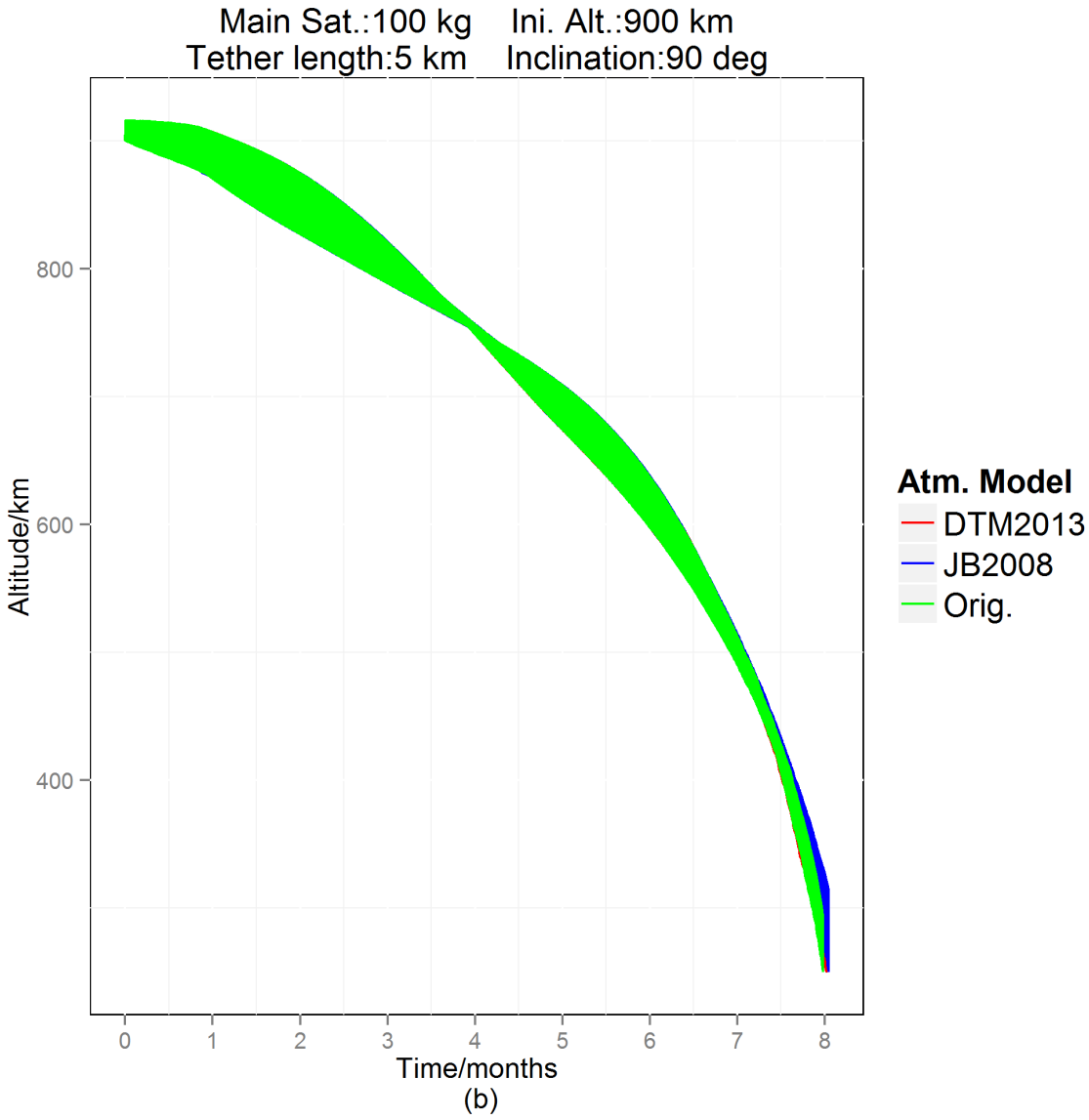
Main Sat.:100 kg Ini. Alt.:900 km
Tether length:5 km Inclination:90 deg
Altitude/km
800
600
400
0
1
2
3
4
5
6
7
8
Time/months
(b)
Atm. Model
DTM2013
JB2008
Orig.

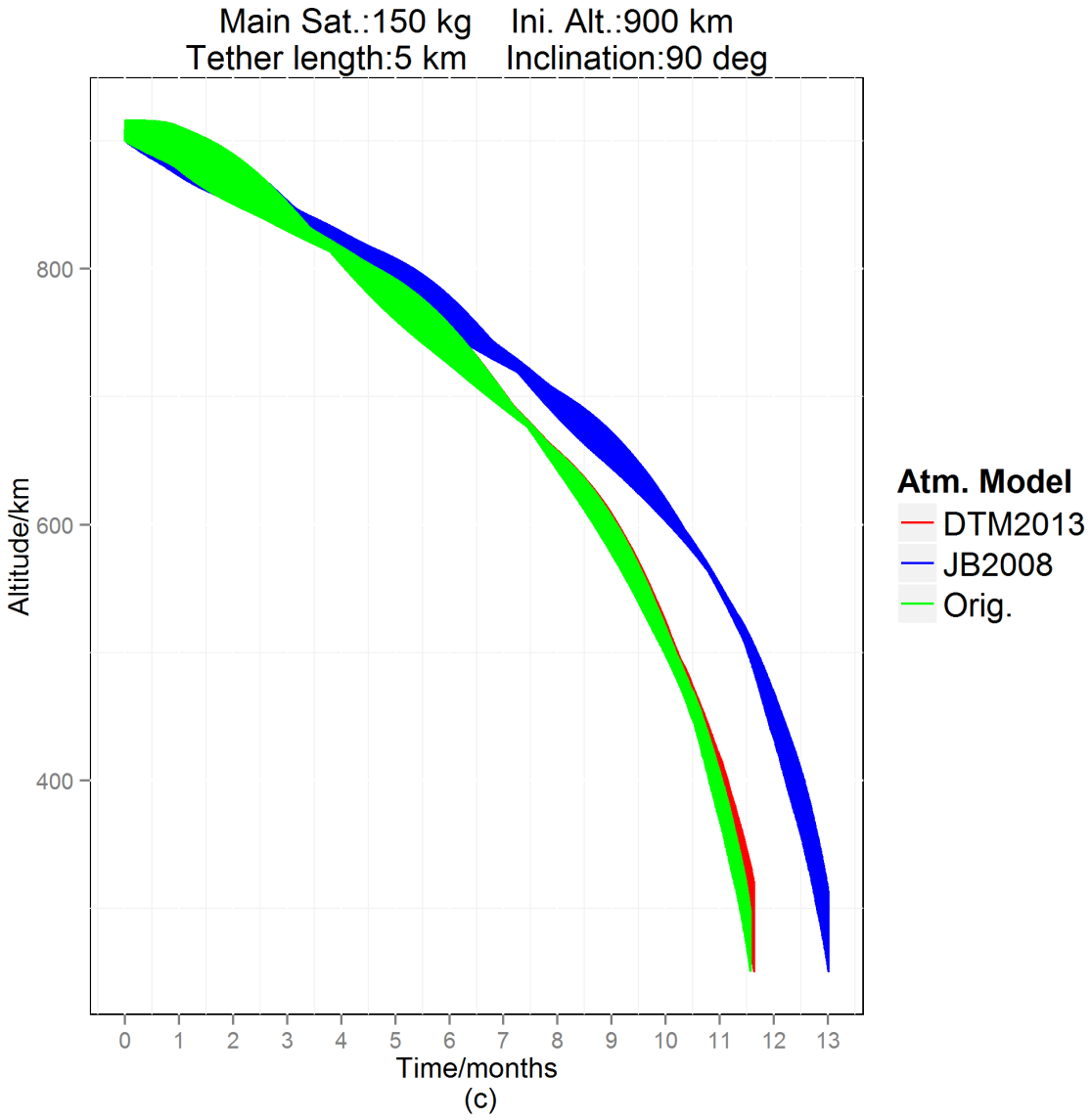

Figure 4.6 Results of the 5 km tether, initial altitude 900 km and main satellite masses of 75 kg, 100 kg, 150 kg (Energy control).

We can safely conclude that the libration energy control is far superior to the angle control. The space tether system almost always completely de-orbits when using libration energy control whereas the opposite is true when using angle control. Additionally, with libration energy control, the atmospheric model seems to be of little consequence during de-orbit.

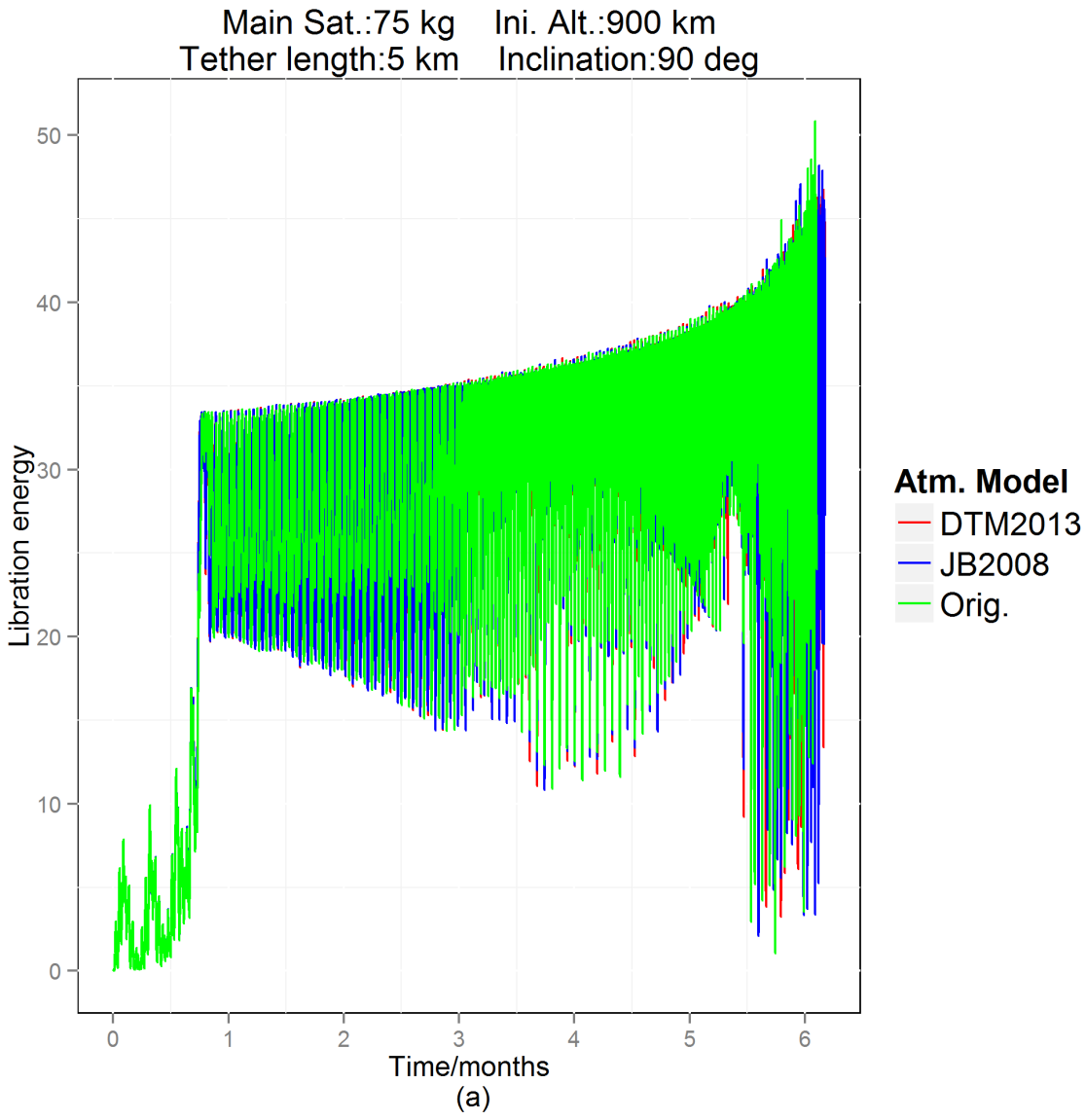
Main Sat.:75 kg Ini. Alt.:900 km
Tether length:5 km Inclination:90 deg
Libration energy
0
10
20
30
40
50
0
1
2
3
4
5
6
Time/months
(a)
Atm. Model
DTM2013
JB2008
Orig.

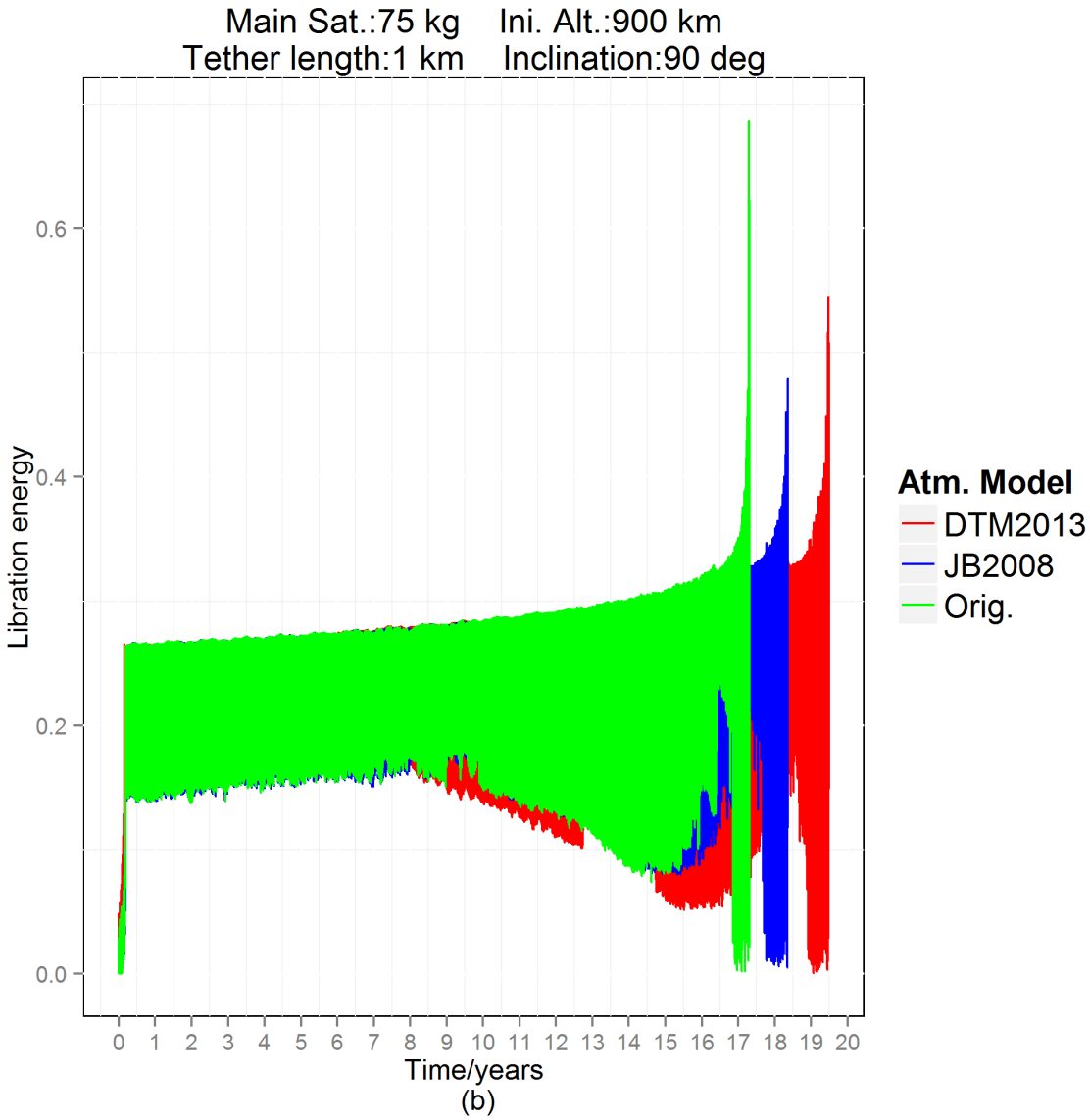
Main Sat.:75 kg Ini. Alt.:900 km
Tether length:1 km Inclination:90 deg
Libration energy
0.0
0.2
0.4
0.6
0 1 2 3 4 5 6 7 8 9 10 11 12 13 14 15 16 17 18 19 20
Time/years
Atm. Model
DTM2013
JB2008
Orig.
(b)

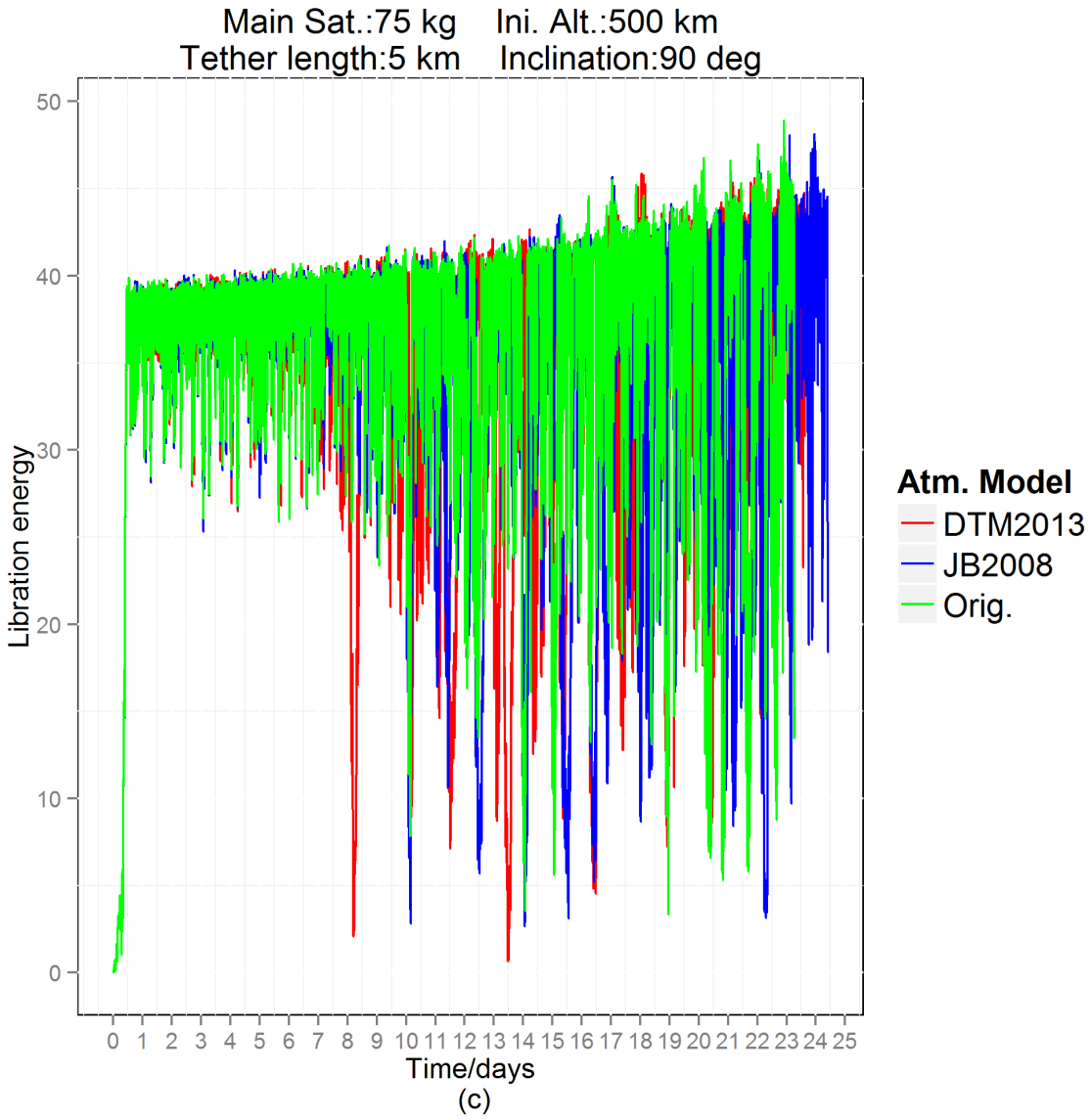
Main Sat.:75 kg Ini. Alt.:500 km
Tether length:5 km Inclination:90 deg
Libration energy
Time/days
(c)
Atm. Model
DTM2013
JB2008
Orig.

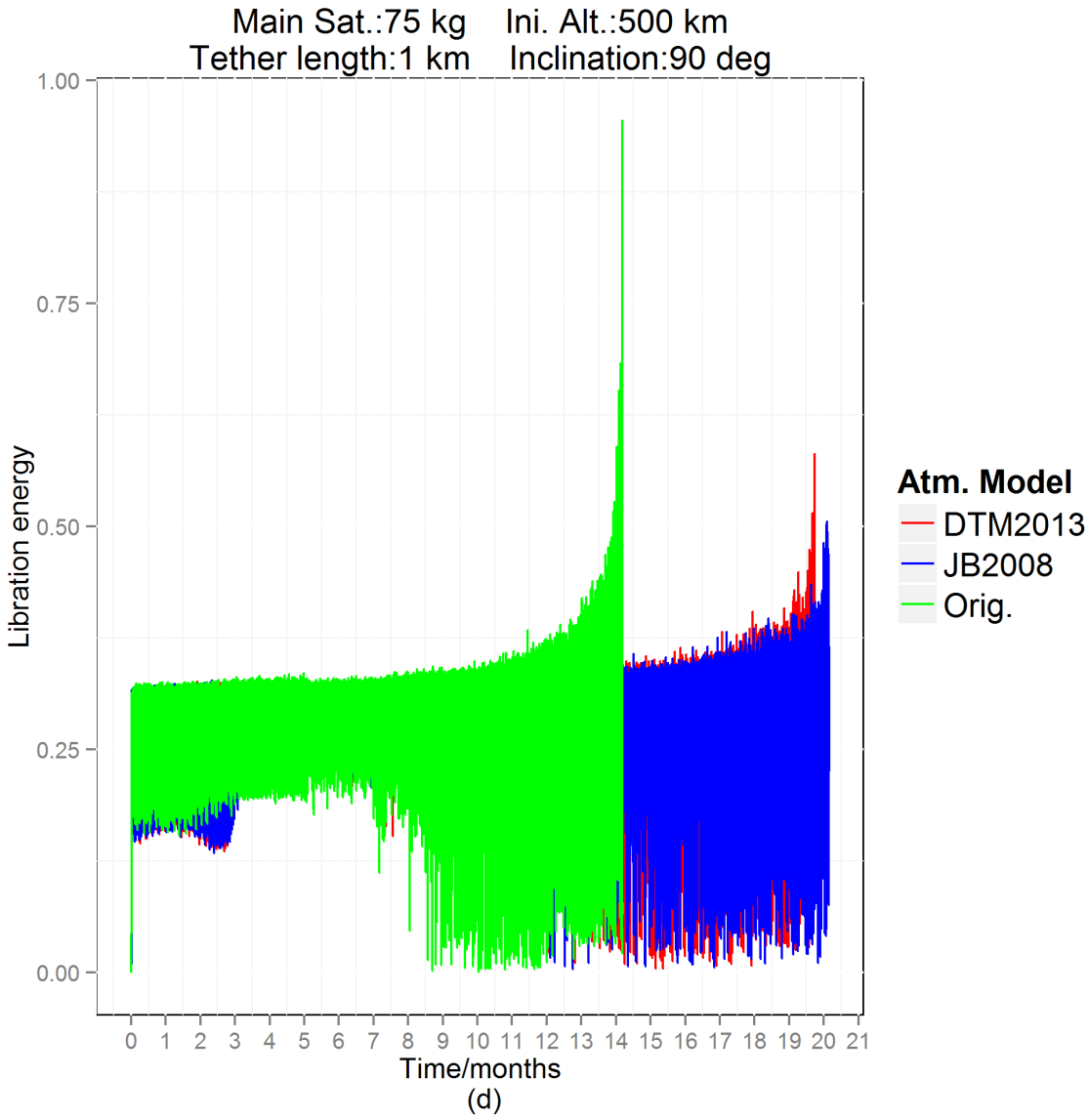

Figure 4.7 Libration energy (Energy control).

Chapter 5 CONCLUSIONS AND FUTURE WORK

5.1 COMDEV Cases

Doubling the mass of the sub-satellite led to longer de-orbit times and to a longer de-orbit. This suggests that the extra mass makes the de-orbit more stable.

The de-orbit times from 500 km initial altitude are considerably shorter than those from 900 km initial altitude.

In the 900 km initial altitude regime, the tether successfully de-orbits the satellite to an altitude where air drag would complete the remainder of the de-orbit for only the 3 km tether and the 5 km tether.

In the 500 km initial altitude regime, the tether was able to successfully de-orbit the satellite for all tether lengths.

5.2 Libration Control Strategy

5.2.1 Simple Pitch/Roll Angle Control

We observed that in the 500 km regime, the old atmospheric model predicted a much sooner de-orbit time than the new atmospheric models predicted. A consequence of de-orbiting for a longer time is that the final altitude the space tether system reached before tumbling was lower when using the new atmospheric models. Also, the results from the new atmospheric models agreed closely with each other. No case reached the final

altitude of 250 km.

In the 900 km altitude regime, the 3 km and 5 km tether led to tumbling in all cases. The new atmospheric models predicted a greater de-orbit time than was originally calculated and managed to de-orbit the space tether system between 450 km and 500 km altitude. For the 1 km tether, all three atmospheric models predicted that the space tether system would continue de-orbiting for some time after the allotted 25 years. However, the same trend that was observed for the 3 km and 5 km tether appear to hold in this case too.

5.2.2 Libration Energy Control

In the 500 km regime, we saw that the space tether system completely de-orbited in all cases unlike the pitch and roll cases. The old atmospheric model predicts a shorter de-orbit time than the new atmospheric models.

In the 900 km regime, almost all of the cases led to complete de-orbit with the atmospheric models performing similar to the 500 km regime. Using libration energy to control the space tether system managed to de-orbit a large number of cases to its final altitude. Therefore, libration energy control is more preferred for de-orbiting a space tether system. The new atmospheric models give us a better sense of how much time is required for the de-orbit.

5.3 Contributions of Thesis Work

This thesis provided insight into several areas of work surrounding the upper atmosphere and space tether systems. First and foremost, it has provided elementary analysis of the effect the new atmospheric models have on the de-orbit of a space tether system. This

work has not been seen before in the literature reviewed for this thesis.

Additionally, we have also made insights into how to further stabilise the de-orbit of our space tether system. The cases that we ran using COMDEV's specifications showed us that doubling the mass of the sub-satellite leads to a more stable de-orbit. The new atmospheric models showed us that the space tether system is more stable than was initially thought. The introduction of libration energy control led us to a better form of control because it lets the space tether system de-orbit successfully in most of the cases run.

Finally, we have made adjustments in our MATLAB/Simulink model of a space tether system by updating the model of the ionosphere and of the Earth's magnetic field.

5.4 Future Work

The most obvious course that one can take in future work surrounding this research is to monitor the most recent publications of atmospheric models. With future atmospheric models, we can make comparisons with the present atmospheric models and with the results obtained from the Simulink/MATLAB model.

Another direction that one could head in is to seek a modification to the current atmospheric models to improve their accuracy. For instance, there has been recent work that makes use of artificial neural networks to better estimate the density of the thermosphere especially during geo-magnetic storms [43] [77] [78].

Currently, the atmospheric models implemented only use the average data from one particular day (January 1st,2011) and repeats these values for each subsequent day. An immediate improvement to this treatment of the atmospheric models would be to use the density data over one solar cycle (approximately 11 years) and repeatedly use these

values.

From here, one could strive to improve the Simulink/MATLAB model that simulates the de-orbit of the space tether system. In particular, one can strive to find control laws that are better suited to keeping the tether vertical throughout the simulation. The two methods that were used in this research (libration energy control and angle control) were not fully robust though they were sufficient for our simulations. There were several instances where the tether lay outside the bounds imposed by the control method. One can either improve upon the current methods of control or make use of alternative methods of control such as fractional order control or non-linear control.

Another avenue to pursue is to investigate the effect a doubled sub-satellite mass has on the space tether system under the influence of the new atmospheric models. This would give us an updated assessment of its effect.

References

1. Williams P. (2012). A review of space tether technology. *Recent patents on Space Technology*, 22-36
2. Wen, H., Jin D. P., Hu H. Y. (2008) Advances in Dynamics and Control of Tethered Satellite Systems. *Acta Mechanica Sinica*, 24, 229-241
3. Chen Y., Huang R., He L., Ren X., Zheng B. (2014) Dynamical modelling and control of space tethers: a review of space tether research. *Non-linear Dynamics*, 77, 1077-1099
4. Sanmartin J. (2010). A review of eletrodynamic tethers for science applications. *Plasma Sources Science and Technology*, 19(3)
5. Cosmo, M.L. and Lorenzini E.C. *Tethers in Space Handbook 3rd Edition.* Smithsonian Astrophysical Observatory. 1997
6. Liu H. T., Zhang Q. B., Yang L. P. et al. Dynamics of tether-tugging re-orbiting with net capture. *Science China Technological Sciences*, 2014, 57
7. Aslanov, V. and Yudintsev V. Dynamics of large space debris removal using tethered space tug. *Acta Astronautica*, 2013, 91, 149-156
8. Schadegg, Maximilian M., Russell, Ryan P., Lantoine, G. (2015) Jovian Orbit Capture and Eccentricity Reduction Using Electrodynamic Tether Propulsion. *Journal of Spacecraft and Rockets*, 52, 2, 506-516
9. Charro, Mario, Sanmartin, Juan R., Bombardelli, Claudio et al. (2012) A Proposed

Two-Stage Two-Tether Scientific Mission at Jupiter. *IEEE Transactions on Plasma Science,* 40, 2, 274-281

10. Beletskii, V. V., Ivanov, M. B., Otstavnov, E. I. (2005) Model problem of a space elevator. *Cosmic Research,* 43, 2, 152-156
11. Yamaigiwa, Y., Hiragi, E., Kishimoto, T. (2005) Dynamic behavior of electrodynamic tether deorbit system on elliptical orbit and its control by Lorentz force. *Aerospace Science and Technology,* 9, 4, 366-373
12. Pardini, C., Hanada, T., Krisko, Paula H. et al. (2007) Are de-orbiting missions possible using electrodynamic tethers? Task review from the space debris perspective. *Acta Astronautica,* 60, 10-11, 916-929
13. Nock, K. T., Aaron, K. M., McKnight, D. (2013) Removing Orbital Debris with Less Risk. *Journal of Spacecraft and Rockets,* 50, 2, 365-379
14. Englert C. R., Bays J. B., Marr K. D., Brown C. M., Nicholas A. C., Finne T. T. (2014) Optical orbital debris spotter. *Acta Astronautica,* 104, 99-105
15. Levin, E., Pearson, J., Carroll, J. (2012) Wholesale debris removal from LEO. *Acta Astronautica*, 73, 100-108
16. Liou, J. -C., Johnson, N. L., Hill, N. M. (2010) Controlling the growth of future LEO debris populations with active debris removal. *Acta Astronautica*, 66, 5-6, 648-653
17. Bayajid Khan, S., Sanmartin, Juan R. (2014) Analysis of tape tether survival in LEO against orbital debris. *Advances in Space Research*, 53, 9, 1370-1376
18. Forward, R. L., Hoyt, R. P., Uphoff, C. W. (2000) Terminator Tether (TM): A spacecraft deorbit device. *Journal of Spacecraft of Rockets*, 37, 2, 187-196

19. Hoyt R. P., Smith, P. (2000) The Remora Remover (TM): A zero-debris method for on-demand disposal of unwanted LEO spacecraft. *2000 IEEE Aerospace Conference Proceedings,* 4, 239-246

20. Pardini, C., Hanada, T., Krisko, Paula H. (2009) Benefits and risks of using electrodynamic tethers to de-orbit spacecraft. *Acta Astronautica,* 64, 5-6, 571-588

21. Perez, D., Bevilacqua, R. (2015) Neural Network based calibration of atmospheric density models. *Acta Astronautica,* 110, 58-76

22. Zhong R., Zhu Z. (2013). Libration dynamics and stability of electrodynamic tethers in satellite de-orbit. *Celestial Mechanics and Dynamical Astronomy,* 116, 279-298

23. Doornbos E., Klinkrad H. (2006) Modelling of space weather effects on satellite drag. *Advances in Space Research,* 37, 6, 1229-1239

24. Aslanov V.S., Ledkov A. S. (2014) Dynamics of towed space large debris taking into account atmospheric disturbance. *Acta Mechanica,* 225, 2685-2697

25. Fejer B.G. (2011) Low Latitude Ionosphere Electrodynamics. *Space Science Reviews,* 158, 1, 145-166

26. Laštovička, J., Solomon, S. C., Qian, L. (2012) Trends in the Neutral and Ionized Upper Atmosphere. *Space Science Reviews,* 168, 1-4, 113-145

27. [27] Clausen, L. B. N., Milan, S. E., Grocott, A. (2014) Thermospheric density perturbations in response to substorms. *Journal of Geophysical Research-Space Physics,* 119, 6, 4441-4455

28. Forbes, J.M., Bruinsma, S., Lemoine, F. G. (2006) Solar rotation effects on the thermospheres of Mars and Earth. *Science,* 312, 5778, 1366-1368

29. Thuillier G., Bruinsma S. (2001) The Mg II index for upper atmosphere modelling. *Annales Geophysicae*, 19, 219-228

30. de Wit, T. D., Bruinsma, S., Shibasaki, K. (2014) Synoptic radio observations as proxies for upper atmosphere modelling. *Journal of Space Weather and Space Climate*, 4, A06

31. Zhu, Z. H., Zhong R. (2013) Long term dynamics and optimal control of nano-satellite deorbit using a short electrodynamic tether. *Advances in Space research,* 52, 1530-1544

32. Zhu, Z. H., Zhong R. (2014) Optimal control of Nanosatellite Fast Deorbit Using Electrodynamic Tether. *Journal of Guidance, Control and Dyanmics,* 37, 4, 1182-1194

33. Zhong, Z. H., Zhong R. (2011) Deorbiting dynamics of Electrodynamic Tether. *International Journal of Aerospace and Lightweight Structures*, 1, 1, 47-66

34. Zhong, Z. H., Zhong R. (2013) Dynamics of Nanosatellite Deorbit by Bare Electrodynamic Tether in Low Earth Orbit. *Journal of Spacecraft and Rockets*, 50, 3, 691-700

35. *U.S. Standard Atmosphere, 1976*. Washington D.C. National Aeronautics and Space Administration. 1976. Print.

36. Cain, J., and Newland, F., "AIM Microsatellite Platform: A Canadian Multi-Mission Satellite Bus Solution," 30th AIAA International Communications Satellite System Conference (ICSSC), AIAA Paper ICSSC-190, 2012.

37. Dafu X., Xianren K., Jun L., Zhengxian Y. & Feng W. (2011). Dynamic modelling and simulation of electrodynamic tether system in stationkeeping phase. *Journal of*

Mechanical Science and Technology, 25(1), 97-102

38. Hoyt R. (2001). Stabilization of Electrodynamic Space Tethers. *Tethers Unlimited, Inc.*

39. Sun G., Zhu Z. H. (2014) Fractional-order Tension Control Law for Deployment of Space Tether System. *Journal of Guidance Control and Dynamics,* 37, 6, 2062-2066

40. Kristiansen K., Palmer P. & Roberts R. (2012). Numerical modelling of elastic space tethers. *Celestial Mechanics and Dynamical Astronomy,* 113, 235-254

41. Montenbruck O., Gill E. (2000). Satellite Orbits: Models, Methods, Applications. New York City, NY: Springer

42. Gaposchkin E., Coster A. (1988). Analysis of Satellite Drag. *The Lincoln Laboratory Journal,* 1

43. Perez, D., Wohlberg, B., Lovell, T. A., et al. (2014) Orbit-centered atmospheric density prediction using artificial neural networks. *Acta Astronuatica,* 98, 9-23

44. Mehta P. (2013). Thermospheric density and satellite drag modelling. Published doctoral dissertation, University of Kansas

45. Vallado D., Finkleman D. (2009). A critical assessment of satellite drag and atmospheric density modeling. *The American Institute of Aeronautics and Astronautics*

46. Doornbos E. (2012). Thermospheric Density and Wind Determination from Satellite Dynamics. New York City, NY: Springer

47. Belehaki, A., Stanislawska, I., Lilensten, J. (2009) An Overview of Ionosphere-Thermosphere Models Available for Space Weather Purposes. *Space Science*

Reviews, 147, 3-4, 271-313

48. Hicks J. (1997). An adaptive thermospheric model to improve the prediction of satellite orbits. Published masters dissertation, University of West Virginia
49. Jacchia L. (1964). Static Diffusion Models of the Upper Atmosphere with Empirical Temperature Profiles. *Smithsonian Contributions to Astrophysics,* 8, 215
50. Jacchia L., Kopal Z. (1951). Atmospheric oscillations and the temperature profile of the upper atmosphere. *Journal of Meteorology,* 9, 13-23
51. COSPAR (2012). COSPAR International Reference Atmosphere-2012: Models of the Earth's upper atmosphere, 1
52. Harris I., Priester W. (1962) Time-Dependent Structure of the Upper Atmosphere. *Journal of the Atmospheric Sciences,* 19, 4, 286-301
53. Jacchia L. (1970). Revised Static Models of the Thermosphere and Exosphere with Empirical Temperature Profiles. *Research in Space Science - Smithsonian Astrophysics Observatory,* Special Report 332, 113
54. Mueller A. (1982). Jacchia-Lineberry upper atmosphere density model. *SAO/NASA ADS Physics Abstract Service*
55. Walker, James C. G. (1965). Analytic Representation of Upper Atmosphere Densities based on Jacchia's Static Diffusion Models. *Journal of the Atmospheric Sciences,* 22, 462-463
56. Bowman B., Tobiska W., Marcos F., Lin C., Valladares C. (2007). The JB2006 empirical thermospheric density model. *Journal of Atmospheric and Solar-Terrestrial Physics,* 70, 774-793
57. Bowman B., Tobiska W., Bouwer S. (2007). The development of solar indices for

use in thermospheric density modeling. *Journal of Atmospheric and Solar-Terrestrial Physics,* 70, 803-819

58. Bowman B., Tobiska W., Marcos F., Huang C., Lin C., Burke W. (2008). A new empirical thermospheric density model JB2008 using new solar and geomagnetic indices. *The American Institute of Aeronautics and Astronautics*

59. Hedin A., Reber C., Newton G., Spencer N., Salah J., Evans J., Kayser D., Alcayde D., Bauer P., Cogger L. (1977). A global thermospheric model based on mass spectrometer and incoherent scatter data MSIS I - N2 density and temperature. *Journal of Geophysical Research,* 82, 2139–2147

60. Hedin A., Reber C., Newton G., Spencer N., Brinton H., Mayr H., Potter W. (1977). A global thermospheric model based on mass spectrometer and incoherent scatter data MSIS II - composition. *Journal of Geophysical Research,* 82, 2148–2156

61. Hedin A. (1983). A revised thermospheric model based on mass spectrometer and incoherent scatter data - MSIS-83. *Journal of Geophysical Research,* 88, 10170–10188

62. Hedin A. (1991). Extension of the MSIS thermospheric model into the middle and lower atmosphere. *Journal of Geophysical Research,* 96(A2), 1159–1172

63. Picone J., Hedin A. , Drob D., Aikin A. (2002) NRLMSISE-00 empirical model of the atmosphere: statistical comparisons and scientific issues. *Journal of Geophysical Research – Space Physics,* 107(A12), 1468

64. Dharwan M., Singh V. (2015) A study of OI 844.6 nm dayglow emission under geomagnetic conditions. *Advances in Space Research,* 55, 11, 2526-2533

65. Barlier F., Berger C., Falin J., Kockarts G., Thuillier G. (1978). A thermospheric model based on satellite drag data. *Année géophysique internationale,* 34(1), 9–24

66. Thuillier G., Bruinsma S., Barlier F. (2003). The DTM-2000 empirical thermosphere model with new data assimilation and constraints at lower boundary: accuracy and properties. *Journal of Atmospheric and Solar-Terrestrial Physics*, 65, 1053 –1070

67. Hedin A.E., M., H.G., Reber, C., et al. (1974). Empirical model of global thermospheric temperature and composition based on data from the OGO-6 quadrupole mass spectrometer

68. Berger C., Biancale R., Ill M., Barlier F. (1998). Improvement of the empirical thermospheric model DTM: DTM-94–a comparative review of various temporal variations and prospects in space geodesy applications. *Journal of Geodesy,* 72(3), 161–178

69. Bruinsma S., Sanchez-Ortiz N., Olmedo E., Guijarro N. (2012). Evaluation of the DTM-2009 thermosphere model for benchmarking purposes. *Journal of Space Weather and Space Climate,* 2

70. Bruinsma, Sean. "DTM 2013 evaluation report". 22 October 2013. Web. 14 May 2015. http://www.atmop.eu/public-documents/evaluation_report_dtm2013.pdf

71. Bruinsma S. (2015) The DTM-2013 thermosphere model. *Journal of Space Weather and Space Climate,* 5, A1

72. Williams P. (2009) Libration Control of Electrodynamic Tethers Using Predictive Control with Time-delayed Feedback. *Journal of Guidance, Control and Dynamics,* 32, 4

73. Zhao G., Sun L., Tan S. (2013) Librational characteristics of a dumbbell modelled tethered satellite under small, continuous, constant thrust. *Journal of Aerospace Engineering,* 227, G5, 857-872

74. Tortora P., Somenzi L., Iess L., Licata R. (2006) Small Mission Design for Testing In-Orbit an Electrodynamic Tether Deorbiting System. *Journal of Spacecraft and Rockets,* 43, 4

75. Corsi J., Iess L. (2001) Stabilty and control of Electrodynamic Tethers for De-orbiting Applications. *Acta Astronautica,* 48, 5-12, 491-501

76. Takeichi N. (2006). Practical Operation Strategy for De-orbit of an Electrodynamic Tethered System. *Journal of Spacecraft and rockets,* 43, 1283-1288

77. Chen, H., Liu, H., Hanada, T. (2014) Storm-time atmospheric density modelling using neural networks and its application in orbit propagation. *Advances in Space Research,* 53, 3, 558-567

78. Cunying X., Xiong H. (2010) Applying Artificial Neural Networks to Modeling the Middle Atmosphere. *Advances in Atmospheric Sciences,* 27, 4, 883-890

79. Chapman, Sydney, and Cowling T.G. *The Mathematical Theory of Non-uniform Gases.* 1953. Print.

80. Boushehri A., Abbaspour A. (1979) Diffusion Thermo-Effect in Gases (The Dufour Effect). *Bulletin of the Chemical Society of Japan,* 52, 7, 2097-2098.

81. Curtis H. D., *Orbital Mechanics for Engineering Students*, Elsevier, Oxford, 1988, Chapter 4

Appendix I. Derivation of Jacchia's Diffusion Equation

Consider a still monatomic gas contained in vessel of height, *h*, and of surface area, *A*. Then, the weight of this column of gas is given by

$$F_{gas} = m_{gas}g(z) = r_{gas}(z)V_{gas}g(z) = r_{gas}(z)Azg(z) \tag{A.1}$$

Then, we can calculate the pressure, *P*, by

$$P = \frac{F_{gas}}{A} = \frac{\rho_{gas}(z)Azg(z)}{A} = \rho(z)zg(z) \tag{A.2}$$

If we now consider a height, *h* + *dh*, where *dh* is a small incremental height, we can find the pressure at this new height. We can then find the difference between the two pressures and write it as follows

$$dP = -\rho(z)g(z)dz \tag{A.3}$$

We include the negative sign because the pressure must decrease with increasing height.

We now consider the ideal gas equation

$$PV_{gas} = n_{mol} R_{gas} T$$
$$PV_{gas} = \frac{m_{gas}}{M_{mol}} R_{gas} T$$
$$P = \frac{\rho R_{gas} T}{M_{mol}}$$
$$\rho = \frac{P M_{mol}}{R_{gas} T} \tag{A.4}$$

Substituting into the above equation for hydrostatic balance,

$$dP = -\frac{P M_{mol}}{R_{gas} T} g dz$$
$$\frac{dP}{dz} = -\frac{M_{mol} g}{R_{gas} T} P \tag{A.5}$$

To derive the diffusion equation that Jacchia used in his model of the upper atmosphere, we must first define some velocities. The following velocities are used for the one-dimensional case.

First, consider a gas that consists of one type of molecule. Let each molecule have velocity, c. Then, the average velocity of the gas, $\bar{c}$, is given by summing all of the individual velocities and dividing by the total number of molecules, n_{tot}.

This gives us an expression for the total number of particles that pass through a unit cross-section of a plane, $n_{tot}\bar{c}$. This is also called the particle transport.

Now assume that the gas is made up of different kinds of molecules. Then, we can define the mean velocity, $\bar{c}$, of this system using the particle transport.

$$n_{tot}\bar{c} = \sum_i n_i \bar{c}_i \tag{A.6}$$

We can further define the mean mass transport velocity as follows.

$$\sum_i n_i m_i \bar{c}_i = \sum_i c_i \rho_i = c_0 \rho \tag{A.7}$$

where m_i is the mass of the ith component of the gas and ρ_i is the density of the i-th component of the gas.

The final velocity that we define is the mean thermal velocity or the peculiar velocity, $\overline{C}_i$. It is defined when one constituent of the gas has a different velocity to the mean velocity.

$$\overline{C}_i = \bar{c}_i - \bar{c} \tag{A.8}$$

It easily follows that, for two constituents,

$$\overline{C}_1 - \overline{C}_2 = \bar{c}_1 - \bar{c}_2 \tag{A.9}$$

Chapman and Cowling [79] give the equations for the conservation of mass, momentum and energy for a system that has many constituents making up the whole gas. In the equation for the conservation of energy, we find a heat flux vector (or rather, the vertical component of the heat flux vector since we are considering one-dimensional motion).

The expression for this component of the heat flux vector contains the last expression written above – the expression involving the difference of the mean thermal velocities. This can be re-written and we will see how in what follows.

This expression encapsulates information about the thermo-diffusion effect or the Dufour effect [80]. Consider an isothermal gas. If we impose a concentration gradient on the gas, then the Dufour effect tells us that the resulting diffusion will induce a temperature gradient on the gas. This temperature gradient is different to the heat

generated by mixing.

The Dufour effect is also the opposite of thermal diffusion. In thermal diffusion, the imposed temperature gradient induces a concentration gradient; in the thermo-diffusion effect, the imposed concentration gradient induces a temperature gradient.

As alluded to earlier, the derivation of the difference of the mean thermal velocities has its roots in non-equilibrium thermodynamics. More specifically, this expression comes from a treatment of Boltzmann's transport equation by Enskog's method of solution. Enskog used perturbation expansions to find a solution for the probability density function found in Boltzmann's equation.

The expression for the difference of the mean thermal velocities in one dimension is given below.

$$\overline{C}_1 - \overline{C}_2 = \frac{n^2}{n_1 n_2} D\left[\frac{\partial(n_1/n_2)}{\partial z} + \frac{n_1 n_2 (m_2 - m_1)}{n\rho}\frac{\partial \log p}{\partial z} + \frac{n_1 n_2}{n^2}\alpha_T \frac{1}{T}\frac{\partial T}{\partial z}\right] \tag{A.10}$$

where D is the diffusion coefficient and α_T is the thermal diffusion factor

Nicolet used this expression together with three assumptions to derive the diffusion equation used by Jacchia. His idea was that we are dealing with minor constituents and, as such, the diffusion equations greatly simplify.

- Diffusion (upwards or downwards) of a minor constituent does not significantly change the pressure of the atmosphere. So,

$$\frac{\partial p}{\partial t} = 0$$

- Since we have a minor constituent, it does not significantly contribute to the

overall number of molecules.

$$n = n_1 + n_2 \cong n_2$$

- There is no net particle flow across any surface.

$$n_1 c_1 + n_2 c_2 = 0$$

Though the discussion is limited to binary gas mixtures, the result is easily extended to gas mixtures with numerous constituents.

With these assumptions, the expression for the difference of mean thermal velocities becomes

$$w = D\left[\frac{1}{n_1}\frac{\partial n_1}{\partial z} + \frac{m_1 g}{kT} + (1+\alpha_T)\frac{1}{T}\frac{\partial T}{\partial z}\right] \tag{A.11}$$

where w is the velocity of the minor constituent

Jacchia took the velocity of the minor constituent to be zero and we now have the diffusion equation used in his models.